

Fall 1990

The Similkameen Batholith of North-Central Washington and South-Central British Columbia: The Petrotectonic Significance of an Alkaline/Calc-Alkaline Magmatic Complex

Andrew M. (Andrew McNair) Buddington
Western Washington University

Follow this and additional works at: <https://cedar.wwu.edu/wwuet>



Part of the [Geology Commons](#)

Recommended Citation

Buddington, Andrew M. (Andrew McNair), "The Similkameen Batholith of North-Central Washington and South-Central British Columbia: The Petrotectonic Significance of an Alkaline/Calc-Alkaline Magmatic Complex" (1990). *WWU Graduate School Collection*. 811.

<https://cedar.wwu.edu/wwuet/811>

This Masters Thesis is brought to you for free and open access by the WWU Graduate and Undergraduate Scholarship at Western CEDAR. It has been accepted for inclusion in WWU Graduate School Collection by an authorized administrator of Western CEDAR. For more information, please contact westerncedar@wwu.edu.

**THE SIMILKAMEEN BATHOLITH OF NORTH-CENTRAL WASHINGTON
AND SOUTH-CENTRAL BRITISH COLUMBIA: THE PETROTECTONIC
SIGNIFICANCE OF AN ALKALINE/CALC-ALKALINE MAGMATIC
COMPLEX**

by

Andrew M. Buddington

**Accepted in Partial Completion
of the Requirements for the Degree
Master of Science**

Dean of Graduate School J

Advisory Committee

Chair

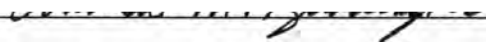
D

D

/

MASTER'S THESIS

In presenting this thesis in partial fulfillment of the requirements for a master's degree at Western Washington University, I agree that the Library shall make its copies freely available for inspection. I further agree that extensive copying of this thesis is allowable only for scholarly purposes. It is understood, however, that any copying or publication of this thesis for commercial purposes, or for financial gain, shall not be allowed without my written permission.

Signature 

Date October 22, 1990

MASTER'S THESIS

In presenting this thesis in partial fulfillment of the requirements for a master's degree at Western Washington University, I grant to Western Washington University the non-exclusive royalty-free right to archive, reproduce, distribute, and display the thesis in any and all forms, including electronic format, via any digital library mechanisms maintained by WWU.

I represent and warrant this is my original work and does not infringe or violate any rights of others. I warrant that I have obtained written permissions from the owner of any third party copyrighted material included in these files.

I acknowledge that I retain ownership rights to the copyright of this work, including but not limited to the right to use all or part of this work in future works, such as articles or books.

Library users are granted permission for individual, research and non-commercial reproduction of this work for educational purposes only. Any further digital posting of this document requires specific permission from the author.

Any copying or publication of this thesis for commercial purposes, or for financial gain, is not allowed without my written permission.

Name: ANDREW Buddington

Signature: [Handwritten Signature]

Date: 6/8/18

**THE SIMILKAMEEN BATHOLITH OF NORTH-CENTRAL WASHINGTON
AND SOUTH-CENTRAL BRITISH COLUMBIA: THE PETROTECTONIC
SIGNIFICANCE OF AN ALKALINE/CALC-ALKALINE MAGMATIC
COMPLEX:**

A Thesis Presented to
The Faculty of
Western Washington University

In Partial Fulfillment
of the Requirements for the Degree
Master of Science

by

Andrew McNair Buddington
October 1990

ABSTRACT

The Similkameen batholith is a 170 Ma plutonic complex that contains coeval mafic alkaline and granitic calc-alkaline assemblages. The marginal mafic alkaline suite is silica-undersaturated, characteristically potassic in composition and comprised of malignite, shonkinite, and mafic syenites (+/- nepheline) with biotite and amphibole-bearing pyroxenite cumulates. The granitic plutons of the core are calc-alkaline, I-type, ranging from monzonite to granodiorite to granite in composition.

Structural and petrofabric studies indicate that the mafic alkaline suite was intruded and deformed by the calc-alkaline granitoids. Magmatic fabrics within the mafic rocks are concentric to the lithologic zonations and have been overprinted by sub-magmatic flow deformation induced by diapiric emplacement of the core. There is no evidence within the batholith for regional deformation associated with the collision of Quesnellia and North America.

Major and trace element variations as well as Sr-isotopic data indicate that the alkaline and calc-alkaline suites are not related by crystal fractionation. However, crystal fractionation appears to have been the dominant process responsible for major element variations within the mafic alkaline suite. Fractionation of the hydrous assemblage clinopyroxene +/- biotite +/- amphibole + apatite + magnetite accounts for compositional variations within the alkaline suite. Calculated modal abundances of the fractionated mineral phases closely approximates observed modal abundances within the pyroxenites, which supports a crystal accumulation origin for the ultramafic rocks.

The alkaline and calc-alkaline suites exhibit a geochemical signature characteristic of subduction-related magmatism. Both suites are enriched in alkali and alkaline earth elements and depleted in high field strength elements. Major and trace element compositions of the mafic alkaline suite are consistent with partial melting of a garnet and phlogopite-bearing peridotite source. However, trace element variations within the alkaline suite demonstrate derivation from a chemically heterogeneous mantle-source. The malignite series contains incompatible element ratios consistent with a depleted MORB-type source, whereas the shonkinite series appears to be enriched, indicative of an OIB-type source. The Ba-enrichments of the malignites relative to the shonkinites probably reflect variations in source mineralogy, i.e., greater amounts of phlogopite in the source, not contamination by pelagic sediments. Furthermore, the low variability of initial-Sr ratios (0.7037-0.7042) indicates contamination of the Similkameen magmas by continental crust was relatively minor.

Variable degree partial melting of a lower crustal mafic granulite source could produce the incompatible element, REE, and isotopic abundances observed within the calc-alkaline granitoids.

Subduction and plate tectonic processes prior to 170 Ma variably enriched (metasomatized) portions of the lithospheric mantle wedge below the western edge of the North American craton. Derivation from this heterogeneous, metasomatized mantle-source resulted in the variably enriched nature of the mafic rocks. The granitoid magmas were the probable result of partial melting related to ponding of hot, hydrous mafic magmas of the alkaline suite at the lower crust-mantle boundary.

ACKNOWLEDGMENTS

My sincere gratitude must go to all the members of my thesis committee. I'm particularly indebted to Professor Scott Babcock, whose enthusiasm toward these strange rocks was greater than mine at times. Scott was instrumental in obtaining much of the geochemical data presented in this thesis. His never-ending ability to provide up-to-date references related to this project was often overwhelming but essential to solving many of the petrologic problems encountered. Dr. Russell Burmester inspired numerous discussions on the problems of petrofabric interpretation and pluton emplacement. Russ taught me that patience was a key toward resolving perplexing scientific problems. To Professor Antoni "Jontek" Wodzicki for the memorable field trips and discussions on geology and the human spirit. Jontek's passion for all branches of geology, particularly economic geology, put me on the path toward the practical application of knowledge. And to Professor James Talbot, many thanks for his help in the field and for teaching me to approach science objectively.

The petrologic avenues of this project benefited immensely from my relations with Dr. Tony Irving, Dr. Stewart McCallum, and Jeffery Tepper from the University of Washington. I'm obliged to Tony for keeping the ICP lab door open to me and for always being receptive to my questions and willing to offer new ideas about the rocks. Stu McCallum was essentially responsible for my work on this project, because it was he who directed me toward the Similkameen as an intriguing petrologic problem. I also extend my thanks to Jeff Tepper, who in the earliest and latest stages of this project offered many helpful ideas and inspired me to pursue several intriguing questions about magmatic processes.

The affordable accessibility to the geochronology laboratory at the University of British Columbia was made possible by Dr. R.L. Armstrong. Both Dick Armstrong and Dita Runkle went out of their way to help me obtain the Sr-isotope data so important for this work; for that I'm grateful. I would also like to thank Keith Stoffel and Bill Phillips of the Washington State Department of Natural Resources for their help in obtaining funding from the State graduate student mapping program.

What would the graduate experience be without fellow grad students? I want to thank my fellow graduate students at Western for putting up with me and for their numerous friendships. Dan McShane, Bernie Dougan, Gary Hurban, and Joe Dragovich offered insightful discussions on plutonic rocks of the North Cascades and were willing to listen to my opinions on igneous fabrics. Paul Riley and Monica Gowan were always there with an ear or a joke to get me through some of the drudgery of grad school.

The most important person by far in the realization of this project is my wife, Teresa. She supported me 110% throughout the toughest of times and for her love and encouragement I am truly thankful. I can't wait to become a real person again and spend the rest of my life with you!

This project was supported in part by a Western Washington University Graduate School research grant, Western Washington University Department of Geology field research grant, and by a State of Washington, Department of Natural Resources (DNR), graduate student state mapping contract. The DNR also provided funding for chemical analyses presented in this thesis.

TABLE OF CONTENTS

Abstract	i
Acknowledgements	iii
Table of Contents	v
List of Figures	vii
List of Tables	viii
List of Plates	viii

CHAPTER I

Introduction	1
Summary of Mesozoic Tectonics for South-Central British Columbia and North-Central Washington	1
Location of Study Areas	5
Previous Work	5
General Character of the Similkameen Batholith	6
Purpose and Scope	7
Methods: Field and Laboratory Work	9

CHAPTER II

Structural and Petrofabric Interpretation for Emplacement of the Similkameen Batholith	10
Introduction	10
Geologic Framework	10
Regional Structure	12
Contact & Porphyroblast Relations	14
Internal Structure of the Batholith	16
Anisotropy of Magnetic Susceptibility	
Magnetic Fabrics	18
Introduction	18
Discussion	18
Petrofabrics	20
Submagmatic Deformational Flow Fabrics	20
Transitional Fabrics	20
Magmatic Flow Fabrics	23
Discussion of Crystallization and Textural Zonation	23

CHAPTER III

Mineralogy, Petrology, and Petrogenetic Evolution of the Similkameen Batholith	32
Introduction	32
Rock Types	33
Ultramafic Assemblages	33
Malignite	35
Shonkinite	37
Mafic Syenite	37
Gneissic Syenite	37

Granitic Rocks	38
Mineral Compositions	40
Clinopyroxene	40
Amphibole	40
Biotite	42
Feldspar	43
Iron Oxides	44
Nepheline	44
Apatite	44
Sphene	44
Zircon	44
Major and Trace Element Geochemistry	44
Major and Trace Element Variations	45
Al ₂ O ₃ versus MgO	45
CaO versus MgO	47
P ₂ O ₅ versus MgO	49
Ni versus Cr	49
Summary of Major and Trace Element Variations	49
Rb-Sr Isotope Geochemistry	49
Petrogenetic Implications of Rb/Sr Isotopes	51
Assimilation and Fractional Crystallization	54
Modeling of Fractional Crystallization and Mixing	55
Alkaline to Calc-Alkaline Suite Fractionation	57
Intrasuite Fractionation for the Alkaline Rocks	58
Granitoids	60
Mixing	60
Source Components for the Alkaline and Calc-Alkaline Suites	62
Calc-Alkaline Granites	64
Mafic Alkaline Suite	67
Discussion	70
Magma Petrogenesis and Tectonic Setting	76

CHAPTER IV

Conclusions	79
References	81
Appendix A	
Petrographic descriptions	91
Appendix B	
XRF Whole Rock, Major and Trace Element Data	105
Appendix C	
Microprobe Data	112
Appendix D	
Rb-Sr Isotopic Compositions	118
Appendix E	
Results of Mass-Balance Calculations	120

LIST OF FIGURES

Figure

1.1: Simplified terrane map of the Canadian Cordillera	2
1.2: Physiographic and tectonic belts of the Canadian Cordillera	3
1.3: Generalized geologic map of the Similkameen batholith	8
2.1: Generalized geologic map of southcentral British Columbia and northcentral Washington	11
2.2: Simplified geologic map of the Similkameen batholith	13
2.3: Photomicrograph of garnet in a pelitic schist	15
2.4: Photomicrograph of randomly oriented biotites	15
2.5: Generalized structural map of the Similkameen batholith	17
2.6: Map of magnetic fabrics	19
2.7: Flinn plot of mean susceptibility values	21
2.8: Hand sample of a medium-grained gneissic syenite	22
2.9: Photomicrograph of gneissic syenite	22
2.10: Outcrop photograph of pseudoleucite-bearing malignite	24
2.11: Photomicrograph of fluid relocation texture	24
2.12: Magmatic flow fabric	25
2.13: Autolith of mafic syenite	25
2.14: Schematic diagram illustrating the sequential development	29
2.15: Schematic cross-sectional diagrams	30
3.1: Photomicrograph of biotite pyroxenite cumulate	34
3.2: Biotite pyroxenite pegmatite	34
3.3: Photomicrograph of nepheline-feldspar intergrowths	36
3.4: Plot of granitoid compositions	39
3.5: Plot of clinopyroxene compositions	41
3.6: Plot of amphibole and biotite compositions	41
3.7: R1-R2 plot	46
3.8: Al ₂ O ₃ versus MgO variation diagram	48
3.9: CaO versus MgO variation diagram	48
3.10: P ₂ O ₅ versus MgO variation diagram	50
3.11: Ni versus Cr variation diagram	50
3.12: Rb-Sr isochron	52
3.13: Sr versus MgO variation diagram	53
3.14: ⁸⁷ Sr/ ⁸⁶ Sr versus 1/Sr (ppm) variation diagram	53
3.15: Fractionation and mixing flow chart	56
3.16: Normalized incompatible element variation diagram	63
3.17: Rb versus Y+Nb granite discrimination diagram	65
3.18: Granitoid discrimination plot	65
3.19: Plot of Na ₂ O+K ₂ O/CaO versus Zr+Nb+Ce+Y	66
3.20: Chondrite normalized REE plot	68
3.21: Plot of Ce/Y versus Zr/Nb	69
3.22: Plot of Y/Nb versus Nb	69
3.23: Plot of Y/Nb versus Zr/Nb	71
3.24: Plot of Ba/Zr versus Nb/Zr	71
3.25: Plot of Ba/Zr versus Mg#	72
3.26: Schematic diagram showing the origin of the Similkameen magmas	77

LIST OF TABLES

Table 3.1: Results From Mass Balance Comparisons	59
Table 3.2: Results From Mass Balance Mixing Runs	61
Table 3.3: Incompatible Element Ratios	75

LIST OF PLATES

(located in back)

- Plate I: Geologic map of the Similkameen batholith, Okanogan County, Washington.
- Plate II: Geologic map of the Similkameen batholith, south-central British Columbia.

CHAPTER I

INTRODUCTION

The Similkameen batholith (the Similkameen-Kruger Alkalic Complex of Daly, 1906; Campbell, 1939) is a Middle Jurassic, alkaline/calc-alkaline plutonic complex located along the 49th parallel in north-central Washington and south-central British Columbia. It is an elongate, concentrically zoned body with the margin composed of a variety of alkaline mafic rocks and the interior of calc-alkaline granitoid rocks.

The batholith intrudes metavolcanic and metasedimentary rocks of the Kobau Formation, a Permo-Triassic oceanic sequence in southwestern Quesnellia (Fig. 1.1). The Similkameen contains at least three distinct plutons within the study area (Plates I, II), but based on the current mapping and petrological interpretation from this study, there may be five or more separate intrusive units.

The batholith is located within the Intermontane Belt approximately 25 km west of the boundary with the Omineca Crystalline Belt (Fig. 1.2). The Omineca Crystalline Belt has been described as a "tectonic welt"; a zone of concentrated intense deformation, regional metamorphism, and granitic magmatism (Monger et al., 1982; Parrish et al., 1985). The initiation and development of the Omineca Crystalline Belt are essentially coincident with the impingement and accretion of Superterrane I to the western margin of North America by the Middle Jurassic (Monger et al., 1982). The relationship of plutonism to regional tectonics following the collision of Superterrane I is still not clearly resolved. Numerous mid-Jurassic plutons that intrude southeastern Quesnellia are deformed and thought to be syntectonic with respect to collision (Archibald et al., 1983). Yet other mid-Jurassic plutons in parts of southcentral and southwestern Quesnellia are post-tectonic with respect to the collisional event (Roback, 1990).

Summary of Mesozoic Tectonics for South-Central British Columbia and North-Central Washington

In the last 10 years much attention has been given to the tectonic evolution of the Canadian Cordillera. In spite of the enormity and diversity of geologic problems, a general picture for the geologic evolution of the Canadian Cordillera has emerged.

The Canadian Cordillera is generally subdivided into five physiographic belts (Fig. 1.2) put forth by Wheeler and Gabrielse (1972) and Monger and Price (1979) among others. However in recent years a major emphasis has been put on regional divisions using the tectonic terrane nomenclature established by Monger and Price (1979), Coney

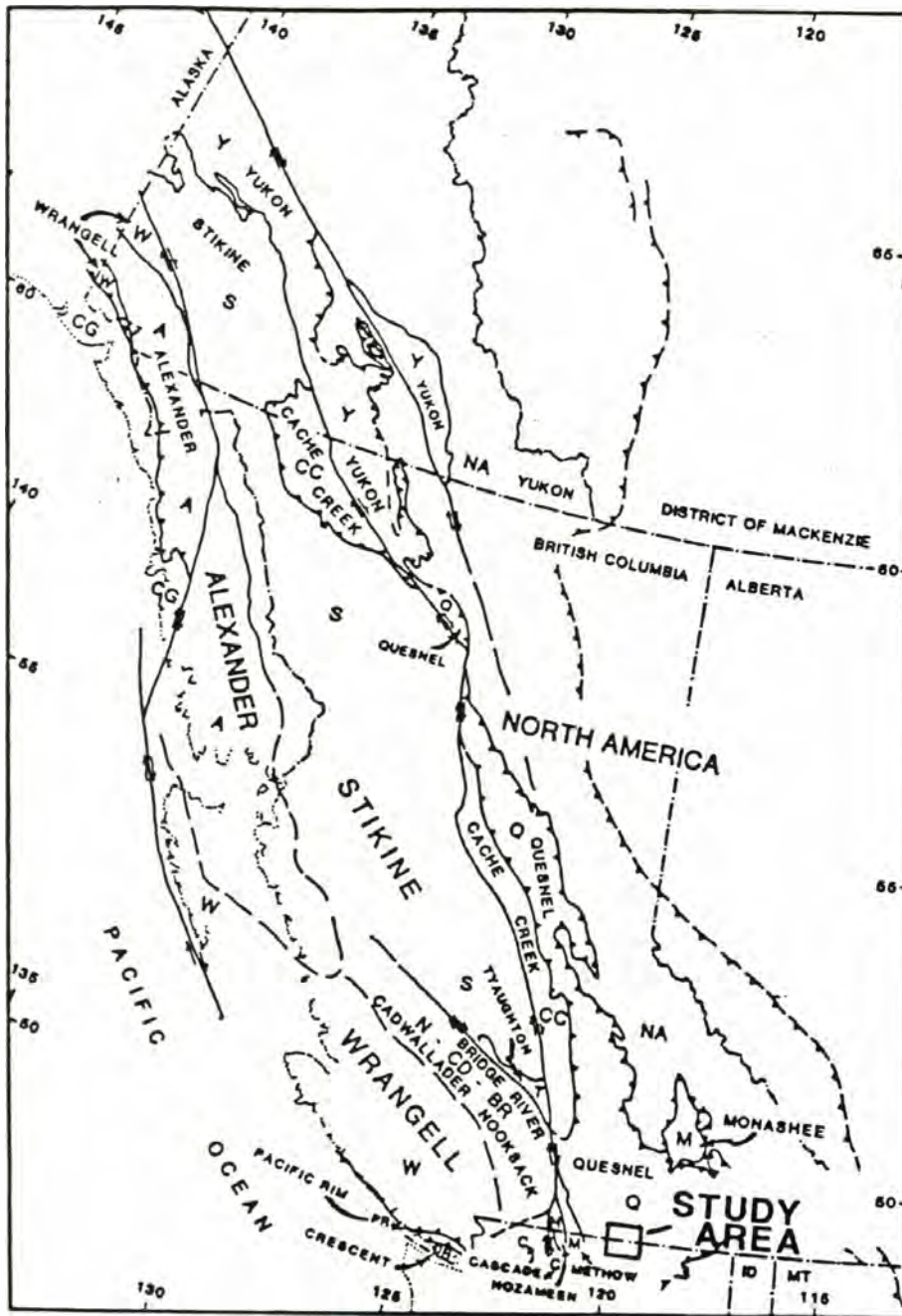


Fig. 1.1: Simplified terrane map of the Canadian Cordillera (from Armstrong, 1988; Monger and Price, 1979). The study area has been enlarged to emphasize that it is located within southcentral Quesnellia.

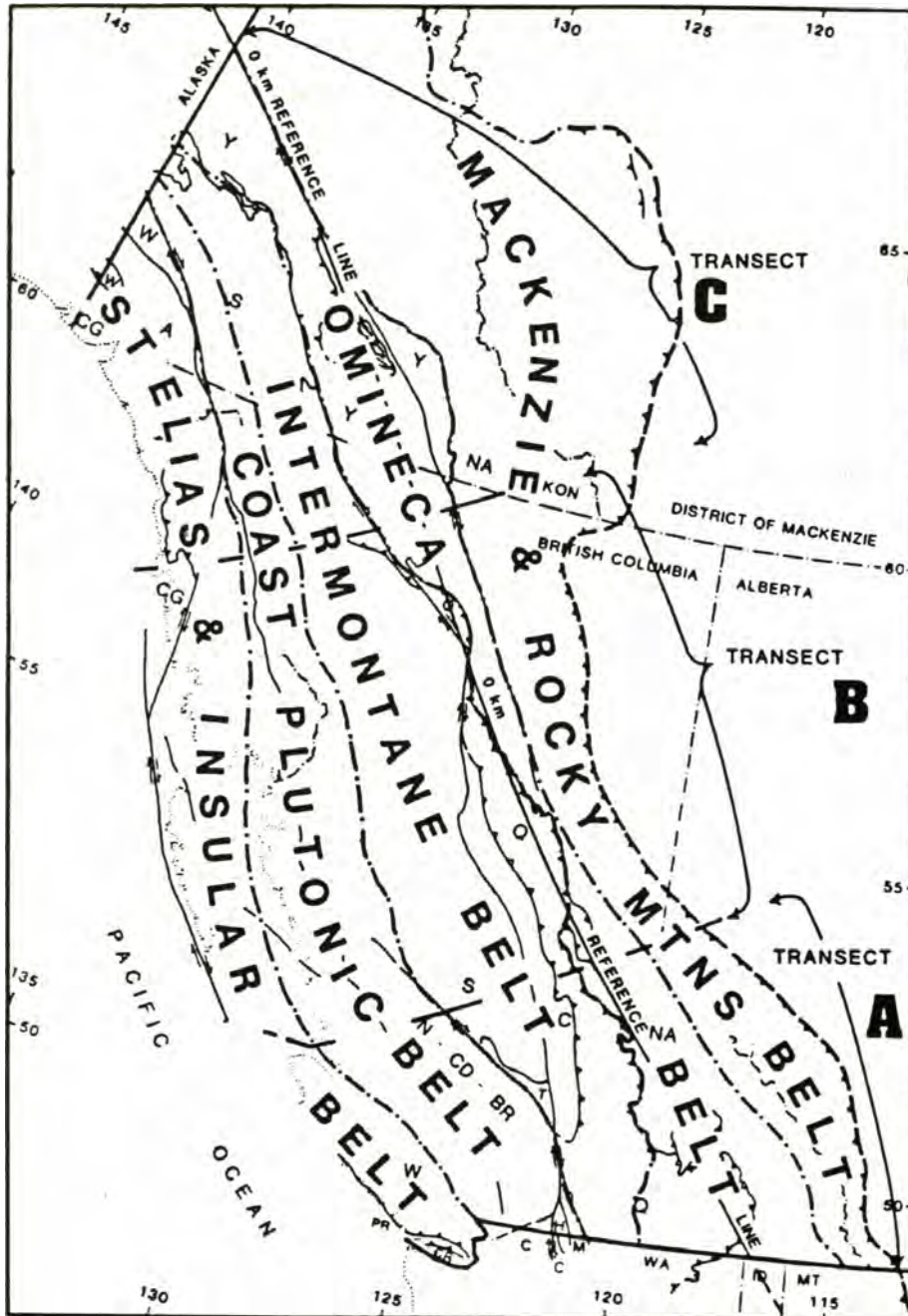


Fig. 1.2: Physiographic and tectonic belts of the Canadian Cordillera (from Armstrong, 1988).

et al. (1980), and Monger et al., (1982) (Fig.1.1). The Omineca Crystalline Belt represents a "tectonic welt", e.g., a suture zone, which consists mainly of granitic intrusions and medium to high-grade metamorphic rocks. The Omineca Belt is believed by many workers (e.g. Monger et al., 1982; Archibald et al., 1983), to have formed from Early Jurassic time onward as a result of collision and accretion of Superterrane I with the North American continental margin. Superterrane I consists mainly of four separate terranes: the Eastern, Stikinia, Cache Creek, and Quesnellia terranes. A second major collisional event between a large composite allocthonous terrane (Superterrane II) and the northwestern margin of North America is believed to have occurred in Late Jurassic to Early Cretaceous time (Monger et al., 1982). Superterrane II consisted of at least three terranes: the Wrangellia, Alexander, and Gravina terranes. Furthermore, the Coast Plutonic Complex has been proposed to be another tectonic welt contemporaneous with the second major collisional event. There is still considerable dispute as to the exact timing for amalgamation of the individual terranes. Moreover, debate rages on as to the timing of collision and the origin of the Coast Plutonic Complex. The reader is referred to Monger et al. (1982) and Armstrong (1988), for specifics on stratigraphic correlations and timing for amalgamation of the individual terranes.

The geochronology of Mesozoic plutons in southern Quesnellia has clarified the timing and role of magmatism with respect to the collision and subsequent suturing of Quesnellia to North America. Magmatism was widespread but somewhat episodic throughout the Canadian Cordillera from the Mesozoic through the Cenozoic (Armstrong, 1988). During the Late Triassic to Early Jurassic (214 to 192 Ma), magmatism was particularly concentrated in southern Quesnellia with intrusion of numerous granitic plutons, some with alkaline affinity (Copper Mountain, Iron Mask, etc.), and the development of Nicola arc (Fig. 1.1). From Middle to Late Jurassic (187 to 155 Ma), magmatism in southern Quesnellia moved eastward into the eastern portions of the Intermontane region and was extensive throughout the Omineca Belt. Numerous Middle Jurassic plutons of southeastern Quesnellia are deformed and probably were emplaced during accretion of Quesnellia to North America (Archibald et al., 1983). The peripheral phases of the Kuskanax Batholith (180-175 Ma, Parrish and Wheeler, 1983) exhibit evidence of involvement with regional deformation, suggesting it is syntectonic. More recent work on the 170 Ma Mount Hadow stock, a satellitic pluton of the Kuskanax, indicates that the stock crosscuts regional structures thus constraining regional deformation prior to 170 Ma in southeastern Quesnellia (Roback, 1990). Yet directly south of the Kuskanax, several 165-163 Ma plutons, the southern tail of the Nelson batholith, the Mount Toby stock (Gabrielse and Reesor, 1974), and the Mine stock,

(Archibald et al., 1983), have structurally concordant and deformed margins indicating late-synkinematic intrusion (Archibald et al., 1983). Early to Middle Jurassic deformed plutons represent magmatic activity synchronous and directly subsequent to the accretion and suturing of Quesnellia with North America (Monger et al., 1982; Archibald et al., 1983; Armstrong, 1988).

In southwestern Quesnellia, west of the Okanogan fault, evidence for high-grade regional metamorphism is lacking. Rocks of the Nicola Group, which unconformably overlie Permo-Triassic metasediments of the Kobau Group, are only gently deformed (Read and Okulitch, 1977). Early to Middle Jurassic plutons of southwestern Quesnellia, some of which include the Hedley Complex and the Pennask batholith, are generally undeformed. This intrusive relationship suggests three possibilities: either the central portions of Quesnellia (the Intermontane region) were relatively sheltered from the ductile deformation that southeastern Quesnellia experienced at that time; or the undeformed plutons were intruded at higher crustal levels above the zone of ductile deformation; or the undeformed Middle Jurassic plutons were emplaced after the regional deformation caused by accretion.

Location of Study Areas

Two separate study areas, the eastern and western study areas (Fig. 1.1; Plates I, II), were chosen to represent the major intrusive units of the complex. The eastern study area spans the International Boundary between the United States and Canada. South of the International Border the eastern study area is located on private and Bureau of Land Management lands within the USGS Nighthawk and Bullfrog Mountain 15' topographic quadrangles. The western study area on the US side of the border is located within the USGS Hurley Peak and Horseshoe Basin 15' topographic quadrangles. On the Canadian side of the border both the eastern and western study areas are located within the Ashnola and Okanogan Provincial Forests within the GSC Keremeos 1:50,000 topographic quadrangle.

Previous Work

The earliest work on the Similkameen-Kruger Complex was general reconnaissance mapping and lithological descriptions of rocks along the 49th parallel by Daly (1906, 1912). Daly mapped approximately 315 km² of the Similkameen batholith exposed along the International Border and described the lithology as primarily monzonite, quartz monzonite, and granodiorite. Daly also concluded that the Similkameen intruded a series of alkaline mafic rocks on the easternmost side of the

batholith. The alkaline rocks were reported to be syenites, nepheline syenites, and malignites, and occupied approximately 45 km² in area. He termed these bordering mafic alkalic rocks the Kruger Alkalic Complex after Mount Kruger, located approximately 2 km to the northeast. Daly concluded that the alkaline nature of the Kruger rocks resulted from reaction of a magma with limestone country rock at depth. Daly also recognized that the Kruger Complex intruded the metasedimentary and metavolcanic rocks of the Anarchist Series (later named the Kobau Formation by Rinehart and Fox, 1972).

Campbell (1939) mapped and carried out the first detailed petrologic study of the Kruger alkaline rocks. Following Daly, Campbell tentatively concluded that the alkaline nature of the Kruger rocks was due to limestone assimilation.

Bostock (1940) mapped the Similkameen and Kruger rocks and other associated units within the Keremeos quadrangle of the Similkameen district of British Columbia. Hibbard (1971) studied in detail the crystalline rocks of the Chopaka Mountain and Toats Coulee areas, which include granitoid phases of the Similkameen batholith. On a regional scale, Fox et al. (1977) included work on the Similkameen and Kruger rocks in his study of alkaline igneous rocks of the Northwest.

In their work on the geology of the Loomis quadrangle, Rinehart and Fox (1972) presented field and geochemical data suggesting a composite or comagmatic relationship between the Similkameen and Kruger rocks. Fox et al. (1975) presented K-Ar data on the Similkameen-Kruger rocks indicating that the age of the batholith is probably between 177 Ma and 191 Ma. Other dates include one K-Ar age (152 \pm 9 Ma: hornblende-augite) from Cannon (1966) and two K-Ar ages (biotite-hornblende: 69.9 \pm 2.1, 170.9 \pm 5.1 Ma, biotite-hornblende: 70.9 \pm 2.1, 177.2 \pm 5.3 Ma) from Engels (1971). A U-Pb age (170 \pm 2 Ma, zircon) for a Similkameen granodiorite was presented in an unpublished thesis by Parkinson (1987). Finally, an unpublished evaluation on the Horn Silver claim was written by W.A. Gewargis for Dankoe Mines Ltd. This report covers geological information and data relevant to precious metal exploration within the Horn Silver claim area. The Horn Silver Mine is located within Similkameen-Kruger syenite and was last operated by Dankoe Mines Ltd. in 1981 for Ag-Au recovery.

General Character of the Similkameen Batholith

Previous workers considered the Similkameen batholith and Kruger Alkalic Complex to be two separate entities (Daly, 1912; Campbell, 1939), but the work of Rinehart and Fox (1972) suggested geochemical and field evidence for a cogenetic relationship. The work of this thesis study supports a coincident magmatism hypothesis

rather than the cogenetic hypothesis of Rinehart and Fox (1972). Nonetheless, hereafter the term Similkameen batholith will be inclusive of the Kruger Alkalic Complex.

The Similkameen batholith is composed of two very distinctive lithologic phases. The bulk of the batholith consists of granitoid rocks of the main phase. The granitoid rocks are comprised of monzonites to granodiorites with a general increase in SiO₂ toward the interior of the batholith. The eastern portion of the main phase is dominated by a monzonitic to granodioritic pluton. Farther to the west in the interior of the main phase at least two separate plutons of quartz monzonite to granodiorite are exposed.

Concentrically bordering the main phase units on the easternmost side of the batholith are the alkaline marginal mafic phases. The marginal phases pinch out farther to the northwest and southwest away from the eastern boundary of the batholith (Fig. 1.3, Plates I, II). The marginal phase units consist of a variety of pyroxenites, malignites, and shonkinites which grade inward to mafic syenite. In general, within the marginal phase units, SiO₂ content increases inward toward the interior phases.

Purpose and Scope

The Similkameen batholith was chosen for study because the coexistence of alkaline and calc-alkaline igneous rocks is relatively uncommon in plutonic environments and the generation of these magma types together is poorly understood. Another reason for studying the Similkameen is its proximity to a possible suture zone. A better understanding of the origin of the magmas that make up the batholith should lead to a better understanding of the tectonic conditions in which the magmas formed.

The primary objectives of this study were to: (1) map and describe the intrusive relations of the individual units within the complex, (2) interpret the origin of fabrics within the intrusive units and the relationships of fabrics to emplacement and/or regional tectonism, (3) establish the petrologic relations of the intrusive phases, and (4) determine the petrotectonic environment and develop a model for the origin, evolution, and emplacement of the magmas.

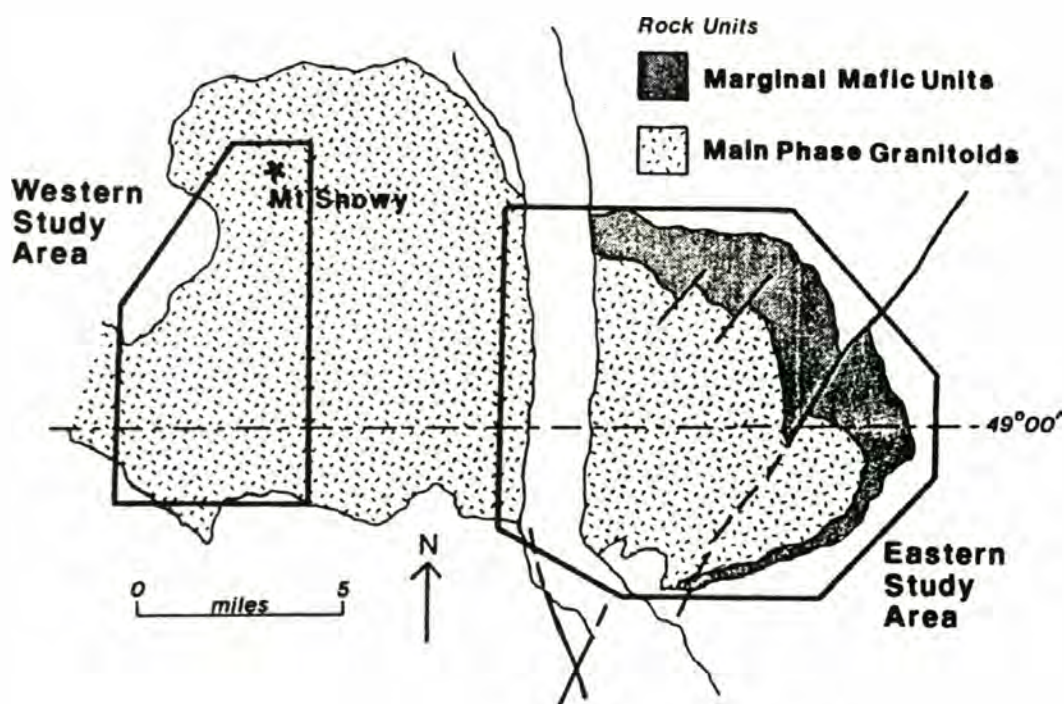


Fig. 1.3: Generalized geologic map of the Similkameen batholith showing the eastern and western study areas.

Methods: Field and Laboratory Work

Fieldwork for this project was conducted during the 1987, 1988, and 1989 field seasons. A total of 60 days was spent working in the field. The majority of the time was spent mapping contacts at a scale of 1:24,000 on USGS quads and 1:50,000 on GSC quads. Simultaneously, emphasis was placed on the collection of suitable samples for petrologic and geochemical analysis. Samples of country rock were representative of the general lithology and metamorphic grades. A total of 264 samples of plutonic, volcanic, and metamorphic rock was collected during the three field seasons, and all samples were sectioned for petrographic analysis.

Modes were determined by point counting slabs etched with HF and stained for potassium feldspar using sodium cobaltinitrite and for plagioclase feldspar using BaCl₂ and amaranth dye. On selected samples, feldspathoids were stained using phosphoric acid and methylene blue. Between 1000 to 1500 points were counted to determine modal percentages of potassium feldspar, plagioclase, quartz, mafics, and feldspathoids. Spacings of 2.0 mm were used for coarse-grained samples and 1.0 mm for medium-grained samples.

Plagioclase compositions were determined by the a-normal method using Rittman's low temperature, plutonic rock curve (Deer et al., 1983). Polished thin sections of six samples were analyzed for plagioclase, pyroxene, amphibole, garnet, and magnetite. Mineral compositions were determined using a Camebax microprobe at the Grant Institute of Geology, University of Edinburgh, by Professor R.S. Babcock. Whole rock major and trace element analyses were performed on 50 representative samples using a Phillips XRF at the Grant Institute of Geology, University of Edinburgh, by Dr. R.S. Babcock and Dodie James. Rb/Sr isotope analyses using a Vacuum-Generators Isomass 54R mass spectrometer were done on 24 samples at the University of British Columbia by the author under supervision of Dr. R.L. Armstrong and Dita Runkle. Details for geochemical and isotopic analytical procedure are given in Appendix B.

CHAPTER II

STRUCTURAL AND PETROFABRIC INTERPRETATION FOR EMPLACEMENT OF THE SIMILKAMEEN BATHOLITH

Introduction

Structural and petrofabric relations in plutonic complexes that reflect the style of intrusion and the mode of emplacement can be used to determine relative ages of pluton emplacement and regional deformational events (Paterson & Tobisch, 1989). In this study we have examined the intrusive relations between the 170 Ma (see Chapters 1 & 3) Similkameen batholith and the surrounding Permo-Triassic rocks of the Kobau Formation in an attempt to understand the emplacement history of the batholith and to constrain the Jurassic deformational history of this portion of southern Quesnellia. Within the Similkameen, later fabrics present indicate a continuum between purely magmatic flow and submagmatic flow. This study utilized detailed petrographic analysis as well as field observation and anisotropy of magnetic susceptibility to distinguish the style of emplacement and the relationships among the fabrics observed.

Geologic Framework

The Similkameen batholith, located in south-central Quesnellia, intrudes Permo-Triassic metamorphic rocks of the Kobau Group (Fig. 2.1, 2.2). In the study area, the Kobau consists of chert, basalt, and pelitic rocks of Permian to Triassic age that have undergone multiphase deformation and greenschist facies regional metamorphism (Rinehart and Fox, 1972). The first major deformation consisted of two periods of folding accompanied by greenschist facies metamorphism (Archibald et al., 1983; Read and Okulitch, 1977). The Chopaka Intrusive Complex that intruded the Kobau rocks has been interpreted as synkinematic with respect to the greenschist facies regional event (Hibbard, 1971). Hibbard (1971) reported a K-Ar date of 190.5 +/-15.6 Ma on actinolite from the Chopaka, but this may be too young because of Ar loss during intrusion by the nearby Loomis pluton (194 Ma). Deformation and regional metamorphism is more likely to be Early Triassic (Read and Okulitch, 1977). An Early Triassic age for metamorphism would correlate with the regional angular unconformity of southern British Columbia described by Read and Okulitch (1977).

Near the study area at Shankers Bend, Rinehart and Fox (1972) described an unconformity between the Kobau metasediments and the overlying Ellemeham Formation. The rocks of the Ellemeham Formation, a sequence of greenstones and

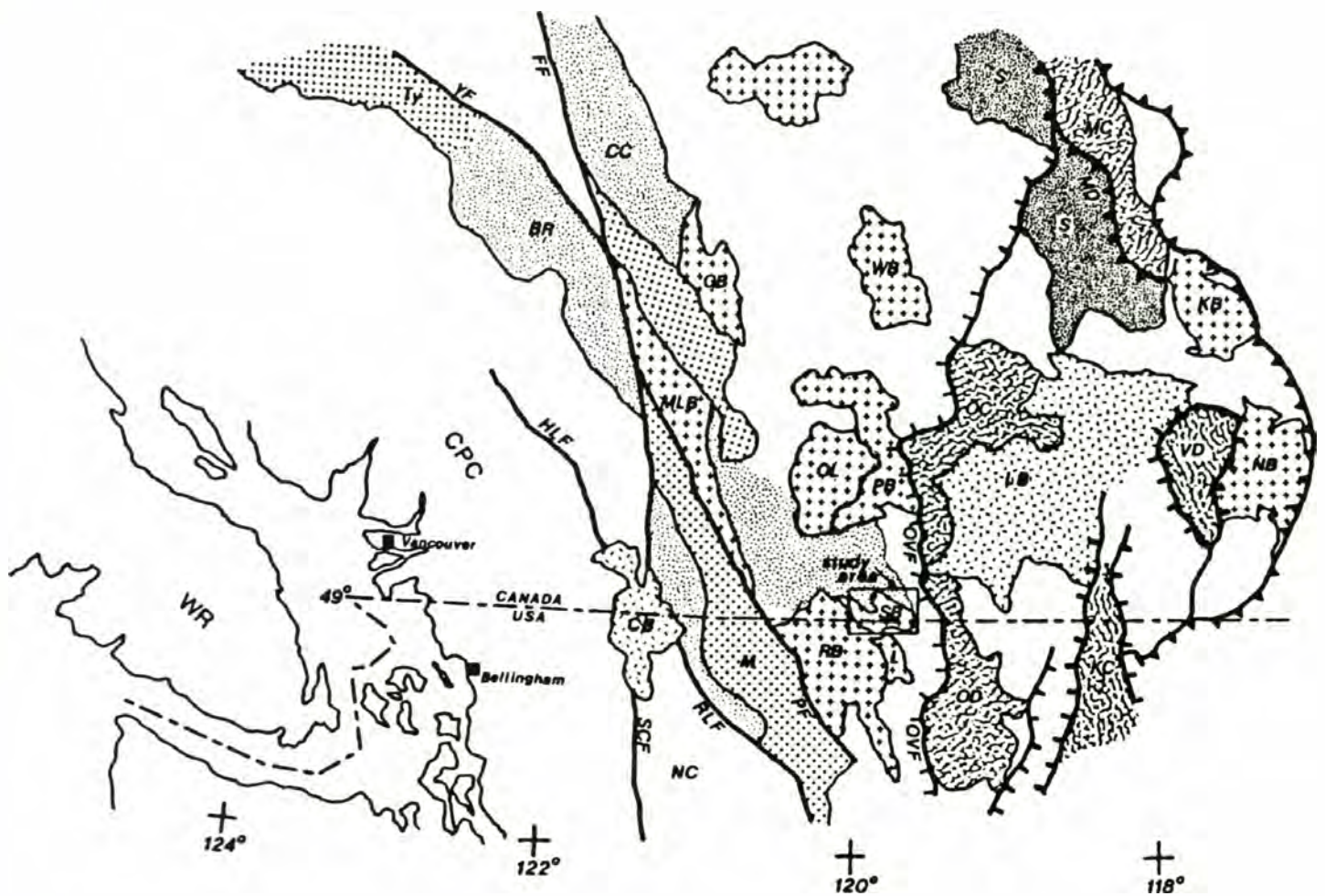


Fig. 2.1: Generalized geologic map of southcentral British Columbia and northcentral Washington. Fraser fault (FF), Yalakom fault (YF), Harrison Lake fault (HLF), Ross Lake fault (RLF), Straight Creek fault (SF), Pasayten fault (PF), Okanogan Valley fault (OVF), Monashee decollement (MD), Okanogan Dome (OD), Okanogan Complex (OC), Kettle Complex (KC), Valhalla Dome (VD), Monashee Complex (MC), Mount Lytton batholith (MLB), Similkameen batholith (SB), Pennask batholith (PB), Rimmel batholith (RB), Kuskanax batholith (KB), Nelson batholith (NB), Shuswap terrane (S), Cache Creek terrane (CC).

tuffaceous siltstones to conglomerates, are only moderately warped and are less metamorphosed than the underlying Kobau. Rinehart and Fox proposed that perhaps metamorphism of the Ellemeham Formation was related to the intrusion of the Similkameen batholith because mafic alkalic rocks similar to those of the border phase of the Similkameen intruded and metamorphosed the Ellemeham near Shankers Bend. Nonetheless, the Ellemeham is older than the Similkameen, being pre-Middle Jurassic, but younger than the metamorphism to which the underlying Kobau rocks were subjected. Read and Okulitch (1977) considered the unconformity between the Kobau and Ellemeham rocks to be correlative with the Early Triassic unconformity between the Kobau and Nicola Groups of British Columbia. Hence, the Ellemeham may be correlative with the Nicola Group.

By Jurassic time, deformation, high-grade metamorphism, and plutonism in the Shuswap and Kootenay Arc regions (Okulitch, 1984; Armstrong, 1988) was well established. Plutonism continued in southern British Columbia until about 155 Ma and was followed by a period of relative magmatic quiescence (Armstrong, 1988).

In many parts of central and eastern British Columbia, Jurassic metamorphic ages were reset by widespread early Cenezoic magmatism and an associated high geothermal gradient (Armstrong, 1988). Crustal extension and high rates of uplift resulted in the development of large low-angle faults and tectonic unroofing of the many scattered metamorphic core complexes. The Kobau country rocks surrounding the Similkameen batholith are part of the upper plate of the Okanogan Valley fault, which is the low-angle detachment fault forming the western boundary of the Okanogan Dome core complex.

Regional Structure

The batholith is elongate NW-SE, roughly parallel to the axis of the Whisky Mountain anticline (Fig.2.2). Northeast of the batholith, the dominant structure is a broad syncline whose northern limbs make up the steeply-dipping units of the Kobau Group metavolcanics on the flanks of Mount Kobau. In general, the Similkameen batholith trends sub-parallel to the overall NW-SE trending structural grain of the region but crosscuts the grain locally, particularly in the northwest and southeast portions of the batholith (see below).

Foliation within the metamorphic country rocks parallels bedding and dips steeply (50°- 90°). The dip of country rock foliation steepens toward the batholith. This steepening and local overturning of beds along the southeast border have been attributed to forceful injection (Rinehart & Fox, 1972).

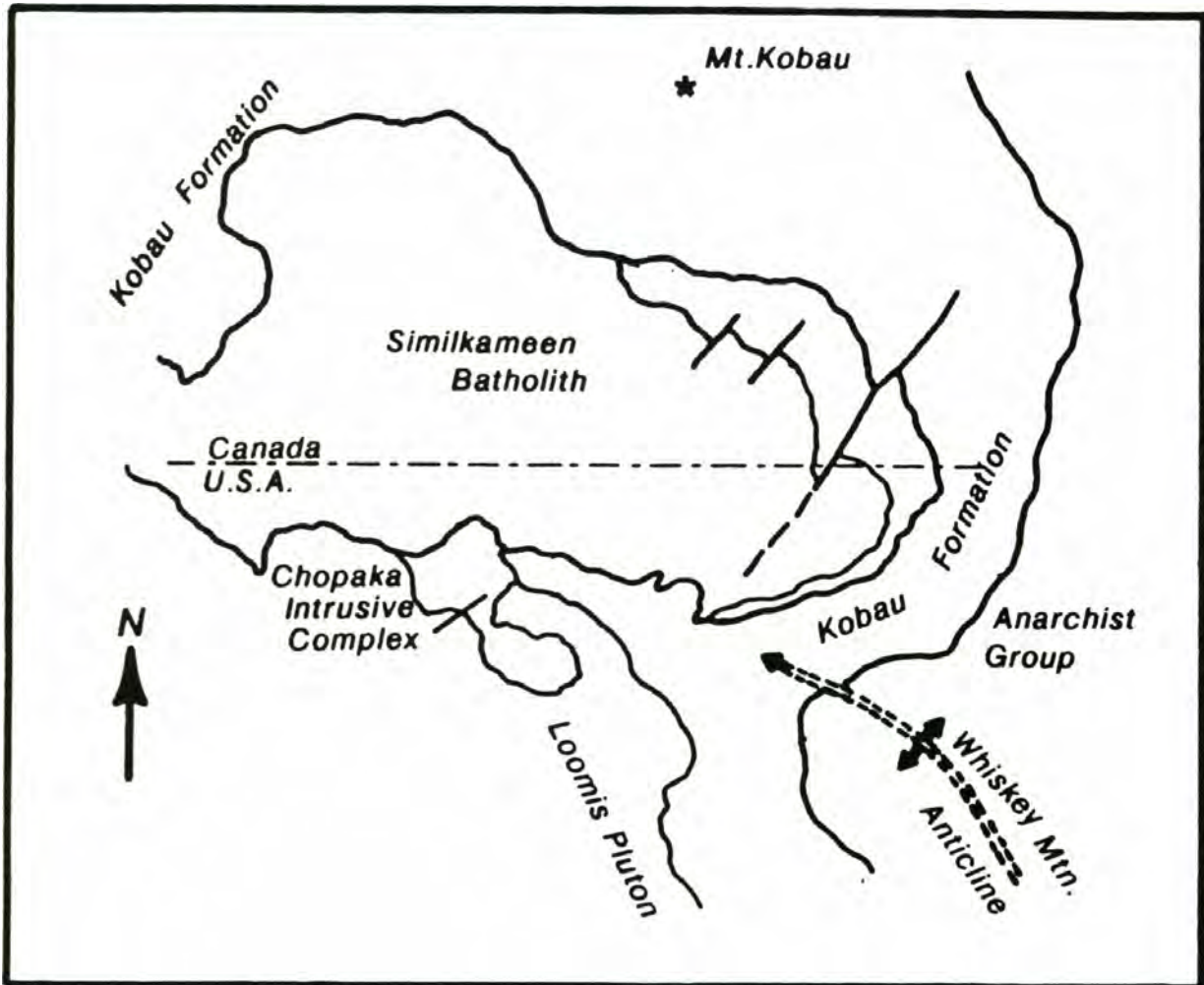


Fig. 2.2: Simplified geologic map of the Similkameen batholith and the associated country rocks.

Contact & Porphyroblast Relations

The contact aureole surrounding the batholith is a relatively narrow (< 100 m), ill-defined zone of weakly hornfelsed Kobau Formation. The intrusive contacts between the batholith and the country rocks are, in all places observed, sharp with little or no physical interaction. In the northwest, contacts between the granitic rocks and metacherts of the Kobau are sharp with small apophyses of granitic material intruded along bedding planes. In the southeastern portions, contacts between the marginal mafic phase and the country rocks are not exposed and xenoliths of country rock material are lacking. Garnets in metapelitic units of the Kobau directly adjacent to contact margins show rotation and have been substantially deformed after their initial growth, indicating that they are pre- to synkinematic (Fig. 2.3). In other locations within the bedded chert units, garnets with biotites along bedding planes exhibit no evidence of rotation or postkinematic deformation. It appears that the deformed garnets were associated with the regional deformation that resulted in the widespread greenschist facies metamorphism of the Kobau Formation whereas the undeformed garnets within the aureole may represent the contact assemblage. In other areas within the aureole, oriented amphiboles that define the pre-existing regional metamorphic foliation are pseudomorphed by non-oriented biotite (Fig. 2.4). This pseudomorph relationship is not seen regionally so it is thought to be a contact metamorphic effect.

Admittedly this study lacks a detailed fabric and structural examination of the Kobau rocks with respect to the contact aureole of the batholith. Porphyroblast relations within the aureole are difficult to establish unequivocally because the aureole is so weakly developed.

The lack of well-developed contact aureoles is common among moderate to deeper level plutons and based on geobarometric considerations, depth of emplacement for the Similkameen batholith was approximately 10 km. Microprobe analyses on igneous hornblende from a main phase granodiorite give pressure estimates for amphibole equilibration ranging from 2.7 to 3.2 Kb (Johnson and Rutherford, 1989) which correlate approximately to depths between 8.1 and 10.8km.

The depth of final emplacement for the batholith may explain the lack of a well-developed contact aureole, but nonetheless, a consistent fabric relationship has been noted in which the country rocks do exhibit multiphase deformation in agreement with Read and Okulitch (1977) for similar rocks observed near Olalla. The final deformation and recrystallization recorded within the Kobau rocks adjacent the batholith, i.e., the overturning of beds and pseudomorphed mineral assemblages, was the result of intrusive

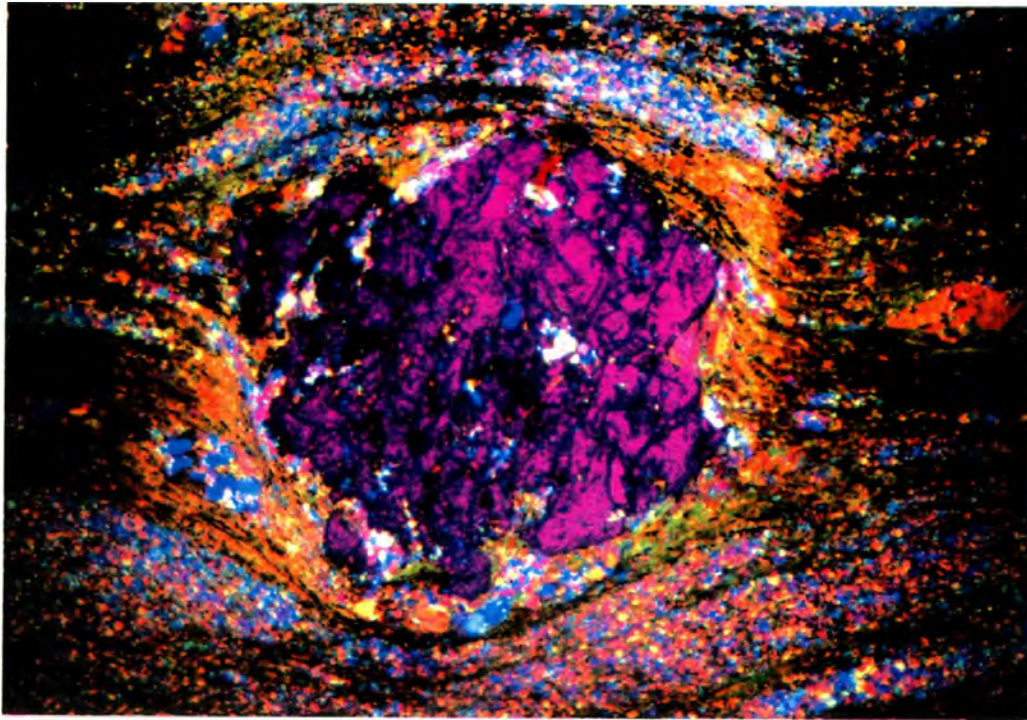


Fig. 2.3: Photomicrograph of garnet in a pelitic schist adjacent to the contact with the Similkameen batholith (xpl with the accessory plate in). The garnet is broken indicating a pre- to synkinematic relationship to the regional fabric. Field of view width is 5 mm.

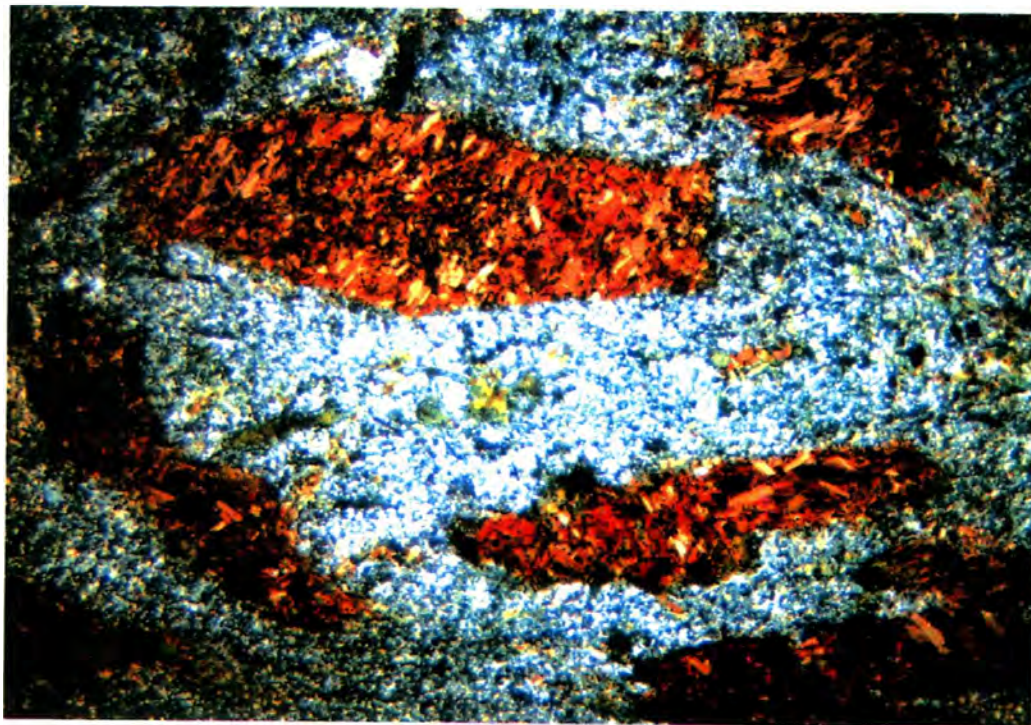


Fig. 2.4: Photomicrograph of randomly oriented biotites pseudomorphed after foliated amphibole within the contact aureole of the batholith.

shouldering and contact thermal metamorphism synchronous with the emplacement of the batholith.

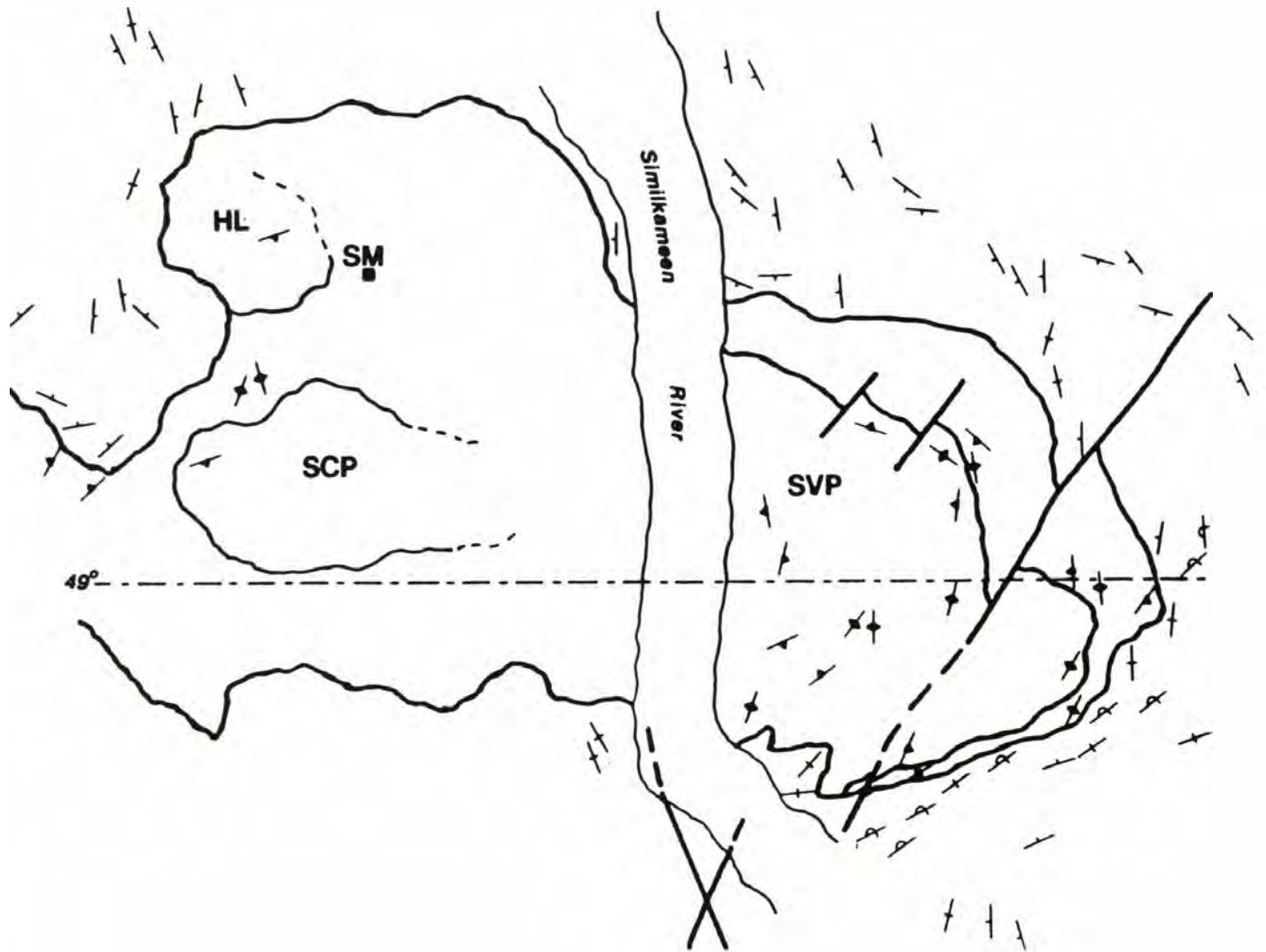
Internal Structure of the Batholith

The eastern end of the batholith is concentrically zoned both compositionally and texturally. The outer portion consists of a suite of marginal mafic (alkaline) rocks, the outermost unit in the SE portion of the batholith being a highly deformed shonkinite to syenite gneiss. Inward, pyroxenitic rocks grade irregularly to malignites and shonkinites which in turn grade inward to mafic nepheline syenite and syenite. Although the specific compositions vary on different radial traverses, there is a consistent overall zonation from very SiO₂-undersaturated (quartz absent) rocks along the margins to SiO₂-saturated rocks inward.

The main phase of the batholith is composed of at least three monzonitic to granodioritic plutons. Within the eastern portion of the complex (Fig. 2.5), the main phase is dominated by one plutonic unit (Similkameen Valley pluton), which has a general compositional zonation with monzonites along the outermost portions gradational to quartz monzonite and eventually granodiorite toward the interior. The central and western portions of the batholith are composed of several individual plutonic bodies (Fig. 2.5), which obscure compositional zonation. Nevertheless there is a general zonation with more SiO₂-rich rocks (granodiorites of the Harry Lake and Snowy Mtn. area) occupying the western portion of the batholith.

Textural zonation is apparent as variations in the intensity of fabric development observed in the field and as deformational style observed in thin section. Fabric zonation is consistent with the concentric compositional zonations observed. In general, the outermost units have the most intense fabric development. There, lineations are recognizable in the syenitic gneisses as elongate biotite aggregates and in the malignites as elongate pseudoleucite megacrysts. Inward, fabric development lessens, with only foliations mappable, except in the nearly isotropic interior main phases. Local departures of fabric attitude, (for example, the pyroxenites appear nearly isotropic in the field) will be discussed in a later section.

Foliations within the outer marginal mafic phases, except for the pyroxenites, are well developed and consistently concordant with the overall contacts of the batholith and the concentric lithologic zonations (Fig. 2.5). The majority of foliations in the marginal phases dip steeply inward (>50° to vertically). Some scattered, small areas contain less steeply dipping foliations. Foliations become less pronounced with higher felsic mineral content. In the main phase granitic rocks, foliations are most easily recognized near



Fig; 2.5: Generalized structural map of the Similkameen batholith showing mapped country rock and igneous foliations. Similkameen Valley pluton (SVP), Snehumpton Creek pluton (SCP), Snowy Mountain (SM).

contacts with the marginal mafic phases or at internal contacts where mafic mineral layers or schlieren are concentrated. Foliations within the contact zones of the main phase granitic rocks are consistently steeply dipping to vertical and parallel to the strike of the contacts.

Anisotropy of Magnetic Susceptibility: Magnetic Fabrics

Introduction

Anisotropy of magnetic susceptibility (AMS) data, i.e., the magnetic fabric, allows for qualitative structural and strain analysis (Henry, 1988). AMS has been shown to accurately predict foliation and lineation directions even where structures are difficult to measure in the field (Cogne and Perroud, 1988). AMS data has also been used to deduce the contribution of contemporary or later regional deformation (Brun and Pons, 1981; Cogne and Perroud, 1988). The magnetic fabric has been measured for representative units from the southeastern portions of the batholith.

Augmenting petrographic fabrics with AMS data allowed for further petrofabric interpretations: 1) fabric analysis was extended into the interior of the Similkameen Valley pluton where fabrics are too poorly developed to measure with confidence, 2) measure elongation directions (lineations) in rocks where lack of suitable foliation surfaces or poor development of mineral lineations made petrographic measurement unreliable, and 3) gain a semiquantitative impression of intensity of fabric development or strain.

The AMS ellipsoid axes represent the directions of greatest, intermediate, and least (K_1, K_2, K_3) magnetic susceptibility within a given sample. The axial ratios K_1/K_2 and K_2/K_3 give a measure of the intensity of the magnetic lineations and foliations respectively. By plotting the axial ratios, it is possible to express the shape and intensity parameters of the susceptibility ellipsoid. The data may be plotted on a corresponding map thus illustrating both the magnetic foliations and lineations or plotted on a Flinn diagram which allows for the characterization of the AMS ellipsoid.

Discussion

A strong correlation exists between visible mapped field fabrics and the magnetic fabrics. All measured magnetic foliations for the batholith dip steeply parallel to lithologic contacts (Fig. 2.6) consistent with the concentric lithologic zonations. The plunge of magnetic lineations varies systematically with location. In the marginal units the plunge of magnetic lineations is consistently steep and nearly downdip of the

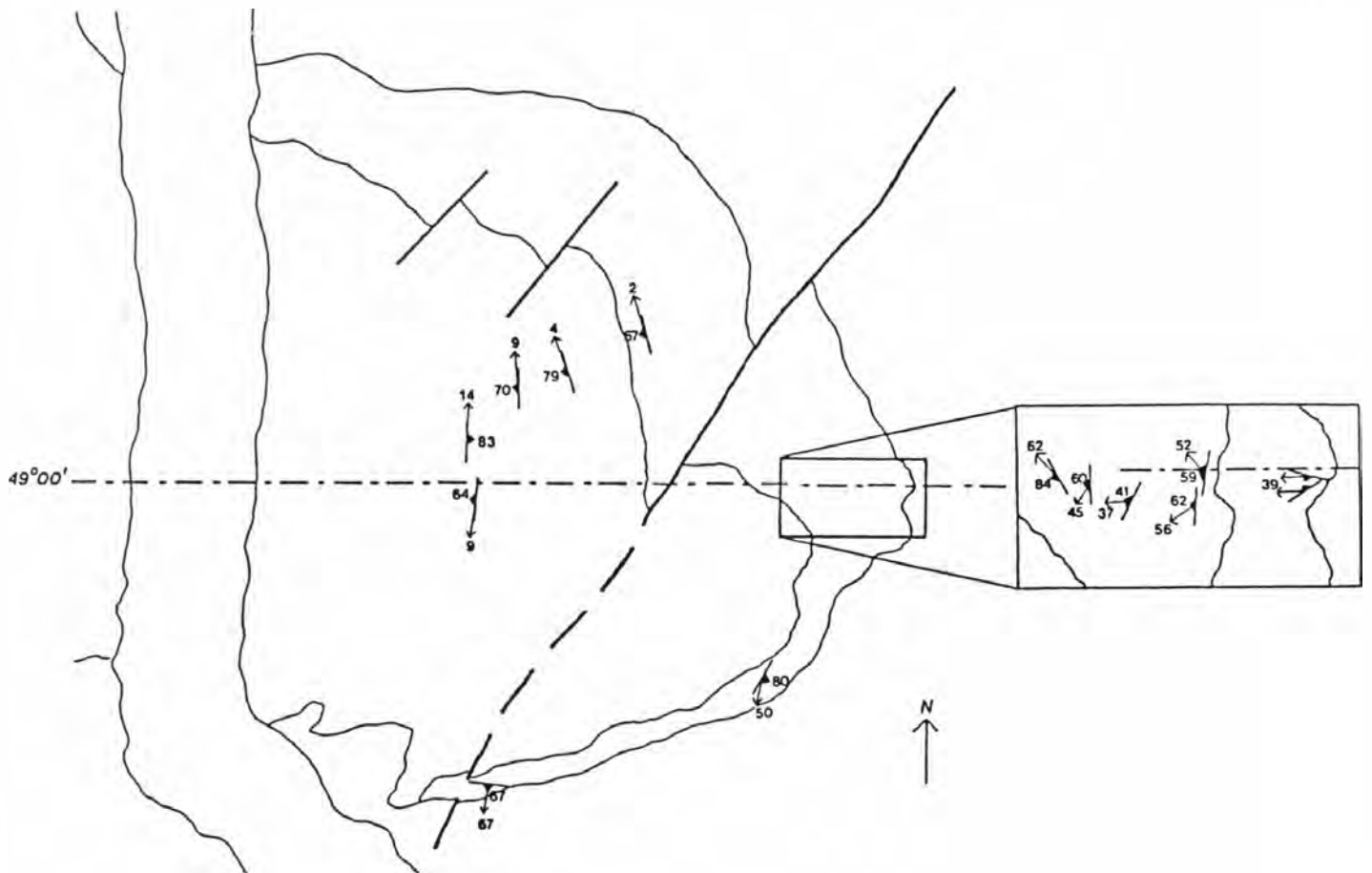


Fig. 2.6: Map of magnetic fabrics within the eastern portions of the batholith. Strike symbols refer to the plane of maximum susceptibility. Arrows indicate direction of maximum susceptibility.

foliations; plunge in the interior granitoids is shallow (Fig. 2.6). Two important relationships are revealed in a Flinn plot of the mean anisotropy of magnetic susceptibility data (Fig. 2.7). All samples show apparent flattening, with strain increasing from the inner quartz monzonite to the marginal alkaline rocks. This increasing strain correlates well with the visible increase in intensity of foliation.

Petrofabrics

Microstructural analysis has revealed two distinctive styles of fabric. In the gneissic rocks of the outer portions of the batholith, submagmatic flow fabrics overprint earlier magmatic flow fabrics. Inward of the gneissic rocks, the shonkinites, malignites, and mafic syenites are dominated by magmatic flow fabrics but some exhibit late-stage fluid relocation textures (Hibbard, 1987). The late-stage relocation textures are indicative of the transition from magmatic to submagmatic flow deformation (Paterson et al., 1989). The interior granitic rocks are characterized by magmatic flow fabrics with only minor sub-solidus deformation, e.g., glide and deformation twinning.

Submagmatic Deformational Flow Fabrics

The gneissic rocks exhibit the most intense fabric development of all the units observed throughout the Similkameen complex. In outcrop this unit shows a distinctive pervasive fine to medium grained gneissic texture; foliations are defined by alternating biotite-rich and microcline-rich layers (Fig. 2.8). The mafic-rich layers commonly contain zones rich in melanite garnet.

In thin section, foliation is defined by the strong alignment of twin planes in microcline and layers rich in oriented biotite intergrown with ovoid clots of garnet (Fig. 2.9). Minor recrystallization has produced fine-grained plagioclase and alkali feldspar along the margins and at the ends of primary feldspar grains. Clinopyroxenes have been replaced by garnet and biotite; primary plagioclases having been completely replaced by sericite and epidote.

Transitional Fabrics

The transitional fabrics are indicative of crystal-liquid deformation but display little or no evidence of recrystallization. Many of the mafic rocks within the marginal zones exhibit microstructures that are consistent with this relationship.

The malignites are characterized by megacrysts (0.5-5.0 cm) of pseudoleucite, which typically are deformed from what was presumed their original icositetrahedral

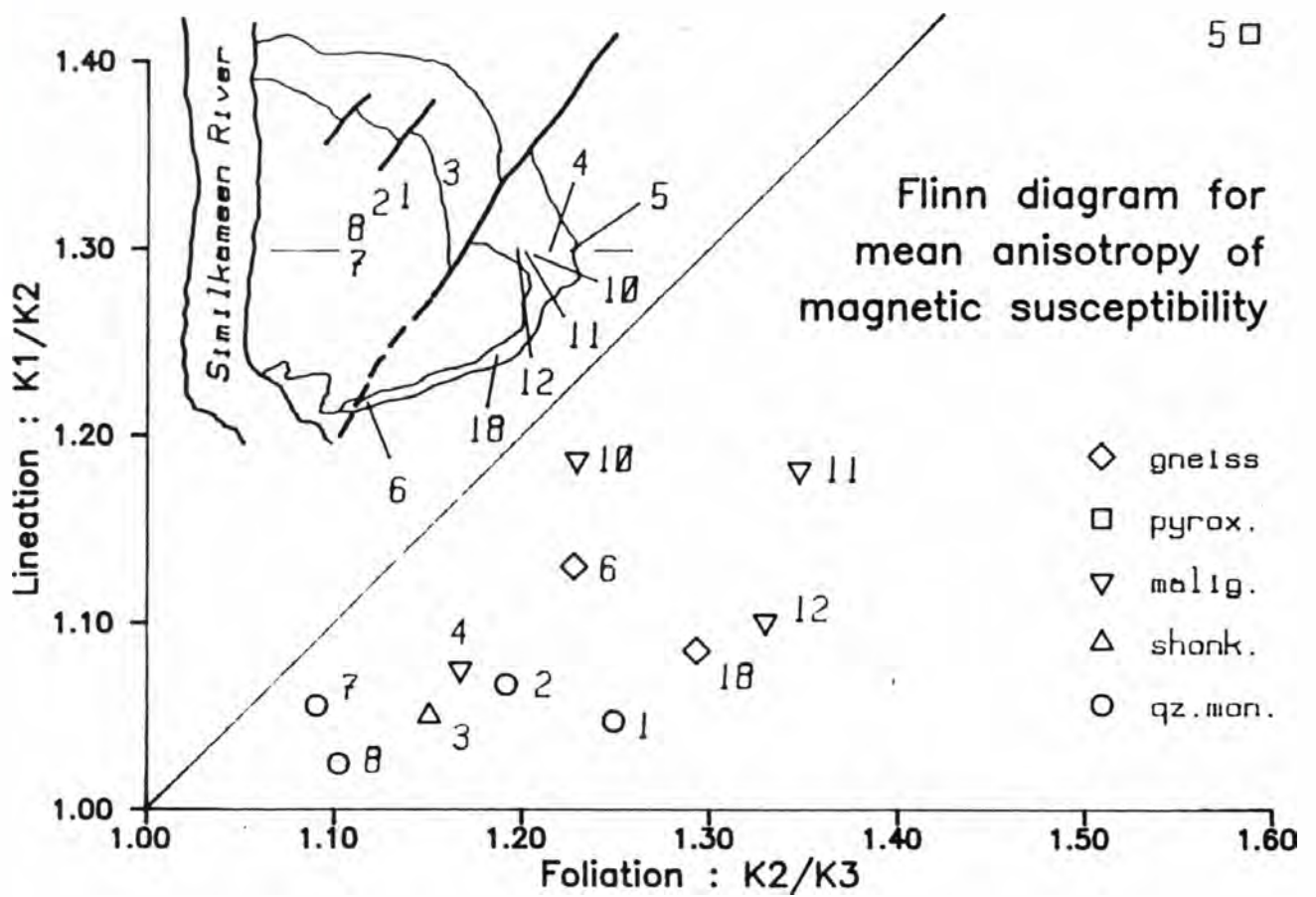


Fig. 2.7: Flinn plot of mean susceptibility values from the Similkameen batholith.



Fig. 2.8: Hand sample of a medium-grained gneissic syenite.

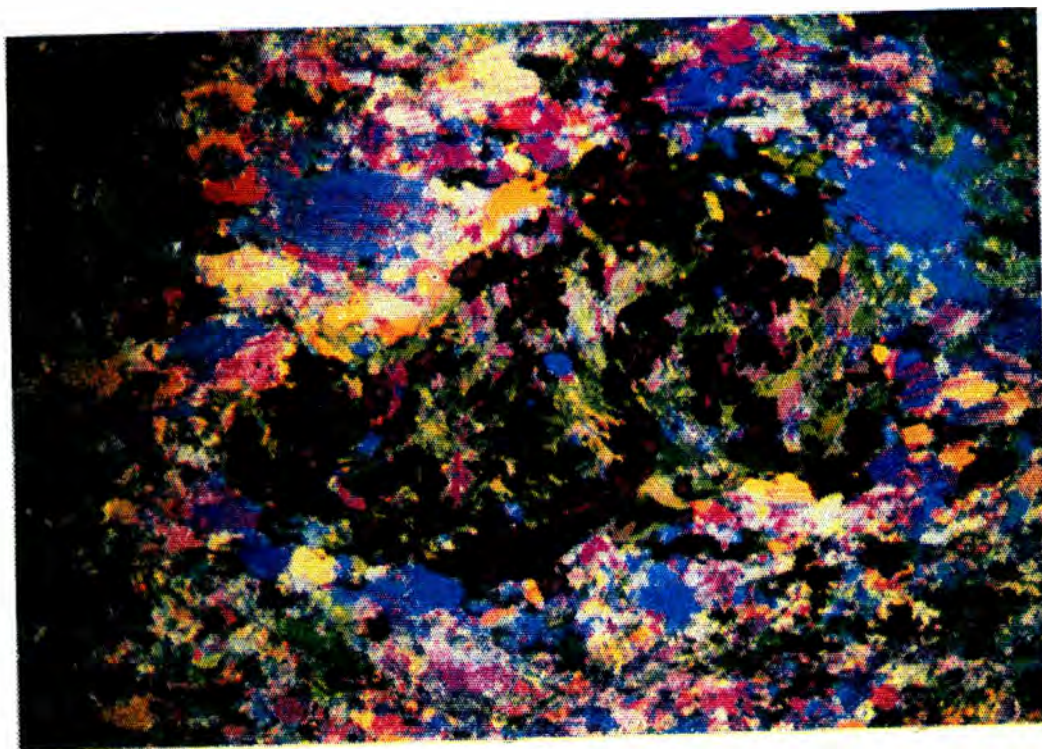


Fig. 2.9: Photomicrograph of gneissic syenite (xpl with accessory plate in). Note the alignment of feldspar twin planes with recrystallized feldspar around the margins of primary feldspar (subhedral) grains. Garnet (red-brown) is subhedral with biotite replacing primary clinopyroxene. Field of view width is 5 mm.

form (Fig. 2.10). These megacrysts with the groundmass of euhedral clinopyroxene and interstitial microcline define the foliation within the rock.

The shonkinites commonly contain ovoid-shaped megacrysts of microcline in a groundmass of aligned euhedral clinopyroxene, amphibole, and microcline. In thin section, both the shonkinites and malignites reveal fractured and bent microcline laths with deformation twinning. A fine-grained polygranular mosaic of plagioclase with minor amounts of microcline fills fractures and interstices between the primary magmatic grains (Fig. 2.11). This fine grained mosaic, similar to that described as microaplite by Hibbard (1987), is interpreted to represent a late-stage fluid relocation texture (see below).

Magmatic Flow Fabrics

Mafic syenite with an unmistakable trachytoid fabric commonly occurs as small unmappable pods between the granitic rocks and the shonkinites. This coarse-grained porphyritic rock contains a trachytoid alignment of euhedral microcline megacrysts (3.0-10.0 cm length) in a foliated groundmass of augite, amphibole, and microcline (Fig. 2.12). The megacrysts exhibit spectacular zoning with small oriented euhedral inclusions of plagioclase within the microcline. Microaplite, similar to that described above, is present surrounding primary groundmass minerals but it is not as prevalent as in the shonkinites.

Within the interior granitic rocks, deformation fabrics are poorly developed except near contact margins. Near contacts, schlieren and adcumulate segregations commonly define a foliation of aligned clinopyroxene, amphibole and elongate mafic enclaves. Magmatic flow is evident at contact margins where foliated autoliths of mafic syenite have been engulfed by main phase monzonite. Both the autoliths and the host monzonite are foliated but in one example the fabrics are not parallel to one another. Furthermore, the foliation within the host is refracted about the inclusions indicating rotation of the inclusions and subsequent flow of the host magma around the autoliths (Fig. 2.13).

Microscopically the alignment of elongate grains is conspicuous. Bent feldspar twins, kinked biotite, glide twins in titanite, and undulose aggregates of sutured quartz indicate that strain continued under solid-state conditions, but these indicators are minor to the dominant magmatic flow fabrics.

Discussion of Crystallization and Textural Zonation

Geochemical data indicate that the marginal mafic phases and the main phase granitoids represent separate distinct intrusions, possibly from different source materials



Fig. 2.10: Outcrop photograph of pseudoleucite-bearing malignite. Note that the pseudoleucite megacrysts (white) are elongate; deformed within the foliation plane.

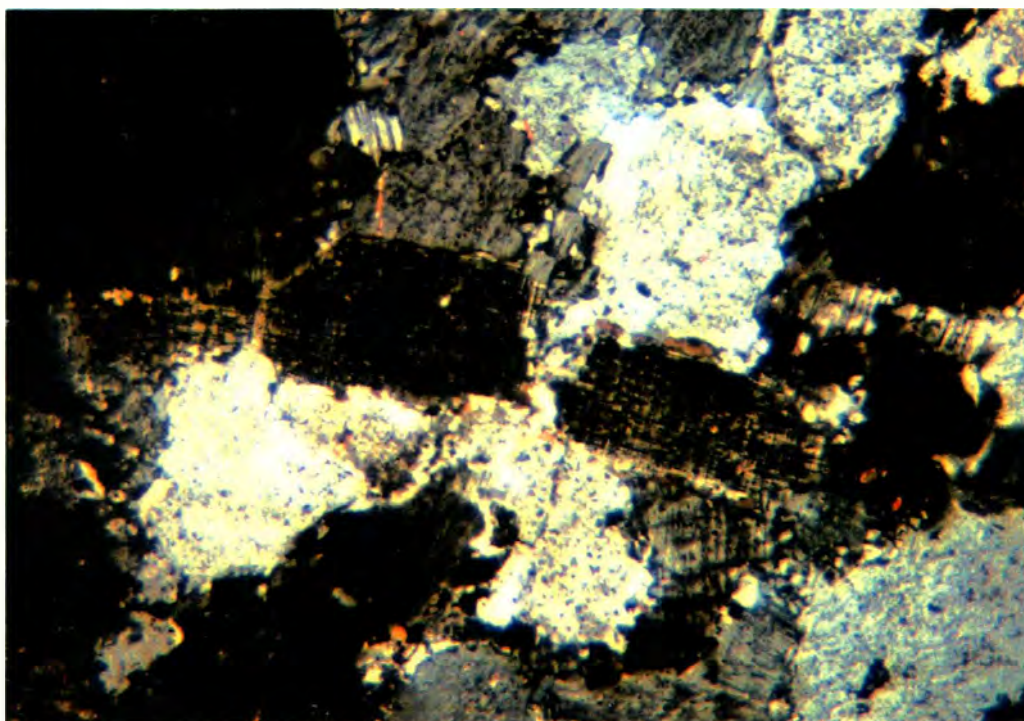


Fig. 2.11: Photomicrograph of fluid relocation texture within a shonkinite (xpl). Note the broken microcline grain with fine-grained feldspar (late-stage fluid) surrounding and filling in the fracture. Field of view width is 5 mm.



Fig. 2.12: Magmatic flow fabric within a mafic syenite. Note the trachytoid alignment of microcline megacrysts. The matrix is composed primarily of clinopyroxene and amphibole.



Fig. 2.13: Autolith of mafic syenite within a flow-foliated monzonite host. Note that the foliation of the host wraps around the autolith and that the foliations of the autolith and monzonite are not parallel.

(see Chapter 3). Nonetheless, Rb-Sr whole rock isotopic analyses of 22 lithologically different samples (Chapter 3) from within the complex and the textural evidence cited above indicate that the separate intrusive phases were closely associated in both space and time during final emplacement.

The earliest crystallizing phases were the marginal mafic phases of the southeast portion of the batholith. Contacts between individual units are characteristically gradational, particularly between the pyroxenites and the shonkinitic rocks. Only one outcrop was observed in which shonkinitic rocks crosscut gneissic rocks; elsewhere this contact is not exposed.

Contacts between the marginal mafic phases and the granitic rocks of the core are sharp to gradational. In several locations shonkinite grades through more felsic-rich material into monzonite with intermittent schlieren of mafic adcumulates. In some contact zones autoliths of shonkinite, some as large as 50 meters in length, occur within the granitoids. Dikes of undeformed alaskite, assumed to be a late-stage differentiated component from the granitic rocks, extend from within the granitic rocks and cut across contacts into the mafic rocks. Intrusive breccias composed of angular blocks of shonkinite or pyroxenite are completely engulfed in a medium-grained matrix of alaskite along some contact margins between the mafic rocks and granites.

The emplacement of the marginal mafic phases was followed by the intrusion of the main phase granitoids. Sharp, crosscutting contacts support this conclusion, but the existence of gradational contacts between the main phase granitoids and marginal mafic units sporadically throughout the complex indicates a close association between the main phase rocks and the marginal alkalic rocks.

The earliest intruded phases, the outermost syenite gneissic units, were originally syenitic to shonkinitic magmas that were later deformed by the intrusion of interior phases such as the malignites and shonkinites. The pervasive gneissic fabrics are interpreted to have originated from magmatic flow. The well developed banding indicates mineral segregation during an intense flow regime. Although primary igneous textures, e.g., subhedral prismatic aligned microcline, are dominant in the gneissic rocks, microstructural evidence indicates that minor recrystallization of feldspar occurred around the original magmatic grains. The recrystallized feldspars are indicative of submagmatic flow deformation (Paterson et al., 1989). Deformation of the gneissic rocks late in the crystallization of the original syenite under conditions at or slightly below the solidus is indicated by a lack of fluid (melt) relocation textures within the gneisses.

Textures within the syenitic to shonkinitic gneisses are difficult to classify based on the criteria reviewed by Paterson et al. (1989). The assumption that high-temperature

aqueous fluids may have been involved in the recrystallization process suggests deformation during what they term "transition from magmatic to solid-state flow". There is a general lack of melt relocation textures indicative of late magmatic deformational processes, yet there are indications that deformation occurred near solidus conditions. In either case deformation was the result of magmatic processes, i.e., emplacement of interior phases and not the result of the regional deformation that affected the Kobau Formation wallrocks.

Inward from the gneissic rocks are the pyroxenites and shonkinites. In the field the pyroxenites exhibit little or no fabric but anisotropy of magnetic susceptibility data indicate that their mean magnetic fabric is consistent with fabrics of surrounding rocks. If the pyroxenites are cumulates from the original magmas of the syenite gneisses, why didn't they sustain as much deformation as the gneisses? Either the pyroxenites were able to partition strain to other areas or they accumulated in low strain zones and were later juxtaposed with the gneisses as large autoliths.

The shonkinitic rocks constitute the bulk of the marginal mafic phase. Mesofstructures are relatively homogeneous; dominance of aligned primary magmatic grains is indicative of crystal-liquid, magmatic flow (>30%liquid). Microstructures are dominated by magmatic flow fabrics as well, but include abundant late-stage melt relocation textures, which are inferred to represent deformation of the body with <30% melt remaining (van der Molen and Paterson, 1979; Hibbard, 1987). This is particularly evident in the malignite unit which contains deformed pseudoleucite megacrysts. There must have been sufficient crystal-crystal interaction after initial flow alignment to deform the megacrysts plastically. The overprinting of late-stage relocation and plastic deformation fabrics indicates that the shonkinites were deformed during the intrusion of the main phase granitoids. There does appear to be partitioning of strain, with the intensity of fabric development greater near the outer margins of shonkinite unit.

Deformation of the outermost gneissic rocks was the result of flattening strain, (see AMS section above) accompanied by minor recrystallization of the earliest intruded magmas. This deformation was due to the ascent and outward expansion during emplacement of interior mafic phases i.e., the shonkinites which in turn were deformed by diapiric "ballooning" of the main phase granitoids.

After careful consideration of the criteria useful in distinguishing emplacement style (Bateman, 1984, 1985; van Den Eeckhout et al., 1986; Hibbard, 1987; Paterson and Tobisch, 1989; Paterson et al., 1989), the observed data are most compatible with a ballooning diapir model (Fig. 2.14).

The early stages in development of the batholith culminated in emplacement of the mafic alkaline magmas; chemical evidence indicates that the mafic assemblages crystallized from at least two separate magma bodies (Chapter 3). During crystallization, fractionation resulted in the crystal cumulate bodies of pyroxenite along the margins and lower portions of the chamber. The syenitic gneisses may have been felsic melts which differentiated from deeper portions of the chamber and subsequently migrated forcibly upward along the margins. Alternatively, the gneissic rocks may have been differentiated melts that were intruded first; then gneissic flow fabrics developing due to forceful injection into fracture zones above the ascending mafic mass.

Emplacement of the shonkinite was most likely the result of sequential growth by successive pulses of mafic magma at depth in the chamber. Pulses of melt ascended through the chamber but more importantly contributed to the pluton's growth by forcible outward expansion (Fig. 2.15). Outward expansion imparted the submagmatic deformation and dominant flattening strain observed in the rocks of the margins.

The granitoids are genetically separate from the marginal mafic rocks (Chapter 3) but intruded soon after the emplacement of the shonkinitic magmas. Melt must have been present in the shonkinites to produce the melt relocation textures observed. Emplacement of the granitic magmas was probably similar to the shonkinites in that sequential pulses of magma fed the chamber resulting in the outward expansion of the upper portions of the body. The outward expansion of material is supported by the dominance of magmatic flow fabrics containing shallow plunging magnetitic lineations. This outward expansion, i.e., ballooning, imparted the flattening dominated strain observed within the shonkinitic rocks.

Bateman (1985) proposed fracture system magma transport for the Cannibal Creek granite. Bateman argued, based on the rigidity of the overlying crust, that realistic ascent velocities could not be attained by a diapir. The Similkameen may have intruded along deeper level zones of pre-existing weakness into the higher level fold axis we see exposed presently. The deeper zones of pre-existing weakness were facilitated by the Early Jurassic collision and accretion of Quesnellia to the cratonic edge of North America (see Chapter 3). Diapiric development and ballooning didn't occur until after the collision and accretion of Quesnellia when the plutons reached crustal levels at or near which they were finally emplaced (Buddington and Burmester, 1990).

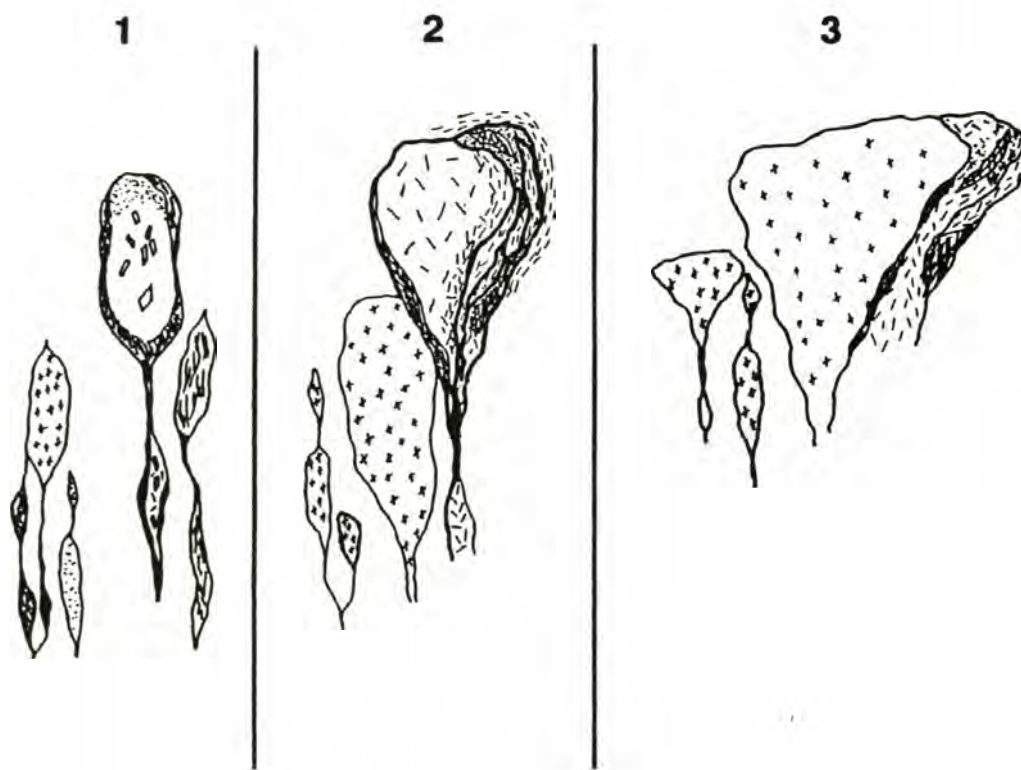


Fig. 2.14: Schematic diagram illustrating the sequential development of the Similkameen batholith: (1) intrusion of mafic magmas and early development of magma chambers: (2) diapiric development by continued injection of mafic crystal-bearing magmas: (3) intrusion and outward expansion of granitic magmas and the resulting deformation to the near-crystalline marginal mafic mass.

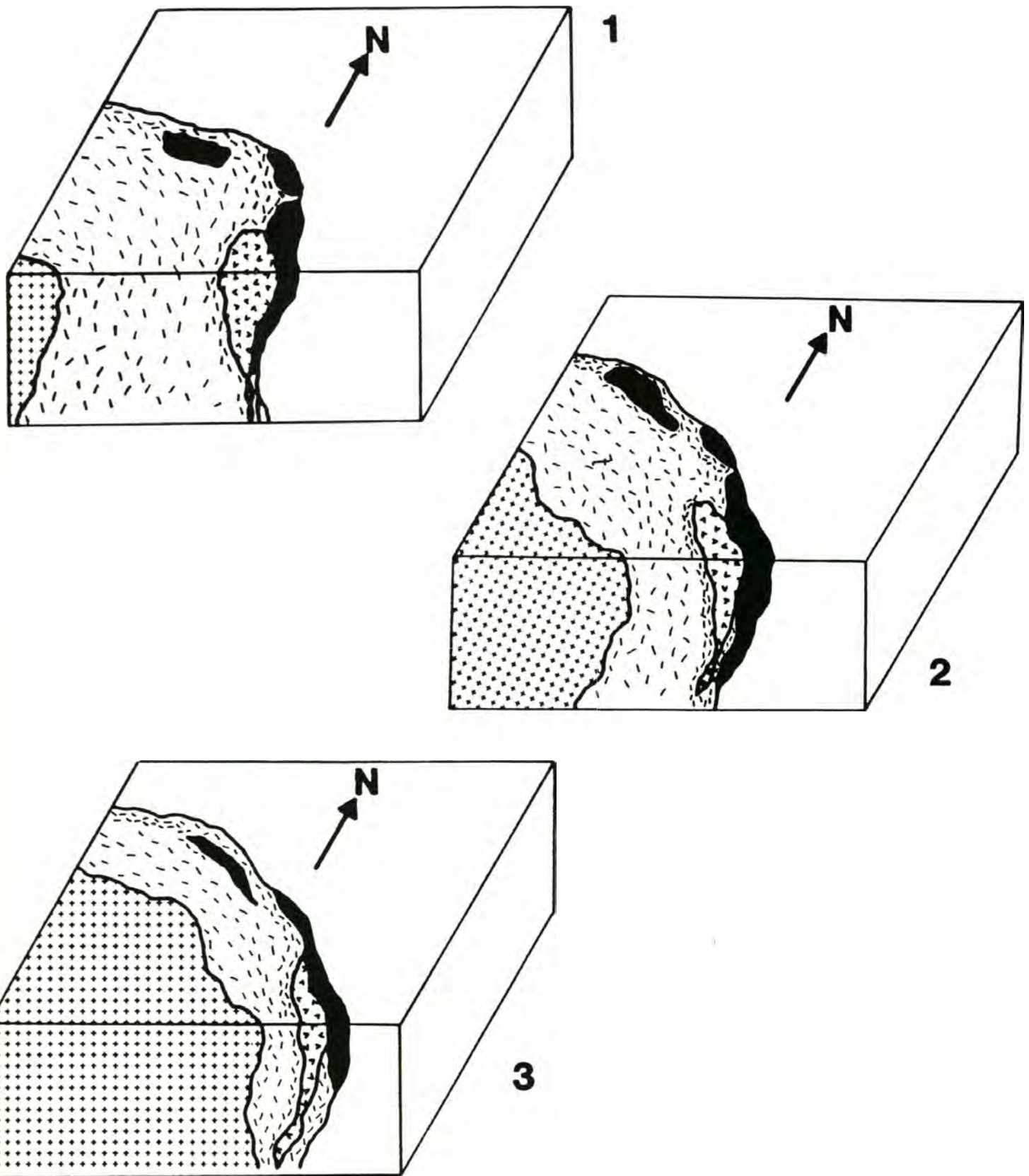


Fig. 2.15: Schematic cross-sectional diagrams showing the sequential growth, outward expansion, and progressive deformation to the marginal mafic phases by the interior main phase granitoids (cross pattern).

In this discussion a ballooning diapir model for emplacement of the Similkameen batholith has been proposed. An alternative model is the intrusion of two distinctively separate magmatic bodies, one deforming the other during a significantly later intrusive episode. Another possibility is that the Similkameen represents a pre-tectonic or syntectonic sequence in which deformation was the result of regional strain.

The first alternative of two separate stages of intrusion can be discounted on the basis of the field evidence, (i.e., gradational contacts), concordant isotopic ages, and the gradational overprinting of microfabrics (i.e., coexistence of submagmatic and crystal-liquid deformation in the earliest intruded phases). This evidence favors a relationship in which the magmas of the individual rock suites (granitoid vs mafic), although not cogenetic in chemistry (see Chapter 3), are associated in time.

The possibility that the marginal mafic rocks were deformed by post-emplacement regional strain is difficult to defend. To date, there has been no documented regional deformation of the wallrocks following emplacement of the batholith. Also, there is no evidence that the regional fabric continues through the batholith. Foliations in some mafic autoliths within main phase granitoids have orientations discordant with flow foliations in the surrounding monzonitic host material. Although detailed analysis of the contact aureole is lacking, it appears that contact assemblages do overprint regional metamorphic fabrics. Finally, magnetic foliation fabrics are concordant to all internal contacts, whereas the plunge of magnetic lineations is steep near the margins and shallow in the interior. The variation in magnetic lineations and the fact that the concentric magnetic fabrics are characterized by flattening strain can be more adequately explained by intrusive mechanisms (i.e., diapirism) rather than regional strain. In summary, there appears to be no evidence of strain within the batholith attributable to regional deformation. Furthermore, intrusion and diapiric growth did not occur until after the collision and accretion of Quesnellia to the North American craton.

CHAPTER III

MINERALOGY, PETROLOGY, AND PETROGENETIC EVOLUTION OF THE SIMILKAMEEN BATHOLITH

Introduction

The Similkameen batholith contains two very distinctive lithologic groups; a marginal group of early, mafic, alkaline (potassic) rocks is intruded by several later calc-alkaline, I-type granitoid plutons. Relative ages of intrusion and crystallization are based on field, petrofabric (Chapter 2), and isotopic data. Although field exposure of the alkaline rocks comprises less than 10 percent of the total area of the batholith, lithologic diversity among the individual phases is striking.

The mafic alkaline assemblage is dominated by shonkinite; a mafic potassic rock containing mainly clinopyroxene, amphibole, alkali feldspar, and nepheline. Also present but in much smaller volumes are malignites. The malignites are similar to the shonkinites but with a higher modal abundance of nepheline. Mafic syenites (nepheline-free) occur throughout the alkaline suite as do ultramafic, biotite and amphibole-bearing pyroxenite cumulates. There is a mineralogic gradation. Clinopyroxene and biotite dominate the ultramafic and malignite assemblages. With increasing SiO₂ and alkali feldspar content, amphibole progressively becomes the primary mafic mineral within the shonkinites and mafic syenites.

The calc-alkaline granitoids consist of three individual plutons ranging from monzonitic to granodioritic in composition. The granitoid rocks are generally hornblende-bearing with minor amounts of biotite, but the Harry Lake pluton on the western side of the batholith contains variable amounts of clinopyroxene.

The coexistence of alkaline (potassic) mafic and granitic calc-alkaline rocks is uncommon in most tectonic settings. In Chapter 2, the study of fabrics and structural relations proposed that the Similkameen magmas intruded after the collision and accretion of Quesnellia. Alkaline magmatism is common to many post-collisional anorogenic regimes; a result of crustal relaxation, extension, and decompression melting. However, it has been suggested by Armstrong (1988) that subduction related magmatism both preceded and continued after the collision of Quesnellia. Recent work in various subduction related settings such as the Mexican volcanic province (Luhr et al., 1989; Verma and Nelson, 1989), the Sunda arc (Stolz et al., 1988), and the Roman province of Italy (Rogers et al., 1985), call for concurrent subduction and extension in the generation of mafic potassic magmas. In the Similkameen region, extensional tectonics during the Jurassic have not been documented, thus the presence of potassic mafic magmatism

coeval with calc-alkaline magmatism is still an enigma. Understanding the geochemical relations between the Similkameen magmas and regional Mesozoic magmatism will allow for better constraints of the tectonic environment within southern Quesnellia during the Jurassic. This study represents but a piece of the tectonic puzzle for later workers to reconstruct.

Major and trace element geochemistries as well as Sr-isotopic data support a subduction related origin for the Similkameen magmas. The relative contributions from individual source components, e.g., slab-derived melts vs. asthenospheric and lithospheric mantle vs. continental crust is still poorly understood. The solution lies with further intensive isotope studies. Regardless, it appears that subduction related enrichment processes and variable source melting within a lithospheric mantle source were dominant processes in the development of the Similkameen system.

The following section briefly summarizes the mineralogy and petrography of representative phases of the mafic alkaline and calc-alkaline rock suites. More detailed descriptions are in Appendix A. Microprobe analyses of selective samples are presented in Appendix C. The final sections review the geochemical data and present a petrogenetic model for the origin for the Similkameen batholith.

Rock Types

Ultramafic Assemblages

The pyroxenites are medium to coarse grained and in thin section exhibit distinctive cumulate textures (Fig. 3.1). The pyroxenites contain euhedral augite with variable amounts of biotite (biotite pyroxenites), magnetite, and apatite. Microcline occurs in the matrix as a minor constituent. Amphibole is relatively uncommon, but in some of the pyroxenites ferroan pargasite is the dominant mafic phase. A rare biotite-pyroxenite pegmatite body with augitic pyroxene, biotite, and amphibole occurs on the southwesternmost margin of the batholith. The pegmatite also contains large (1-4 mm) prismatic apatite grains and interstitial carbonate with straight grain boundaries (Fig. 3.2) and is assumed to be a late magmatic phase.

Biotite is present in all of the pyroxenites as fresh intergranular grains or books and as euhedral inclusions in clinopyroxene and amphibole. The abundance of biotite and the occurrence of pegmatitic pyroxenite indicates that hydrous conditions prevailed during crystallization.

Common to all the pyroxenite bodies are vapor and fluid-rich inclusions (Appendix A). The fluid inclusions occur primarily in apatite, but in the pegmatitic pyroxenite

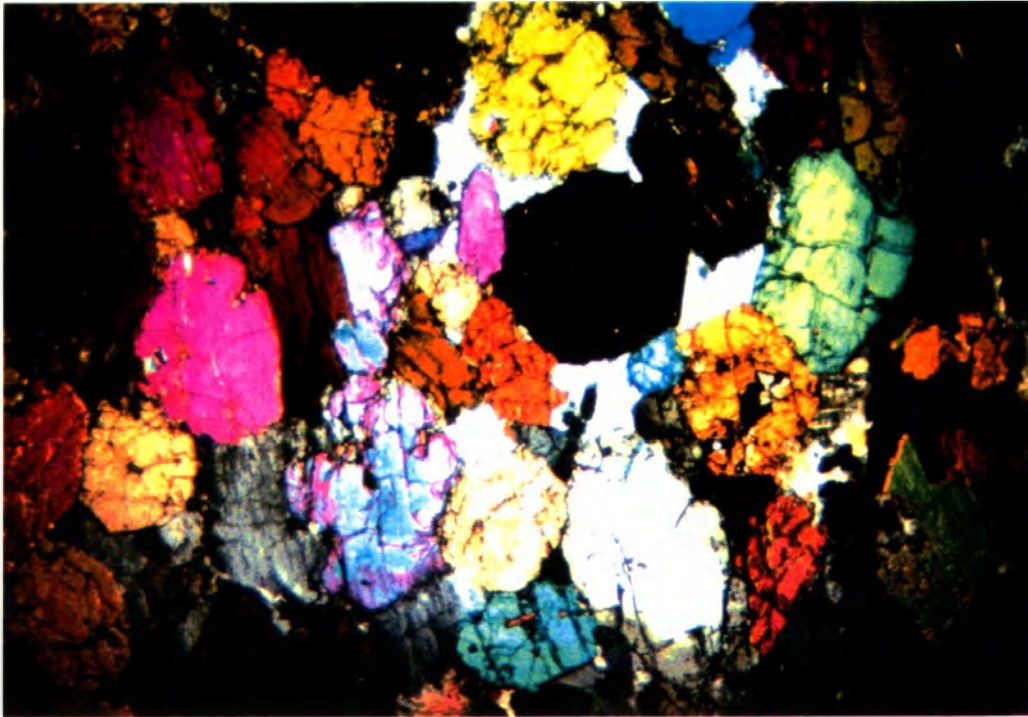


Fig. 3.1: Photomicrograph of biotite pyroxenite cumulate with euhedral clinopyroxene (augite) and subhedral biotite (left center) and interstitial microcline (right center). Cross polarized light and field of view width is 5 mm.

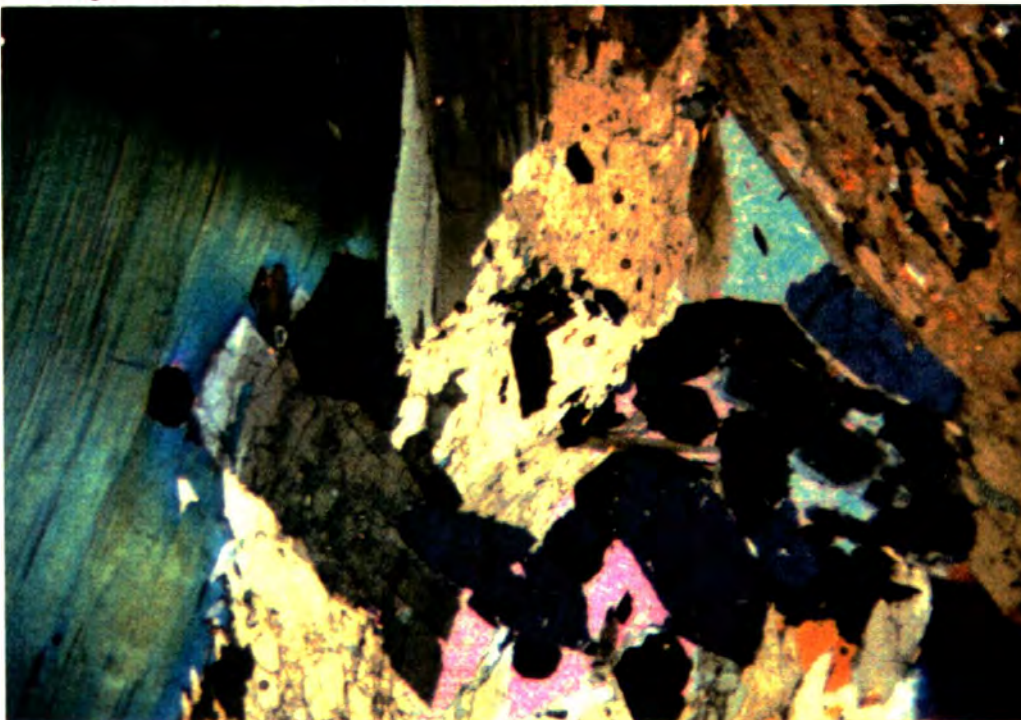


Fig. 3.2: Biotite pyroxenite pegmatite (SMK-126). The clinopyroxene has been partially replaced uralite the biotite cleavages are kinked. Note the euhedral apatite (gray) and interstitial carbonate (twinned). Field of view width is 5 mm.

(SMK-26), inclusions are in primary clinopyroxene, amphibole, and biotite. The majority of the inclusions are fluid-rich but some vapor-rich inclusions have been identified. One sample (SMK-159) contained NaCl crystals (<1 μm) within the liquid-rich inclusions. The inclusions are interpreted to be primary because they occur sporadically throughout grains and exclusively in primary magmatic minerals. A preliminary study on the fluid inclusion compositions indicates that the fluids are dilute, composed of H_2O with little to no CO_2 or CH_4 component (Wodzicki, personal communication).

Malignite

Malignite is a minor lithology confined to a small intrusive unit along the 49th parallel (Plate I). In outcrop the appearance of the malignite is distinctive, typified by ovoid megacrysts of pseudoleucite. The groundmass is coarse-grained and composed of augite + microcline + pargasitic amphibole + nepheline + apatite + magnetite +/- plagioclase. The malignite is heterogeneous with biotite-rich and garnet-rich (melanite) zones alternating with more felsic alkali feldspar-rich layers.

The megacrysts contain intergrowths of microcline and vermiform or rod-like nepheline (Fig. 3.3). Although somewhat flattened, the megacrysts commonly exhibit the icositetrahedral form of leucite, hence the name pseudoleucite (see Chapter 2). Pseudoleucite intergrowths identical to those described here also occur in alkaline rocks from Kaminak Lake, Northwest Territories (Davidson 1970) and in a phonolite dike in the Bearpaw Mountains (Fudali 1963). Gittins et al. (1980) described very similar intergrowths in alkaline ultramafic rocks of the Batbjerg intrusion in East Greenland. The origin of the intergrowths in each place has been attributed to recrystallization of leucite (Fudali, 1963; Taylor and MacKenzie, 1975; Gittins et al., 1980).

Amphiboles in the malignites are ferroan pargasitic in composition and occur as primary grains or as late overgrowths mantling clinopyroxene (salitic augite). Melanite garnet (Ti-andradite) is poikilitic with inclusions of microcline and biotite suggesting later crystallization of these minerals. In the biotite-rich zones, biotite is subhedral with straight boundaries and occurs as early inclusions in clinopyroxene. Biotite compositions within the malignite unit are Fe and K-rich and Si-poor (see below and Appendix C). Ti values for the biotites are relatively low, which indicates that available Ti was partitioned into melanite and amphibole during crystallization.

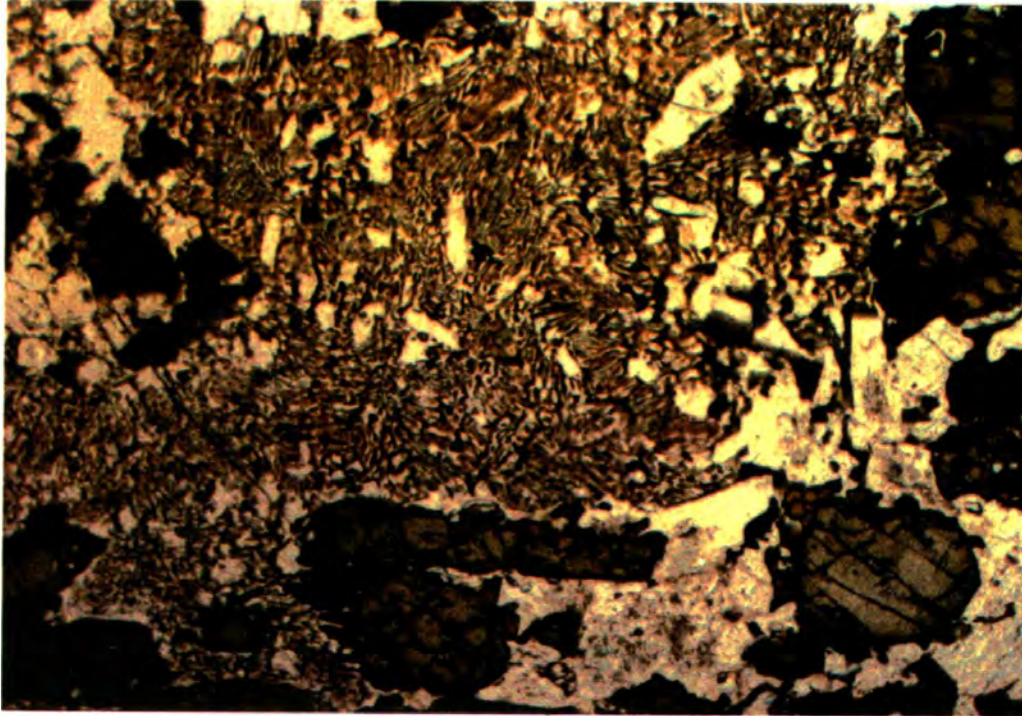


Fig. 3.3: Photomicrograph (plane polarized light) of vermicular intergrowths of nepheline (brown) and micricline (light). Note the euhedral augite (green). Field of view is 3 mm.

Shonkinite

The shonkinites are equigranular and coarse-grained, although porphyritic varieties with microcline phenocrysts occur sporadically throughout. Minerals present include salitic clinopyroxene + microcline + ferroan pargasite + nepheline + apatite + magnetite +/- plagioclase +/- sphene +/- melanite +/- biotite. Clinopyroxene is the dominant mafic constituent and compositions vary only slightly between samples. In general, with increasing modal microcline, modal amphibole content (vs. clinopyroxene) increases. Prismatic, subhedral to euhedral amphibole in the shonkinites is assumed to be an early primary phase, whereas the mantled overgrowths to clinopyroxene and a sieve-like intergrowth with microcline indicates crystallization later in the paragenetic sequence. Biotite is found only as small inclusions within clinopyroxene and amphibole, suggesting early crystallization. Accessory apatite occurs as intergranular prismatic grains and as early inclusions within clinopyroxene. Both varieties contain fluid inclusions similar to those found within apatites of the pyroxenites.

Mafic Syenite

Texturally, the mafic syenites are identical to the shonkinites with the exception of the trachytoid mafic syenites (see Chapter 2). The trachytoid rocks are mafic in overall appearance but modally range from monzonites to syenites and are here considered mafic syenites because of their consistent geochemical correlations with the alkaline mafic assemblages. Shonkinites differ from mafic syenites in that they lack nepheline and have a generally higher modal content of felsic components. In thin section the abundance of ferroan pargasite relative to clinopyroxene in the mafic syenites is obvious. Salitic clinopyroxene is present as ragged cores to amphibole and rarely as discrete grains.

Gneissic Syenite

The marginal zone along the southeastern border contains a texturally unique syenite lithology (see Chapter 2). Based on the major and trace element geochemical trends, these gneissic alkali syenites represent the most fractionated magmas of the older alkaline suite (see Major Element Geochemistry below). The gneissic structure is defined by mafic-rich and felsic-rich layering, presumably formed by mineral segregation during magmatic flow (Chapter 2). The felsic-rich layers contain prismatic euhedral to subhedral alkali feldspar with subordinate amounts of plagioclase that has been altered to epidote and sericite. Minor recrystallization has produced fine-grained interstitial feldspar. Rare clinopyroxene has been replaced by melanite, biotite, epidote, and magnetite within the mafic-rich layers. Orange-brown melanite occurs with biotite in foliated masses or clots. The biotites are distinctively deep green in color, unlike biotites

observed in any of the other rock types. The magmatic mineralogy for the gneissic syenites is; microcline + plagioclase +/- clinopyroxene. The relationship of the garnet and biotite appears to be a late magmatic replacement of earlier mafic minerals within the syenite. Similar garnets occur as primary magmatic phases within the malignites and are common in many alkaline igneous complexes, thus a magmatic origin for the garnets can not be discounted.

In summary, from petrographic analysis there appears to be a mineralogic gradation with Ca-rich clinopyroxene dominating the ultramafic and malignite assemblages. Biotite is abundant within the pyroxenites and malignites but occurs only as inclusions in the shonkinites. With increasing SiO₂ and alkali feldspar content, amphibole progressively becomes the primary mafic mineral phase within the shonkinites and mafic syenites. Alkali feldspar is the dominant feldspar in the alkaline rocks; plagioclase only becomes an important phase in the calc-alkaline granitoids. Quartz is absent in the alkaline rocks.

Granitic Rocks

This study has identified three lithologically distinct granitoid plutons within the Similkameen complex (see Chapter 2). The eastern half of the batholith is composed of a zoned granitic pluton (Similkameen Valley pluton) that grades from monzonite along its margins inward to quartz monzonite or quartz monzodiorite and granodiorite in the core (Fig. 3.4). All of the phases have coarse-grained porphyritic textures with megacrysts of microcline. Hornblende is the dominant mafic mineral supplemented with ragged clinopyroxenes in some of the border monzonites. These clinopyroxenes possibly are xenocrysts from assimilated inclusions of the marginal mafic alkaline rocks (see Mixing etc. below). Biotite is rare and occurs only as ragged resorbed grains or as early inclusions within hornblende. Monzonites of the Snowy Mountain area are lithologically and chemically similar to the monzonites of the eastern area, and thus are considered to be the western exposure of the Similkameen Valley pluton.

Within the western field area two other granitic plutons were identified. The Harry Lake pluton is an equigranular, medium-grained quartz monzonite that contains variable amounts of hornblende and clinopyroxene (augite). In thin section, augite is euhedral prismatic to equant indicating that it was a primary magmatic phase. Major element variations will be discussed below, but it is interesting to note here that the Harry Lake pluton consistently plots off the main granitoid trend indicating that the Harry Lake unit is a separate plutonic phase.

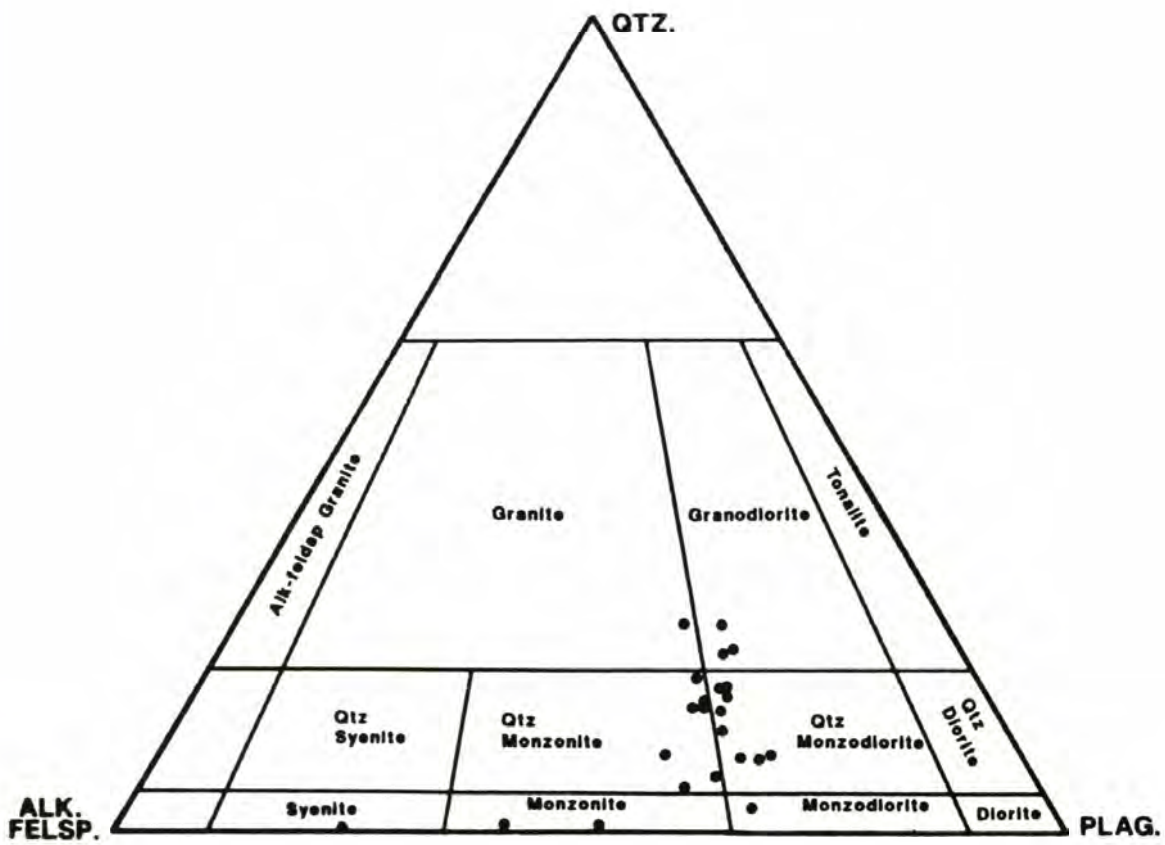


Fig. 3.4: Plot of granitoid compositions from the Similkameen batholith.

The granodiorite of upper Snehumption Creek is texturally similar to the Harry Lake pluton, but compositionally this pluton is distinct from either the Harry Lake pluton or the granitoids of the eastern field area. In major element oxide variation diagrams, this unit plots well away from the main trend at the most fractionated end of the spectrum. It contains the highest SiO₂ and lowest CaO and MgO concentrations. Biotite is the primary mafic mineral with variable amounts of amphibole, and quartz clots are ubiquitous.

In summary, three distinctive granitoid plutons have been identified within the Similkameen batholith. The Similkameen Valley pluton and the granodiorite of the upper Snehumption Creek area are hornblende and biotite bearing whereas the Harry Lake pluton contains variable amounts of augitic pyroxene and hornblende. Plagioclase dominates microcline although megacrysts of microcline are common to all phases. Quartz is present in variable amounts except for the granodiorite of upper Snehumption Creek where it occurs as obvious clots. Accessory minerals include magnetite, sphene, apatite, and zircon.

Mineral Compositions

The following summary of mineral compositions is based on microprobe analyses of representative samples throughout the complex. Mineral composition data appear in Appendix C along with a discussion of analytical methods.

Clinopyroxene

Clinopyroxene, present in all the mafic rocks, is generally salitic in composition (WO=48-54:EN=31-42:FS=8-21, Fig. 3.5). In thin section, compositional zoning is sporadically discernible and microprobe data confirm that zoning is present within individual grains (Appendix C). Because there are very few analyses, compositional zoning trends for pyroxenes of the individual rock suites are tentative. It appears that the shonkinitic pyroxenes (SMK-125, SMK-142) trend from salitic cores toward more diopsidic-rim compositions whereas the malignites (SMK-111) exhibit consistent Ca-salite compositions. The most diopsidic clinopyroxene was from an amphibole-rich pyroxenite (SMK-159).

Amphibole

Amphibole compositions vary from ferroan pargasite to hastingsite in the marginal mafic rocks to exclusively hornblende (edenitic hornblende) in the granitoids (nomenclature based on Leake, 1978), (Fig. 3.6). Modal amphibole contents generally

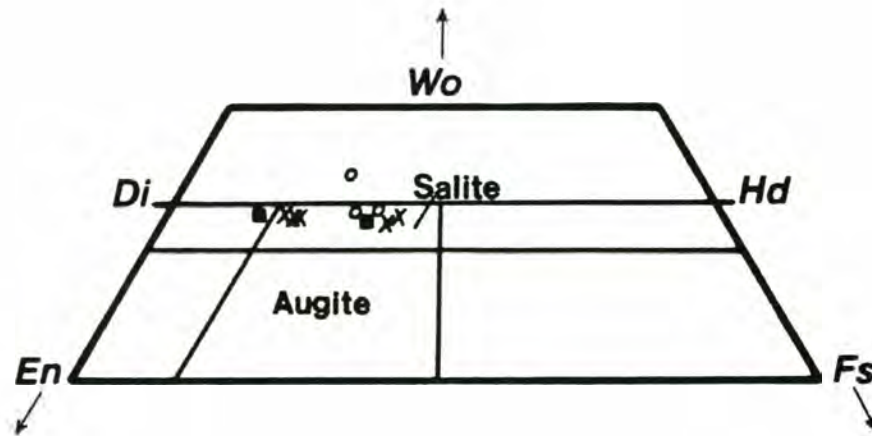


Fig. 3.5: Plot of clinopyroxene compositions in percent wollastonite, enstatite, and ferrosilite component.

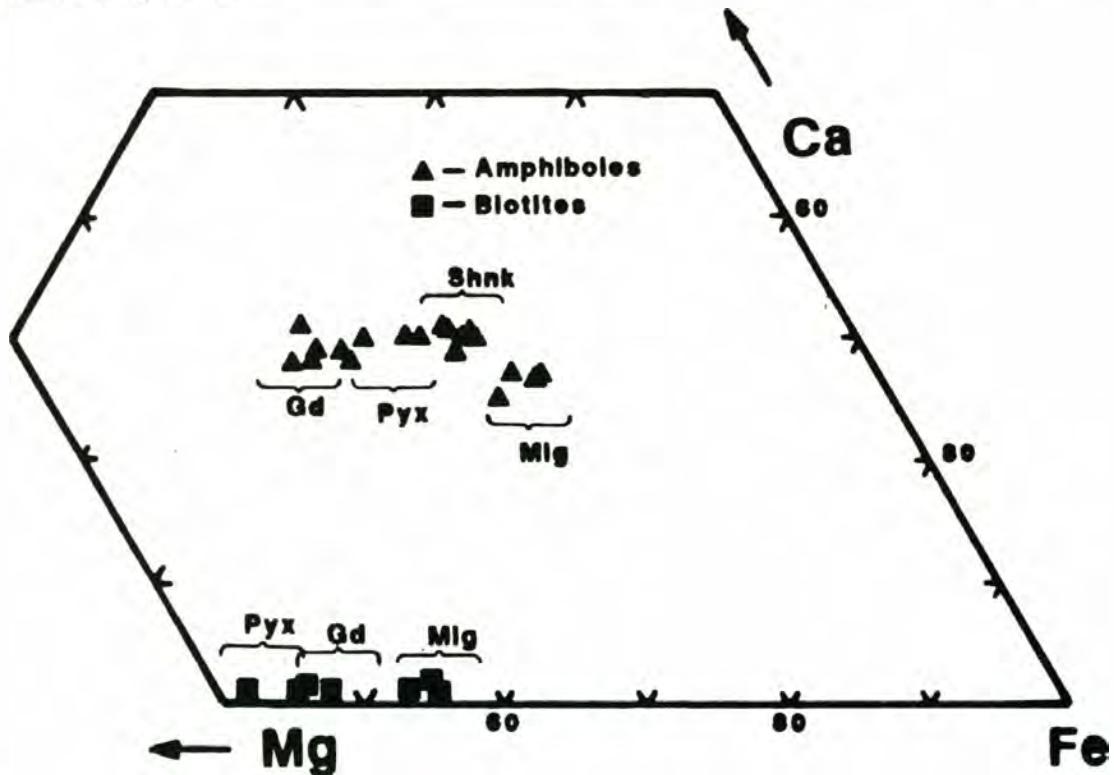


Fig. 3.6: Plot of amphibole and biotite compositions based on weight percent Ca, Mg, and Fe.

increase relative to pyroxene with increasing microcline content. For the mafic rocks, amphiboles were analyzed from two amphibole-rich pyroxenites (SMK-159, SMK-206), one malignite (SMK-111), and two shonkinites (SMK-125, SMK-142) (Appendix C). Compositional variation within the pyroxenite amphiboles is relatively erratic as displayed by the evolution index $Fe/(Fe+Mg)$ (atomic ratio; where Fe =total iron as Fe^{+2}). Amphiboles from the pyroxenites are the most Mg-rich and Fe-poor in the complex and have $Fe/(Fe+Mg)$ ratios that vary from 0.58 to 0.71. Shonkinite amphiboles show a trend of increasing $Fe/(Fe+Mg)$ ratios (0.68 to 0.74) with decreasing Al and Ca as the amphiboles become more Fe-rich. The malignite amphiboles contain the highest $Fe/(Fe+Mg)$ and lowest Ca, Ti, and Al values which correlates with the relatively more evolved nature of the malignites when compared to the shonkinites. The K contents remain comparatively constant while Si and Na values increase from the pyroxenites through to the shonkinites.

Amphibole compositional trends for the few samples analyzed indicate that Fe-enrichments can be directly correlated to whole rock compositional trends. In the mafic alkaline suite, the more fractionated rocks contain amphiboles with the highest Fe concentrations. Furthermore, amphiboles from the alkaline rocks display the coupled substitution $Ca(M4)Al(IV) - Na(M4)Si(IV)$ indicative of magmatic differentiation in silica-undersaturated magmas (Giret et al., 1980; Bonin and Giret, 1984; Henderson et al., 1989).

Amphiboles (ferro-edenitic hornblende) from an interior calc-alkaline granodiorite (SMK-120) have higher Si and Mg values and considerably lower Fe, Al, Na, K, and Ti than amphiboles of the marginal mafic rocks. A more detailed study is needed to identify any compositional variations within amphiboles of the granitoid rocks and to understand the relationships, if any, between amphiboles of the alkaline and calc-alkaline suites.

Biotite

Biotite is abundant in the pyroxenites as inclusions in clinopyroxene or as discrete euhedral grains. In a pegmatitic biotite pyroxenite (SMK87-26) books as large as 3-6 cm occur with clinopyroxene and apatite. Malignite is the only other mafic lithology that contains appreciable biotite. Biotite is relatively uncommon in the majority of the granitic plutons, occurring only as ragged anhedral grains or as small inclusions in amphibole.

Compositional variation (Fig. 3.6) between biotites of the pyroxenite (SMK-159) and the malignite are most significant for Fe and Mg (Appendix C). The pyroxenite biotites contain higher concentrations of Mg, which is reflected in the lower $Fe/(Fe+Mg)$

ratios (0.55-0.59) compared to the malignite biotites (0.67-0.68). Si and Al values are similar although the malignite biotites exhibit some Al-enrichments from core to rim and there is a marked increase in Mn from the pyroxenite biotites to the malignites. Na and K values are consistent for both rock types. The low analytical totals for the biotite analyses are typical and reflect substantial amounts of F, Cl, and/or OH.

Biotites from mafic alkaline rocks of the Similkameen were compared to biotites from mafic potassic rocks of the Highwood Mountains (O'Brien, 1988). Si and Al contents for biotites from several Highwoods rock types including biotite pyroxenite, mafic phonolite, and shonkinite are similar to the Similkameen biotites but the Highwoods biotites contain significantly lower Fe/Fe+Mg ratios (0.45-0.48) than the Similkameen, consistent with the less evolved whole rock chemistry of the Highwoods. The Highwoods biotites have much higher Ti contents as well.

Feldspar

Microcline is ubiquitous in the Similkameen batholith and is by far the dominant feldspar in the mafic alkaline rocks. In the pyroxenites, microcline is a late crystallizing interstitial phase. In all other units microcline occurs either as megacrysts or micro- to coarse braided perthites with tartan twinning. Microcline megacrysts are euhedral, commonly with plagioclase inclusions (attached presumably by synneusis) parallel to internal crystal faces. In the mafic alkaline assemblages, plagioclase is subordinate to alkali feldspar, or commonly absent. In the granitic units, plagioclase is the dominant feldspar, occurring as complexly zoned euhedral to subhedral grains.

Based on the limited data, it appears that the alkali feldspars exhibit little to no compositional variation except for Ba contents and minor differences in K and Na between the mafic units and the granitoids (see Appendix C). Alkali feldspar compositions are strongly potassic throughout the complex ranging from Or₉₃Ab₇ in the pyroxenite (SMK-206) to Or₉₀Ab₉An₁ - Or₉₂Ab₈ in the shonkinites (SMK-125, SMK-142) and Or₉₁Ab₉ in the malignite (SMK-111) sample. BaO concentrations (1.78 wt.%) are highest in the pyroxenite. Alkali feldspar from the granodiorite (SMK-120) exhibits the highest K values with the composition Or₉₅Ab₅.

Plagioclase compositions in the alkaline rocks were difficult to obtain optically because of the lack of twinning and small grain size. The narrow range in plagioclase compositions (An₃₀₋₃₃) was consistent throughout the alkaline rocks except for one sample, SMK-134, which contained the most sodic plagioclases (An₁₃₋₂₀) observed. The granitic rocks exhibit greater compositional variation with cores ranging from An₃₇ to An₃₂ and rims from An₂₈ to An₂₃. Most granitic plagioclases are complexly

zoned with normal to oscillatory zoning and have groups of plagioclase in synneis relation.

Iron Oxides

Magnetite is the dominant opaque oxide present in the alkaline rocks of the Similkameen complex and occurs as euhedral intergranular grains or as inclusions in the mafic minerals. Compositions are exclusively magnetite, surprisingly devoid of Ti and Mg with very little solid solution to ulvospinel (Appendix C). No analytical data on opaque oxides have been obtained for the granitic rocks.

Nepheline

Nepheline is abundant (up to 30 modal %) in the malignites but has been replaced by hydronepheline, cancrinite, and various other unidentified zeolites in most rocks. Grains of unaltered subhedral nepheline (up to 10 modal %) occur in the shonkinites and mafic syenites.

Apatite

Apatite is present in all rocks of the Similkameen batholith but is most evident in the mafic alkaline rocks where it occurs as early prismatic inclusions and as euhedral grains. In the pyroxenites apatite commonly occurs as small (0.5-2.0 mm) clusters with euhedral magnetite. Cathode luminescence reveals that apatites in the alkaline rocks are more enriched in LREE's (lavender luminescence) relative to those of the granitoids (yellow luminescence) (Mariano, 1989).

Sphene

Sphene is abundant in both the alkaline rocks and the granitoids as euhedral wedge-shaped grains. In the alkaline rocks sphene is found with magnetite as a late-stage replacement product of clinopyroxene, amphibole, and/or biotite. A sphene composition is presented in Appendix C.

Zircon

Zircon occurs in all rocks but is most abundant in the granitoid rocks. Xenotime (YPO₄) also has been identified by cathode luminescence in a variety of the alkaline mafic rocks.

Major and Trace Element Geochemistry

The diversity in lithology and mineralogy of the Similkameen rocks is reflected in a wide range of major and trace element compositions. The mafic alkaline suite (Fig.

3.7) is typically potassic ($K_2O:Na_2O = 1.5$) and high in Sr and Ba relative to the granitic rocks. The granitoids can be characterized as calc-alkaline, I-types that are metaluminous with molar $Al_2O_3/CaO + Na_2O + K_2O$ (A/CNK) ratios generally < 1.1 . Primary magmatic compositions from the alkaline and calc-alkaline suites are comparatively evolved (average Mg# = 40-42). Ni, Cr, and Pb are consistently depleted in the alkaline suite (<15 ppm Ni, <25 ppm Cr, <19 ppm Pb) except for Ni and Cr in the pyroxenites which are considered crystal cumulates. Both suites display light rare-earth element (LREE) enrichments with the alkaline suite being more LREE enriched. Both suites also display relative depletions in the high field strength elements Th, Nb, Ti, and presumably Ta. The high Ce/Y and LREE/HREE ratios of the mafic rocks are consistent with residual garnet in the source region.

Based on the major and trace element chemistry, it appears that magmas of the alkaline and calc-alkaline suites were not cogenetic. Furthermore, there are significant variations in incompatible element ratios within the mafic alkaline suite, indicating the possibility that two geochemically separate series exist. The "shonkinite" series displays oceanic island basalt (OIB) type composition and is enriched in incompatible elements relative to the mid-ocean ridge-basalt (MORB) type "malignite" series. However, it is possible that those compositional variations could be explained by fractional crystallization and/or different degrees of partial melting of a similar source region. If the alkaline series are not cogenetic, melting from a heterogeneous source region may be the alternative. This hypothesis will be tested in the section on Source Components.

Major and Trace Element Variations

Whole rock major and trace element analyses were obtained from 50 representative samples (analyses presented in Appendix B) from throughout the Similkameen complex (see Plates I, II for locations). To evaluate possible fractional crystallization trends, selected major element oxides are plotted against MgO wt.%.

Al_2O_3 versus MgO (Fig. 3.8)

It is apparent from the plot of Al_2O_3 versus MgO, that it is unreasonable to relate the granitoids to the mafic alkaline rocks via a similar liquid line of descent. The granitoids exhibit an opposite sloping trend with decreasing MgO with the two alaskite samples representing late differentiates from the granitoids. In contrast, the alkaline

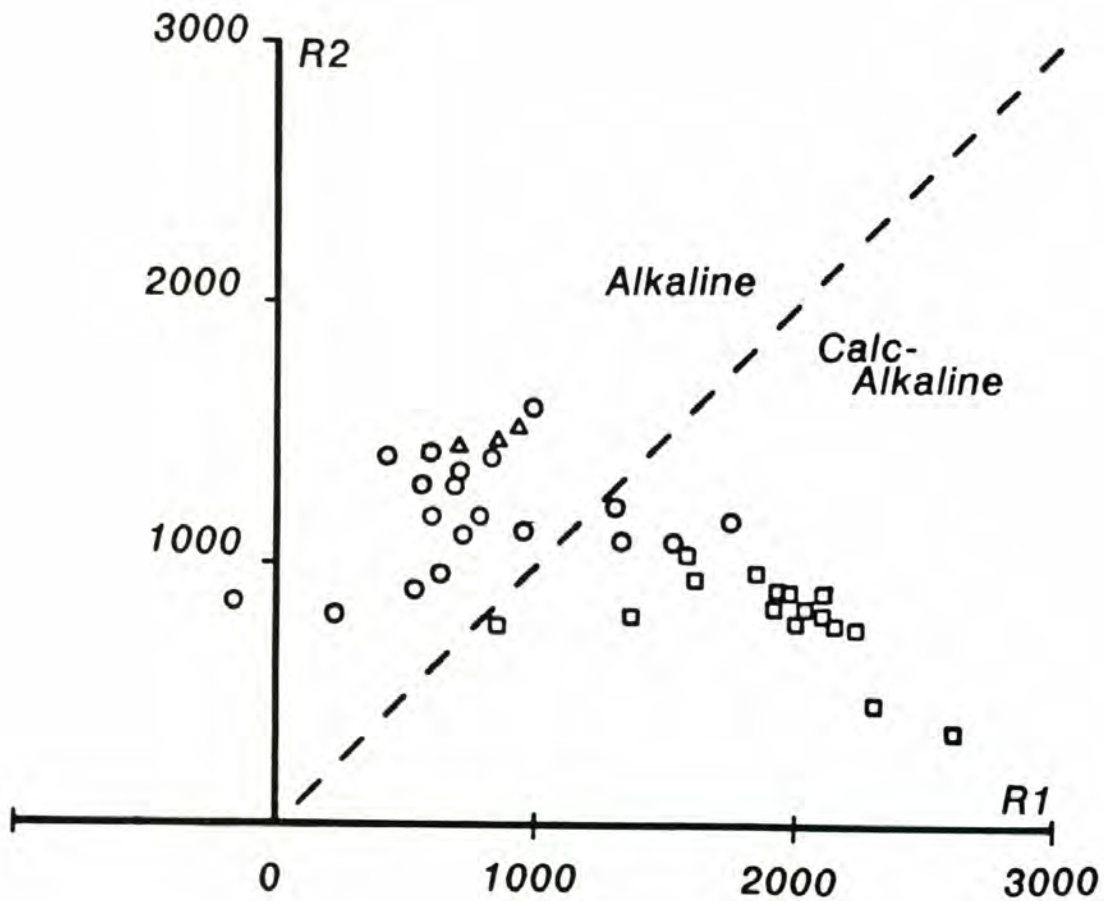


Fig. 3.7: R1-R2 plot (after de la Rouche et al., 1980) of the Similkameen rocks showing alkaline/calc-alkaline division. Circles < 50% SiO₂, diamonds < 60% SiO₂, squares > 60% SiO₂.

$$R1 = 4Si - 11(Na + K) - 2(Fe + Ti)$$

$$R2 = 6Ca + 2Mg + Al$$

rocks exhibit increasing Al_2O_3 with decreasing MgO in a linear array away from the pyroxenites. This trend reflects increasing potassium feldspar crystallization. Note that the gneissic syenites plot in a co-linear array within the alkaline trend.

CaO versus MgO (Fig. 3.9)

Fractionation of clinopyroxene was likely responsible for the observed CaO trend within the alkaline rocks because plagioclase is such a minor phase. Clinopyroxene is common throughout the alkaline rocks, particularly in the high MgO samples. The pyroxenites are most likely crystal extracts from the shonkinites and malignites based on the linear relation between the two.

Some scatter exists between the shonkinites and malignites and this relationship is consistent throughout most of the major and trace element variation plots. The scatter may reflect varying clinopyroxene, apatite and amphibole fractionation. For example, sample SMK-137 is dominated by amphibole versus clinopyroxene and contains 8% modal apatite which is unusually high for the pyroxenites. An alternative explanation is that the malignites and shonkinites represent sub-suites unrelated to each other by fractional crystallization. This aspect will be explored further in the discussions on fractionation modeling and magma petrogenesis below.

The shonkinite SMK-207 is not a crystal cumulate, yet plots well off the main alkaline trend (in all plots) and may represent the least evolved magma composition of the alkaline suite. There is no demonstrated relationship between SMK-207 and the fractionation series displayed by the main alkaline trend. No olivine has been identified in any of the mafic rocks nor has any olivine cumulate been identified. However, SMK-207 may be an isolated sample of the parental magmas of the mafic alkaline suite. The pyroxenites which lie on a linear trend with SMK-207 (SMK-159, 198, and 219) may be crystal cumulates extracted from either SMK-207 or a parental magma to SMK-207.

The linear granitic trend overlaps the more evolved mafic syenites (e.g. SMK-158, 169) of the alkaline trend and at approximately 2.0% MgO there is a break in the granitic trend. The mafic syenites are located in contact zones with the granitoids and may possibly represent assimilated materials. The break in the granitic trend may also indicate various amounts of assimilation of mafic material by the granitoids with the group of high MgO granitic rocks being the mixing or assimilation end-members. This process will be discussed further in the section: Mixing etc..

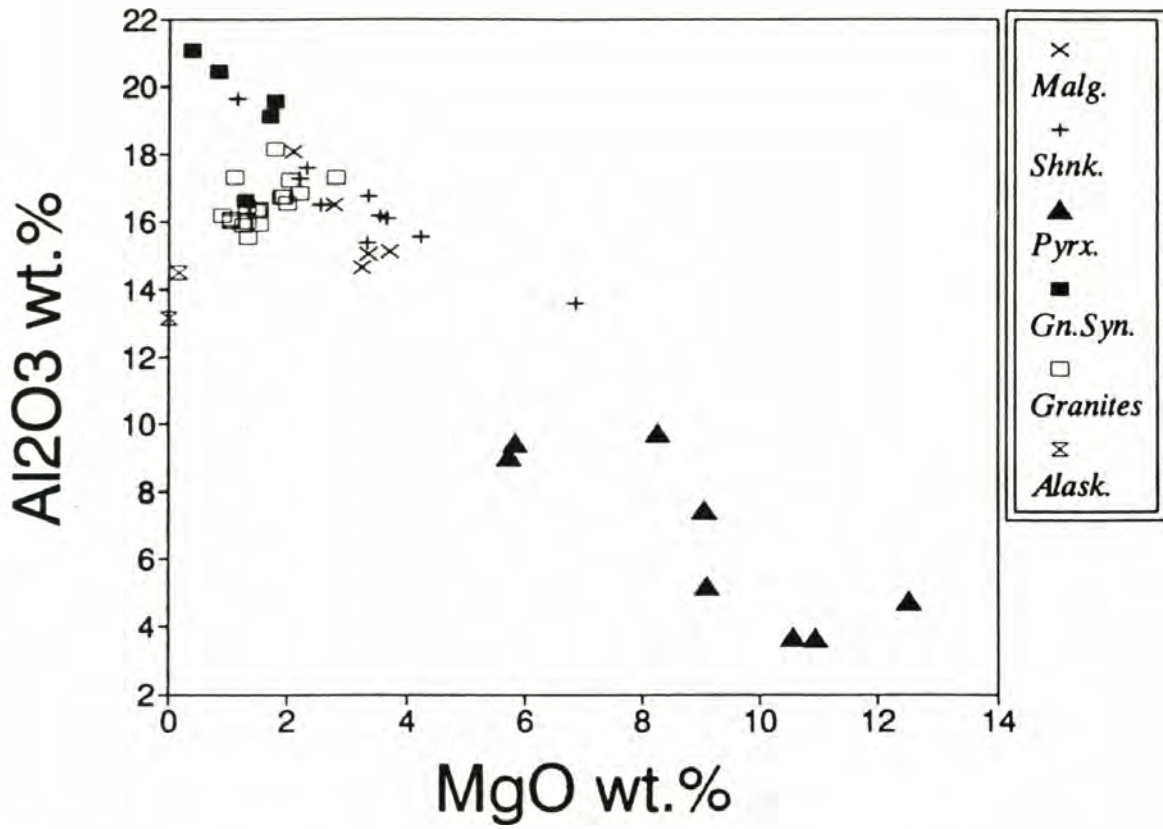


Fig. 3.8: Al₂O₃ versus MgO variation diagram.

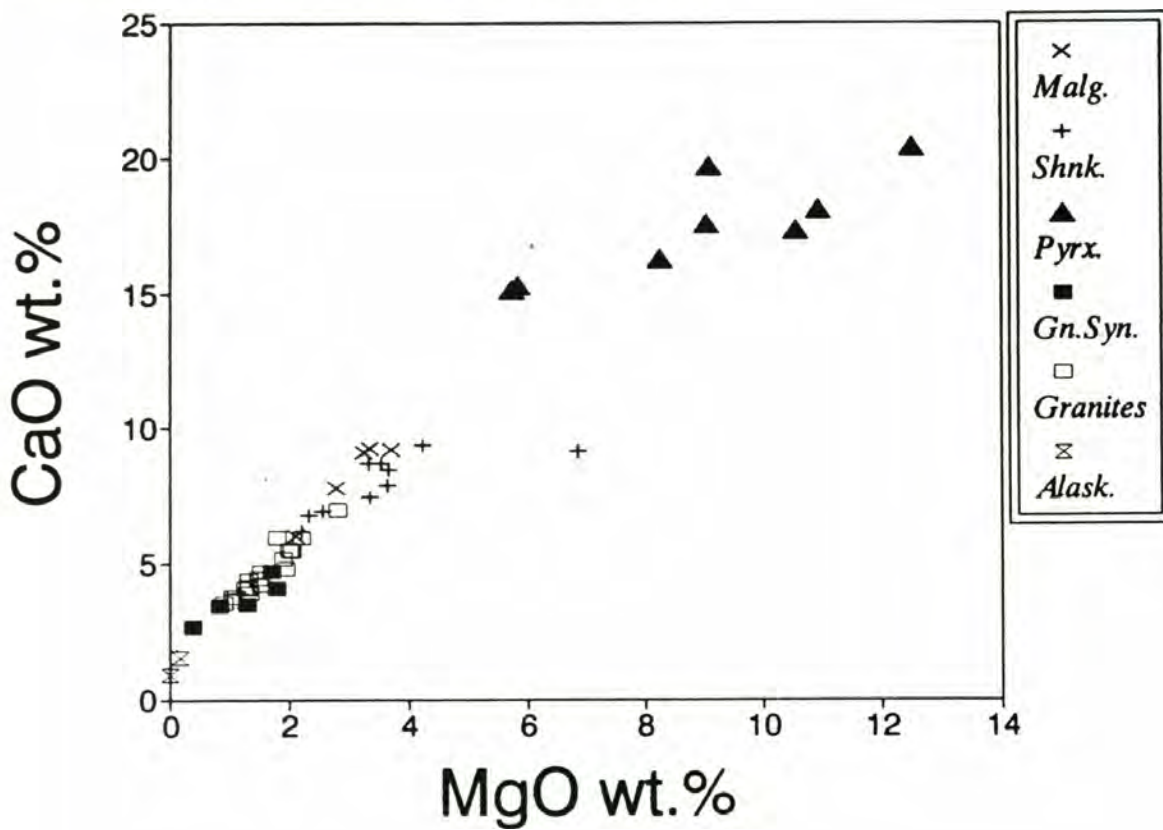


Fig. 3.9: CaO versus MgO variation diagram.

P₂O₅ versus MgO (Fig. 3.10)

The P₂O₅ trend is controlled by apatite which correlates directly to observed petrographic relationships. The high P₂O₅ pyroxenites contain up to 8 wt.% modal apatite whereas the low P₂O₅ pyroxenites contain accessory amounts of apatite. Apatite is abundant in all the mafic alkaline rocks but essentially absent from the low P₂O₅ gneissic syenites. All the granitoids contain trace amounts of apatite. The variations in FeO*, TiO₂, and V are similar to the P₂O₅ trend.

Ni versus Cr (Fig. 3.11)

The low abundances of these compatible elements suggests the highly evolved nature for the Similkameen magmas. Notable are the higher Ni and Cr concentrations in the high MgO shonkinite (SMK-207), and the two pyroxenites (SMK-159, 219), which suggests derivation from relatively more primitive magmas.

Summary of Major and Trace Element Variations

A cogenetic origin for the mafic alkaline and calc-alkaline granitoid rocks is not strongly supported by the observed variations in the major and trace elements. Harker plots of oxides versus MgO are somewhat misleading because in most cases both suites define an overlapping coherent linear trend, but the plot of Al₂O₃ vs. MgO precludes the possibility of a realistic liquid line of descent between the two suites. Some scatter in the trends of major and trace elements between the shonkinites and the malignites suggests that these units possibly were of separate origins as well.

Most analyses of the gneissic syenites plot along linear trends with their more mafic counterparts and chemical variations indicate that the gneissic syenites are indeed part of the alkaline suite. The pyroxenites contain erratic elemental variations but plots indicate a relationship to the shonkinites and malignites by clinopyroxene + apatite +/- biotite +/- amphibole +/- magnetite removal from assumed parent compositions, consistent with a cumulate origin.

Rb-Sr Isotope Geochemistry

Rb-Sr whole rock isotopic analyses were performed on 24 representative samples that span the range of rock types from the Similkameen batholith. The analyses were done at the geochronology laboratory of the University of British Columbia by the author under the supervision of R.L. Armstrong and D. Runkle. Analytical procedures and results are presented in Appendix D.

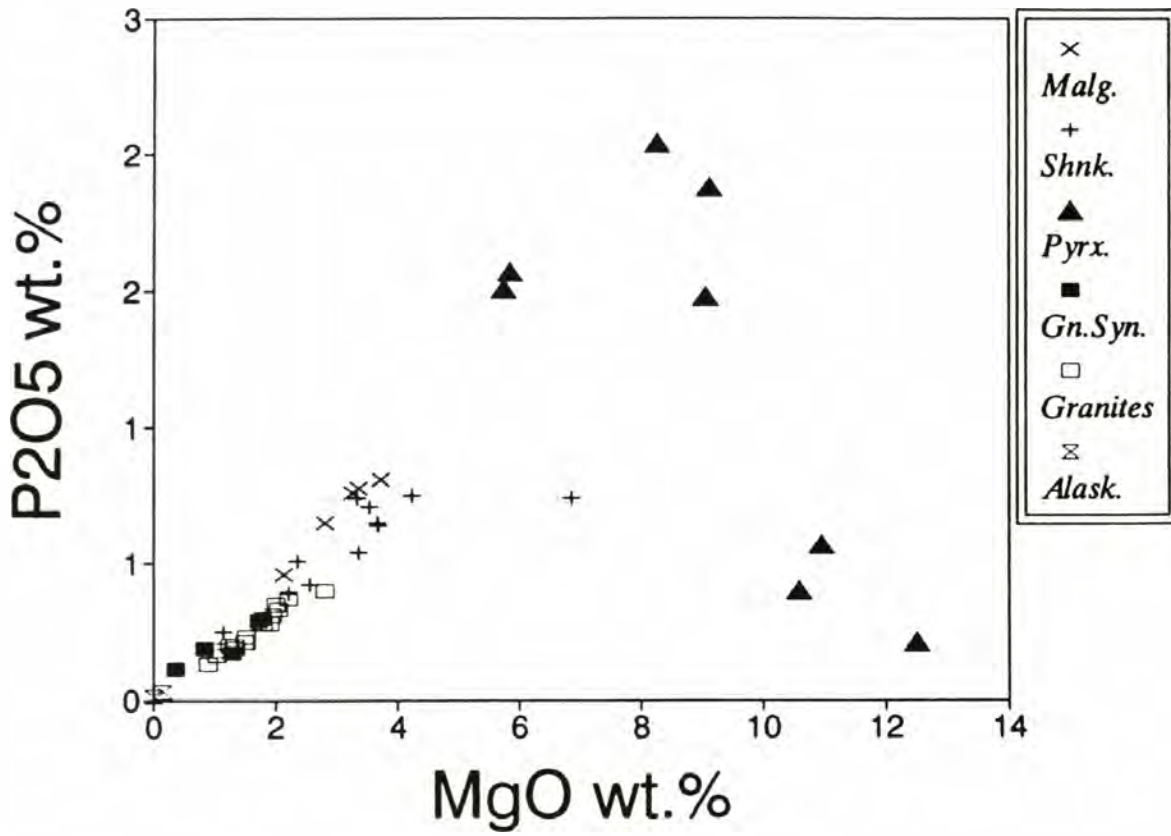


Fig. 3.10: P₂O₅ versus MgO variation diagram.

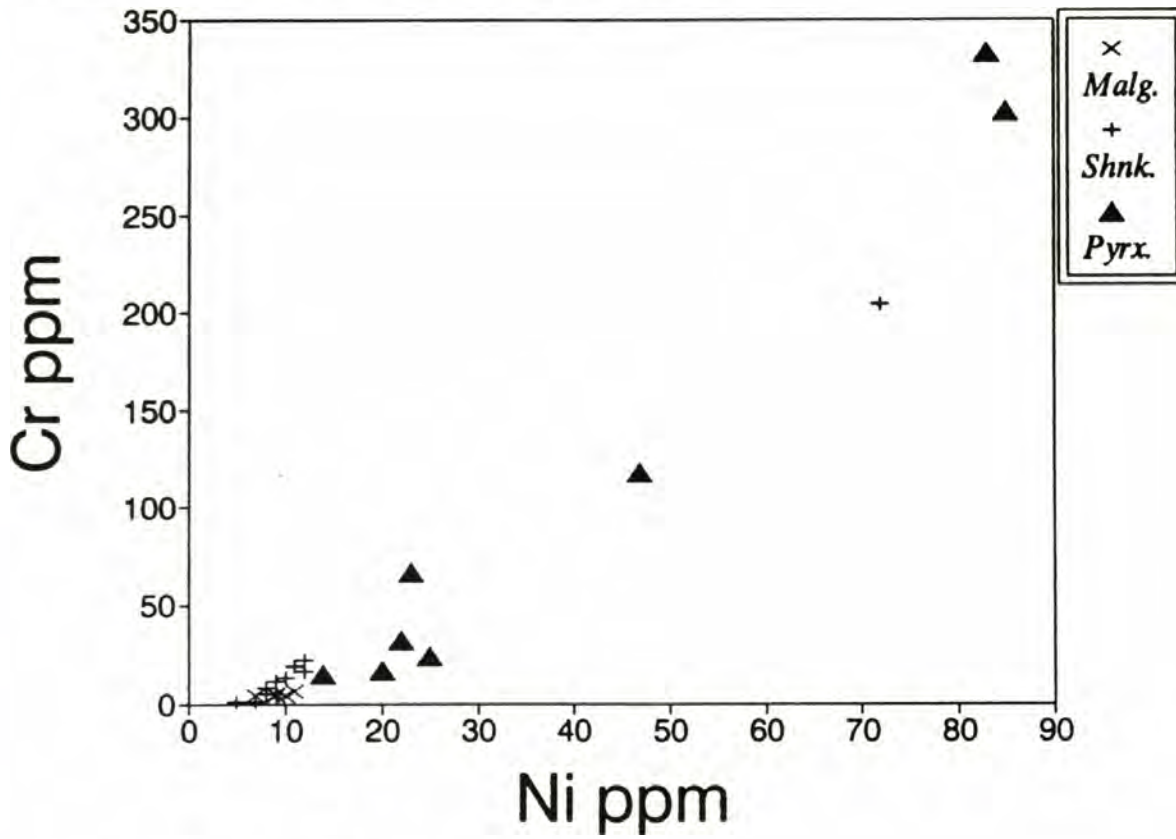


Fig. 3.11: Ni versus Cr variation diagram.

A Rb-Sr isochron age of 165 \pm 6 Ma with an initial-Sr ratio of 0.7039 was calculated for the Similkameen based on these samples (Fig. 3.12). This Rb-Sr age is in agreement with previous isotopic ages obtained for the Similkameen. Fox et al. (1977) published K-Ar ages of 170.9 \pm 5 and 177.2 \pm 5.3 Ma (hornblende), and Parkinson (1987) presented a concordant U-Pb (zircon) age of 170 \pm 2 Ma obtained from an interior granodiorite phase of the batholith.

The alkaline suite is characterized by high Sr concentrations (1350-2773 ppm Sr) with the shonkinites exhibiting considerable scatter but distinctively lower Sr concentrations than the malignites (Fig. 3.13). The pyroxenites and the calc-alkaline granitoids contain lower Sr concentrations than the main alkaline suite. Initial $^{87}\text{Sr}/^{86}\text{Sr}$ ratios (calculated to 170 Ma based on the U-Pb zircon date cited above) of primary magmatic phases have a narrow range (0.7037 to 0.7042), consistent with mantle derived values (MORB source=0.7020 - 0.7040, OIB source =0.7025 - 0.7060). The range in Rb/Sr (0.014 -0.183: alaskites excluded) is narrow as well.

Petrogenetic Implications of Rb/Sr Isotopes

The Similkameen reference isochron shows a moderate amount of scatter but does fit the U-Pb age reported by Parkinson (1985). This relationship indicates that the Similkameen represents an undisturbed isotopic system, i.e., the Rb-Sr isotopes have not been reequilibrated by any later thermal event. Therefore the Sr-isotope data can be used for petrogenetic interpretations.

Magmatic mechanisms that may account for the variations in the $^{87}\text{Sr}/^{86}\text{Sr}$ ratios include: varying degrees of country rock assimilation; melting of an isotopically heterogeneous source; and/or mixing of isotopically distinct magmas (DePaolo, 1981; Arculus and Powell, 1986; Ellam and Hawkesworth, 1988; Arth et al., 1989).

To investigate the possibilities of an isotopically heterogeneous source or mixing of isotopically distinct magmas, initial-Sr ratios (corrected to 170 Ma) were examined (Fig. 3.14). The low variation in initial-Sr ratios (essentially horizontal on Fig. 3.14) indicates that the Similkameen magmas originated from an isotopically homogeneous source (Arth et al., 1989). Mixing of isotopically different magmas would create compositional mixing trends away from a horizontal line.

If assimilation processes played an important role during magma evolution, then the assimilated material must have had initial-Sr ratios similar to the Similkameen magmas or the amount of assimilated material was insignificant. Contamination by isotopically distinct material would have resulted in considerable variations in the initial-Sr ratios.

Similkameen Batholith Rb/Sr Data

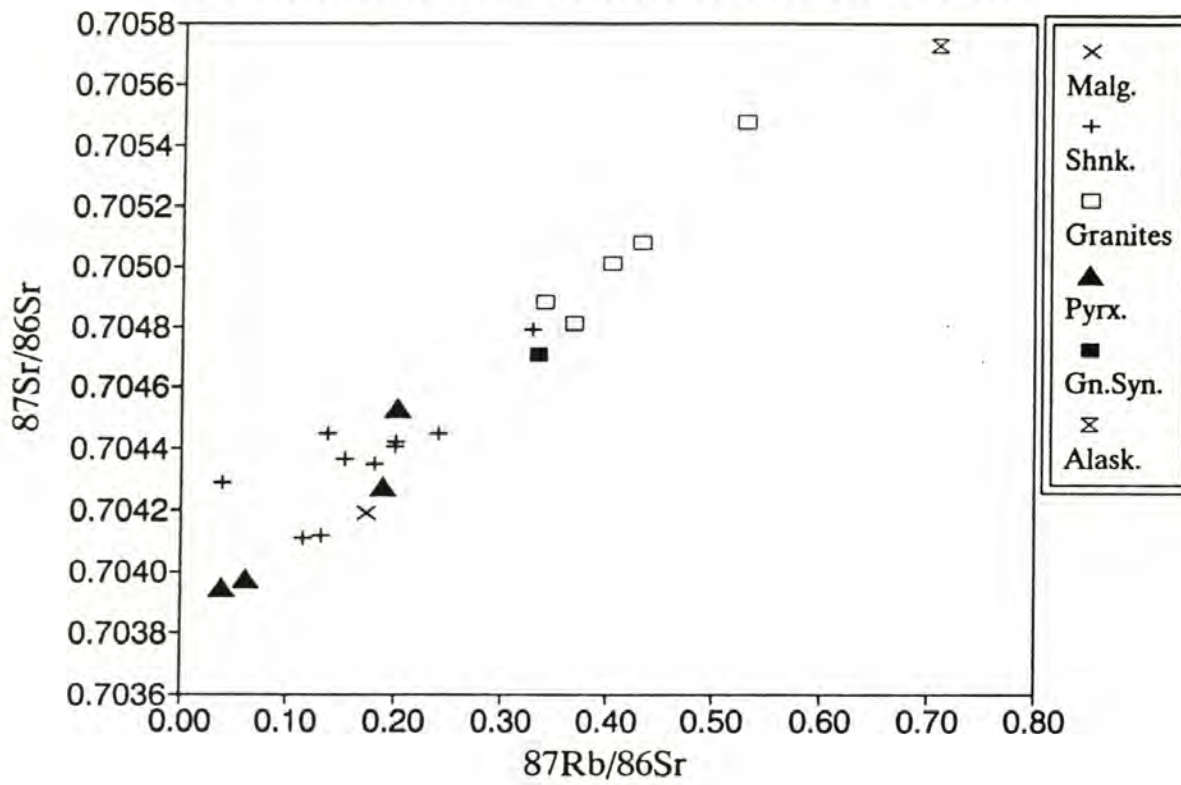


Fig. 3.12: Rb-Sr isochron for the Similkameen batholith.

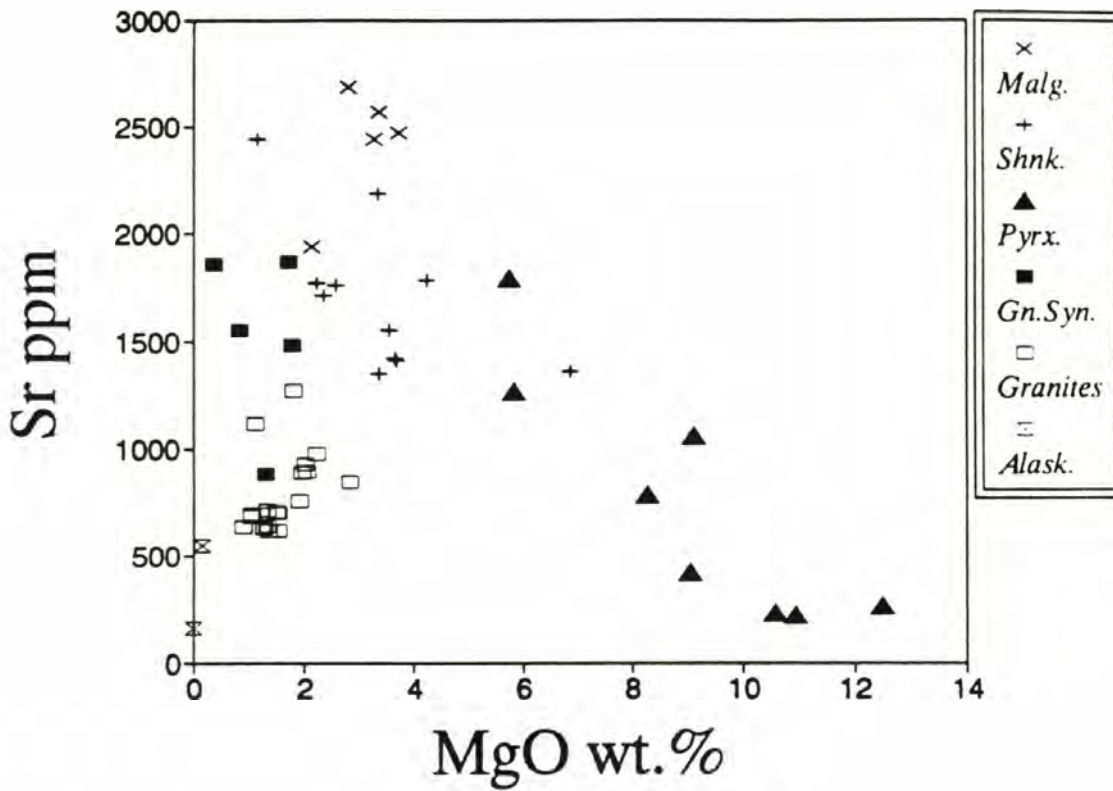


Fig. 3.13: Sr versus MgO variation diagram.

Similkameen Batholith Rb/Sr Data *170 Ma

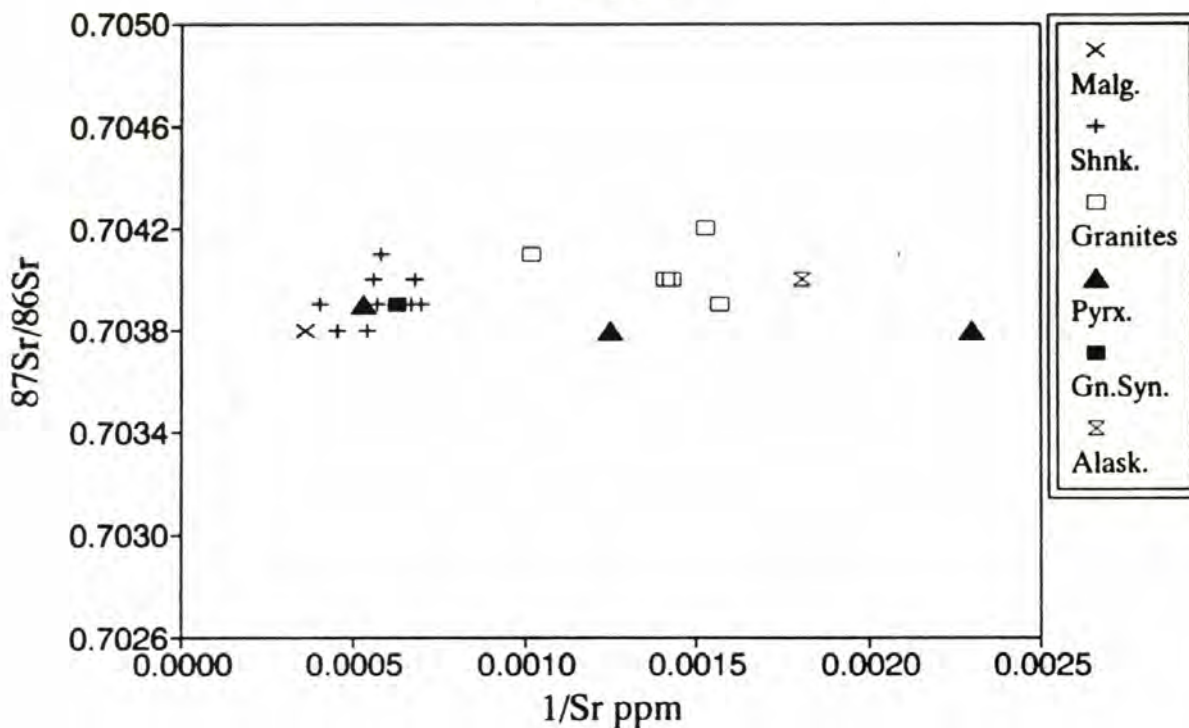


Fig. 3.14: $^{87}\text{Sr}/^{86}\text{Sr}$ versus 1/Sr (ppm) variation diagram. The initial-Sr ratios have been corrected to 170 Ma.

As discussed in previous sections, fractional crystallization played an important role in the geochemical evolution of the Similkameen suites. The tight horizontal cluster of data points (Fig. 3.14) for the alkaline suite rocks is in agreement with magmatic variation due to fractional crystallization (Arth et al., 1989). Note that the only malignite sample (SMK-111) plots away from the main cluster of the shonkinites suggesting it had a different source. The granitoids plot along a protracted horizontal line and are considerably displaced from the alkaline suite indicating a non-cogenetic or non-fractional crystallization relationship, but derivation from an isotopically similar source. The data points SMK-175 and SMK-183 are from separate granitoid plutons (Upper Snehumption Creek and Harry Lake plutons) and plot well away from the cluster of points for the Similkameen Valley pluton (SMK-179,195,120) also suggest derivation from different sources.

Assimilation and Fractional Crystallization

From the discussion above, assimilation of middle to upper-crustal materials was probably minor due to the low variations in the initial-Sr ratios. However, zircon fractions separated from the Horn Silver unit of the batholith yield 1.9 Ga upper intercepts on a U-Pb discordia trajectory (Armstrong, personal communication). The U-Pb data indicate some incorporation of continental crustal material within the Similkameen system.

The effects of assimilation and fractional crystallization (AFC) processes on initial isotope ratios and element concentrations of a parent magma may be evaluated quantitatively by the equations of DePaolo (1981). Based on the bulk distribution coefficient (K_d) of Sr, the effects of assimilation and/or fractionation can be monitored by constraining the rate of assimilation vs. crystallization. Table D.2 (Appendix D) shows the Sr isotope data of Similkameen magmas and crystalline rocks (from the southern Quesnellia region) used in the AFC modeling. All initial-Sr ratios and Sr concentrations have been adjusted to 170 Ma and all calculations have Sr K_d values = 0.60.

From the Sr-isotope calculations (Appendix D), several general conclusions about assimilation and fractionation processes operating within the Similkameen system may be offered. First, it appears that fractionation was the dominant process responsible for the variations in Sr concentrations observed within the shonkinites and malignites. Starting with initial concentrations of Sr (170 Ma) for a proposed parent composition (SMK-126), the observed trends in Sr concentrations could be generated by fractionation

of approximately 30 to 50% of the parent composition. SMK-189 is the approximated daughter composition.

Second, considering that the contaminants (SH-A, SH-D, SH-T) used are representative of lower to middle crustal rocks of the southern Quesnel region (Parkinson, 1987; Armstrong and Van der Heyden, 1989; Armstrong, personal communication), assimilation probably was not more than roughly 15% of the total volume of the system. At approximately 10 - 15% assimilation when Sr concentrations reach those of the proposed daughter composition, the calculated initial-Sr ratio has increased to or beyond the observed initial-Sr ratio of the daughter.

The calc-alkaline granitoids have slightly higher initial-Sr ratios (0.7039-0.7042) indicating the possibility of relatively more interaction with crustal components. Yet the initial ratios of the granitoids are low enough to imply a dominant mantle source or a crustal source of recent mantle derivation.

In summary, based on the low variation in the initial-Sr ratios, it appears that the alkaline and calc-alkaline suites were derived from isotopically similar sources. Fractional crystallization (+/-mixing with isotopically similar sources) may have produced some of the intrasuite variations in $1/Sr$ values. The significant differences in Sr concentrations between the alkaline and calc-alkaline suites as well as within the individual granitoid plutons is more likely the result of melting of different sources (refer to section, Source Components etc.). Assimilation of continental crustal material was not an important process during magma evolution of the two suites.

Modeling of Fractional Crystallization and Mixing

To test possible mineral fractionation schemes for the observed major element variations, mass-balance calculations based on the least-squares approximation method (Bryan et al., 1969; Bryan, 1986) using the computer-based analysis of Baker et al. (1987) were employed. The goal of the method is to determine if an end-member residual liquid can be derived from a known parent composition (magma) by the removal of mineral phases of known compositions (Fig. 3.15). Rayleigh fractionation is assumed for all runs. The calculated modal abundances of the removed mineral phases (cumulates) are then compared with the known modal abundances of the suspected cumulate samples (see above) to test the validity of possible crystal fractionation processes involved in the evolution of the Similkameen magmas.

A similar exercise was undertaken to evaluate mixing between the individual rock suites. The term mixing is not meant to imply magma mixing but is meant to infer an

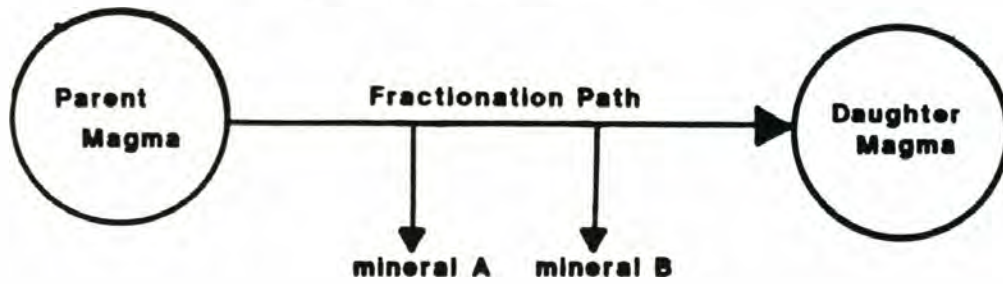
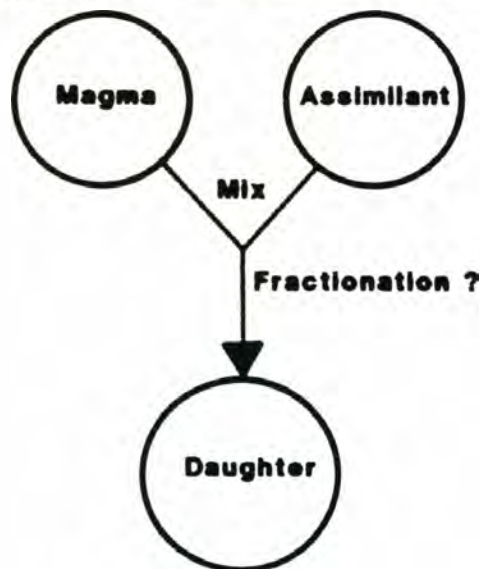
A**Crystal Fractionation****B****Mixing +/- Fractionation**

Fig. 3.15: (a) schematic flow chart showing hypothetical fractionation scheme. Minerals removed from a parent composition represent the cumulate assemblage; (b) schematic flow chart showing hypothetical mixing scheme (+/- fractionation) between endmember compositions.

interaction between mafic and silicic materials (see below). The goal of this approach is to determine if various intermediate compositions between the alkaline and calc-alkaline suites could be generated by mixing of selected end-member compositions (Fig. 3.15).

The plot of CaO vs MgO (Fig. 3.9) is used as an index of differentiation to compare end-member and intermediate compositions. The pyroxenites as well as samples SMK-158, 169, 190 were not used in any of the mass-balance calculations because these compositions do not represent equilibrium assemblages (see Appendix A). Several end-member compositions from the mafic alkaline and calc-alkaline suites were compared using combinations of various mineral compositions from both suites and the cumulate pyroxenites. This approach attempts to derive known calc-alkaline suite compositions from known compositions of the mafic alkaline suite via mineral fractionation. Intrasuite fractionation schemes are also tested. Because the mineral composition data from the Similkameen is limited, it should be stressed that the mass-balance comparisons can only be considered as first order approximations.

Mineral and liquid compositions used are listed under INPUT DATA in Appendix E. The calculated composition of the derivative liquid (daughter calc) is compared to the known composition, and weight proportions of the minerals removed and the derivative liquid are presented under SOLUTION. R-squared values represent the sum of the squares of the elemental residuals. Hence, lower R-squared values indicate closer fits between calculated and known daughter compositions. R-squared values < 1.0 are considered acceptable for mineral fractionation modeling schemes. All mineral compositions used are from the Similkameen batholith (see Appendix C) except for apatite and olivine compositions which were taken from an evolved mafic phonolite of the Highwood Mountains (O'Brien, 1988).

Alkaline to Calc-Alkaline Suite Fractionation

Over 50 mass-balance fractionation comparisons between the mafic alkaline rocks and the calc-alkaline granitoids were made. Mass-balance comparisons included the most evolved alkaline compositions (SMK-125, 142, 189, see Fig. 3.9) and the least evolved granitoid compositions (SMK-136, 163, 192) with various single and multiminerale combinations. Minerals used included amphibole (hastingsite), clinopyroxene, biotite, plagioclase, K-feldspar, apatite, and magnetite. In all comparisons, R-squared values were > 8.0 with the majority being >> 10, and proportions of fractionated mineral phases were unrealistic. Thus, combinations of end-member and mineral compositions, revealed no acceptable solutions attributing the alkaline and calc-alkaline suites to crystal fractionation schemes.

Intrasuite Fractionation for the Alkaline Rocks

Major element oxide plots indicate a generally linear relationship throughout the alkaline suite rocks yet there is considerable variation particularly between the malignites and the shonkinites (see above). Numerous mass-balance comparisons were made to relate the malignites and shonkinites by variable phase mineral fractionation processes but no acceptable fits were obtained for any of the fractionation combinations.

Table 3.1 gives the results of mass-balance calculations for samples within the malignite and shonkinite series. Note that stepwise comparisons from the least evolved to the most evolved samples within each series indicates that multimineral fractionation could indeed produce the observed end-member compositions for each series.

For the malignite series, runs between compositional endmembers (SMK188-204) as well as intermediate compositions (SMK188-111.a, 111.a-204), yield acceptable R-squared values and realistic proportions for cumulate assemblages which approximate modal abundances within the pyroxenites. The fractionating assemblage is: clinopyroxene + biotite + magnetite + apatite. Stepwise comparisons for the shonkinite series yield similar results (Table 3.1). Runs between the compositional endmember (SMK-209) to intermediate compositions (SMK-125, 142) require 3 or 4-phase fractionation schemes involving clinopyroxene + biotite + magnetite +/- apatite. For runs from the intermediate compositions (SMK-125, 142) to the most evolved shonkinitic endmembers (SMK-189), the required fractionating assemblage includes clinopyroxene +/- biotite +/- amphibole (hastingsite) +/- magnetite +/- apatite. Runs with both biotite and amphibole together produced unacceptable results. Runs between compositional endmembers (SMK-209, 189) were difficult to match and it appears that stepwise, variable phase mineral fractionation can best explain the observed compositional trends. The early to middle part of the fractionation sequence includes clinopyroxene + biotite + magnetite + apatite, whereas the middle to more evolved portions can include either clinopyroxene + biotite + magnetite + apatite or clinopyroxene + amphibole + magnetite. The calculated assemblages have modal abundances approximating those observed in the biotite and amphibole-bearing pyroxenites (see Appendix A, Appendix E).

Runs between the most primitive shonkinite (SMK-207, see Fig. 3.9) and the main trend of shonkinites did yield acceptable results when the fractionating assemblage diopsidic clinopyroxene + olivine + K-feldspar + biotite was used. However, petrographic and trace element data show no evidence of olivine fractionation.

The results from runs between the shonkinites and the gneissic syenites are in agreement with the observed modal abundances of the pyroxenites (Table 3.1). Removal

	Malignites			
Parent	SMK188	SMK111.a	SMK188	
Daughter	SMK111.a	SMK204	SMK204	
Cumulate	Cpx,Bi,Mt,Ap	Cpx,Bi,Mt,Ap	Cpx,Bi,Mt,Ap	
R-square	0.827	0.366	0.659	
	Shonkinites			
Parent	SMK209	SMK209	SMK125	SMK142
Daughter	SMK125	SMK142	SMK189	SMK189
Cumulate	Cpx,Bi,Mt,Ap	Cpx,Bi,Mt,Ap	Cpx,Am,Ap	Cpx,Bi,Mt,Ap
R-square	0.742	0.354	0.752	0.594
	Gneissic Syenites			
Parent	SMK142	SMK142		
Daughter	SMK211	SMK167		
Cumulate	Cpx,Am,Mt,Ap	Cpx,Bi,Mt,Ap		
R-square	0.085	0.628		
	Granitoids			
Parent	*SMK125	SMK120	SMK192	SMK176
Daughter	SMK120	SMK195	SMK136	SMK195
Cumulate	Cpx,Bi,Mt,Ap	Am,Pl,Kf,Mt,Ap	Am,Pl	Am,Pl,Kf,Mt
R-square	16.45	0.01	0.175	0.065
	* Shonkinite/Granitoid Run			
Parent	SMK195	SMK183	SMK183	
Daughter	SMK175	SMK192	SMK175	
Cumulate	Am,Kf,Mt,Ap	Am,Pl,Kf,Mt,Ap	Am,Pl,Kf,Mt,Ap	
R-square	0.008	0.366	3.520	

Table 3.1: Results From Mass Balance Comparisons

of clinopyroxene + biotite + magnetite + apatite from a parent shonkinite (SMK-142) could yield liquids similar in composition to the gneissic syenites (SMK-167, 211). Therefore, it appears that the gneissic syenites were derived from the shonkinites by crystal fractionation.

Granitoids

The lithologic and chemical variations exhibited by the calc-alkaline granitoids has led to the identification of three intrusive units (see above, Appendix A). Mass-balance calculations indicate that the compositional variations within the granitoids is mainly related to varying degrees of fractional crystallization.

Runs of end-member and intermediate compositions, within and between the separate units (see below) yielded several acceptable R-squared values (Table 3.1). Mineral assemblages used include analyzed mineral compositions from a quartz monzonite (SMK-120) phase of the Similkameen Valley pluton.

The Harry Lake pluton (SMK-183) can be linked to the monzonites of the Similkameen Valley pluton by hornblende + plagioclase + K-feldspar + magnetite + apatite fractionation. Runs between the Harry Lake pluton and the granodiorite of Upper Snehumption Creek (SMK-175) produced unacceptable results (R-squared > 10.0), which may indicate a different source for the Harry Lake pluton (see Rb-Sr geochemistry), but several mass-balance comparisons gave acceptable results for a fractionation relationship between the Similkameen Valley pluton and the monzonites of the Snowy Mountain area (see Table 3.1)

Mixing

Although no appropriate fractionating assemblages were found to link the alkaline and calc-alkaline suites, several mixing assemblages between the two suites were determined which produced compositions approximating known intermediate compositions, i.e., compositions within the major element overlap between the two suites (Fig. 3.9).

Table 3.2 gives the results of mixing comparisons using the computer program MULTIFIT (Bryan, 1986). Similar to the mass-balance comparisons discussed above, this analysis takes endmember compositions (variable arrays) and "fits" the endmember compositions to known intermediate compositions (solution arrays) and determines the best fit solution (Appendix E). For each solution array, weight fractions and a corresponding sum of the squared residuals are computed. As with the fractionation mass-balance calculations, low R-squared values (< 1.0) for the mixing assemblages

Results From Mass-Balance Mixing Runs

Parent A	SMK209	SMK209	SMK209	SMK188
Parent B	SMK194	SMK194	SMK194	SMK195
Mixed Daughte	SMK179	SMK120	SMK136	SMK179
R-squared	0.2887	0.0344	0.672	0.2894

Results of Mass-Balance
Comparisons From Mixed End Members

Mixed Parent	SMK134.CA
Daughter	SMK189
Cumulates	Cpx,Am,Mt,Ap
R-squared	0.295

Table 3.2: Results From Mass Balance Mixing Runs

indicates a positive correlation between the variable array and the individual solution arrays.

Mixing between the shonkinite SMK188 and various granitoid compositions (SMK-183, 194, 195) did produce intermediate compositions approximating several of the observed mafic syenite compositions (SMK-134, 158, 169), (Table 3.2, Appendix E). Table 3.2 also shows the results of mixing runs of selected mafic alkaline (SMK-188, 209) and calc-alkaline compositions (SMK-194, 195) that produced good fits with several of the higher MgO granitoids.

The samples SMK-158 and SMK-169, which were not used in the fractionation comparisons (non-equilibrium assemblages, see above and Appendix A), were used in the mixing comparisons. These samples are located within or near contact zones between the mafic alkaline and calc-alkaline rocks and the results of mixing calculations are consistent with derivation of these compositionally anomalous rocks by mixing of the two suites.

Fractional crystallization superimposed upon mixing is another process which explains some of the observed major and trace element chemical variance. Both processes acting simultaneously produce compositions that can not be explained by either process alone. Similar mass-balance calculations yielded acceptable results for the fractionation of clinopyroxene +/- biotite +/- amphibole + magnetite + apatite to generate some mafic syenites (e.g., SMK-189) from mixed compositions (SMK-134.CA), (see Table 3.2).

The discussion above suggests that mixing (+/- crystal fractionation) of mafic and silicic compositions could produce daughter compositions similar to several of the compositions that can not be explained by crystal fractionation alone. Taken in this context, mixing was a process by which silicic magmas incorporated mafic materials. The mafic materials were likely to have been crystal-liquid mushes because liquid-liquid mixing textures (e.g., magma mixing) have not been observed yet clinopyroxene xenocrysts are found in some of the mixed granitoid assemblages.

Source Components for the Alkaline and Calc-Alkaline Suites

The data presented above demonstrate that the mafic alkaline and calc-alkaline suites are not related by crystal fractionation, yet many major and trace element similarities exist between the two suites. Normalized element profiles (Fig. 3.16) for the two suites show very distinctive and, in general, similar trends. Both suites are enriched in Ba, K, Rb, and Sr and both exhibit negative spikes in Th, Nb, P, and Ti. The alkaline

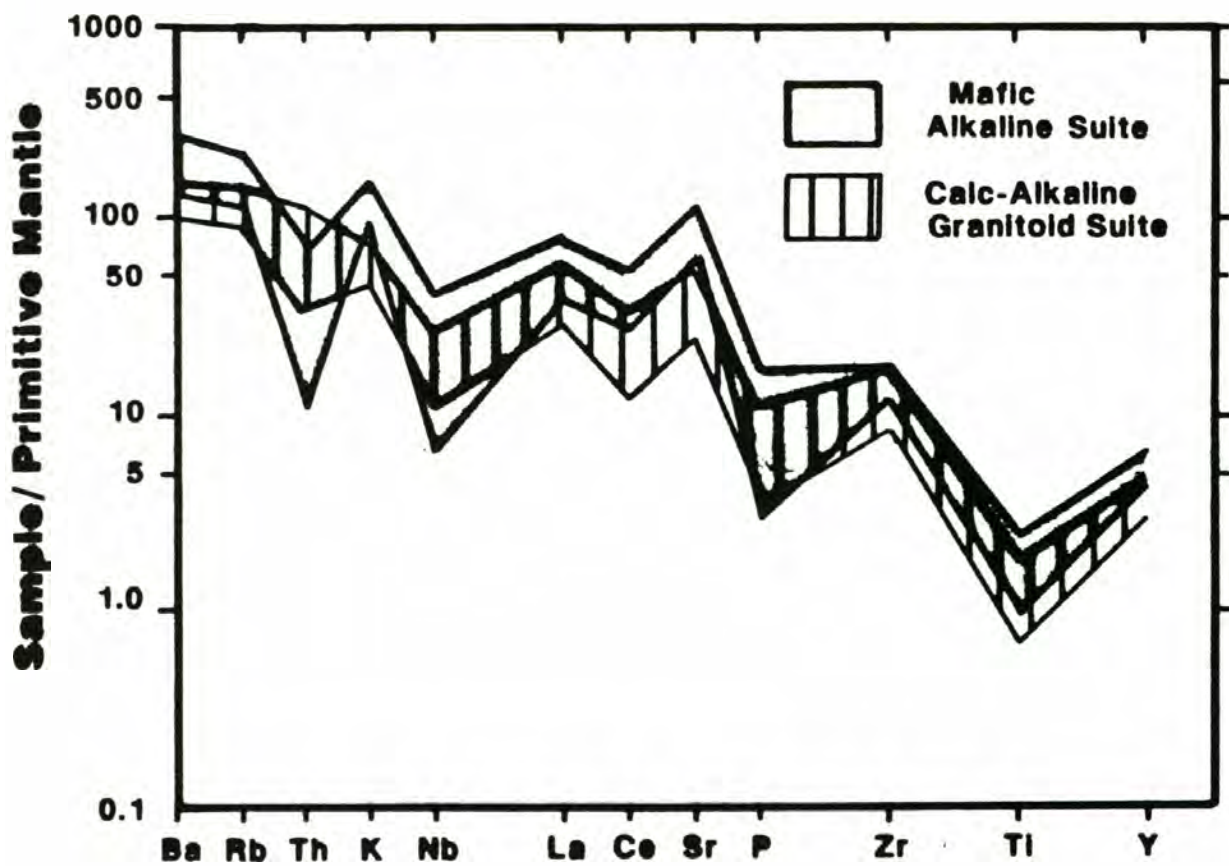


Fig. 3.16: Normalized incompatible element variation diagram for the mafic alkaline and calc-alkaline suites. Normalization values are from Wood, 1979.

suite is enriched in Ba, Rb, K, Sr, and Ce with greater depletions in Th and Nb relative to the calc-alkaline granitoids. The observed depletions in Ti, Th, and Nb, (Ta assumed) and enrichments in incompatible elements for both suites are characteristic of subduction zone magmas (Perfit et al., 1980; Arculus and Powell, 1986; Luhr, et al., 1989). A mantle origin for the mafic rocks is assumed based on the rare earth element (REE) and Sr isotopic evidence as well as their mafic character.

Calc-Alkaline Granites

Major and trace element discrimination diagrams of the granitic rocks confirm a magmatic arc affinity. In Figure 3.17 all the granites plot within the volcanic arc field, which indicates a crustal source (Pearce et al., 1984). Using the tectonic discrimination scheme of Maniar and Piccoli (1989), the majority of the samples plot within the continental arc granite field although a group (with consistently higher molar Na₂O) plots within the continental collision granite field (Fig. 3.18). The granitic rocks are I-type in character based on their chemical and mineralogical properties (Chappell and White, 1974), (Fig. 3.19).

In Figure 3.20, REE compositions of two granitoids (SMK-183 and SMK-195) are plotted with the mafic alkaline rocks. In general, the granitoids exhibit REE patterns similar to the mafic rocks; they are moderately LREE enriched and lack negative Eu anomalies. These rocks have distinctive concave upward REE patterns (Dy < Lu) which indicates either amphibole fractionation or melting from a source dominated by amphibole. The lack of negative Eu anomalies implies either feldspar was not an important fractionating phase or that the granitoid magmas were derived from a source containing little to no residual feldspar.

The granitoids display similar patterns but have quite a range in normalized abundances. The least evolved sample (SMK-183, see Major Element Geochemistry above) contains higher REE abundances, which suggests that either SMK-183 was derived from a relatively more enriched source (than SMK-195) or that SMK-183 represents earlier, lower-degree partial melts with respect to SMK-195.

The observed REE patterns of the granitoids preclude the possibility that the granitoids originated from the same source as the mafic rocks. The systematically lower REE abundances of the granitoids, particularly the LREE's, might suggest that the granite melts were higher degree partial melts from the same source region as the mafic rocks. But, the silicic nature of the granitoids precludes this possibility. The possibility that the mafic rocks themselves were a source is doubtful because of the same arguments; the granitoid LREE abundances are lower, not higher, than the mafic rocks. Any partial

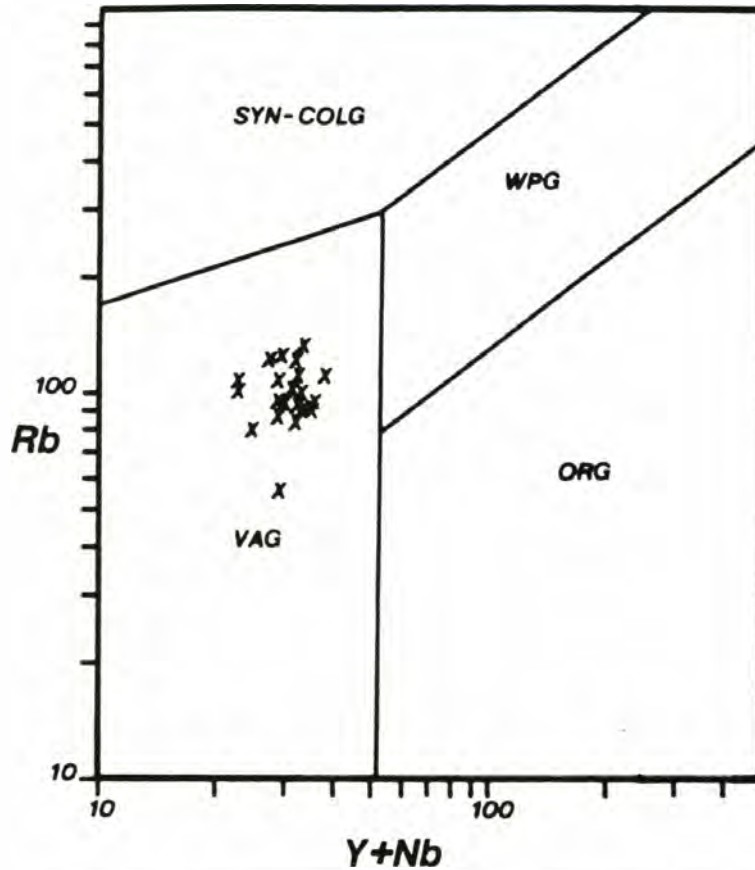


Fig. 3.17: Rb versus Y+Nb granite discrimination diagram (after Pearce et al., 1984) for the Similkameen batholith granitoids. This plot shows a strong crustal component for the granitoids.

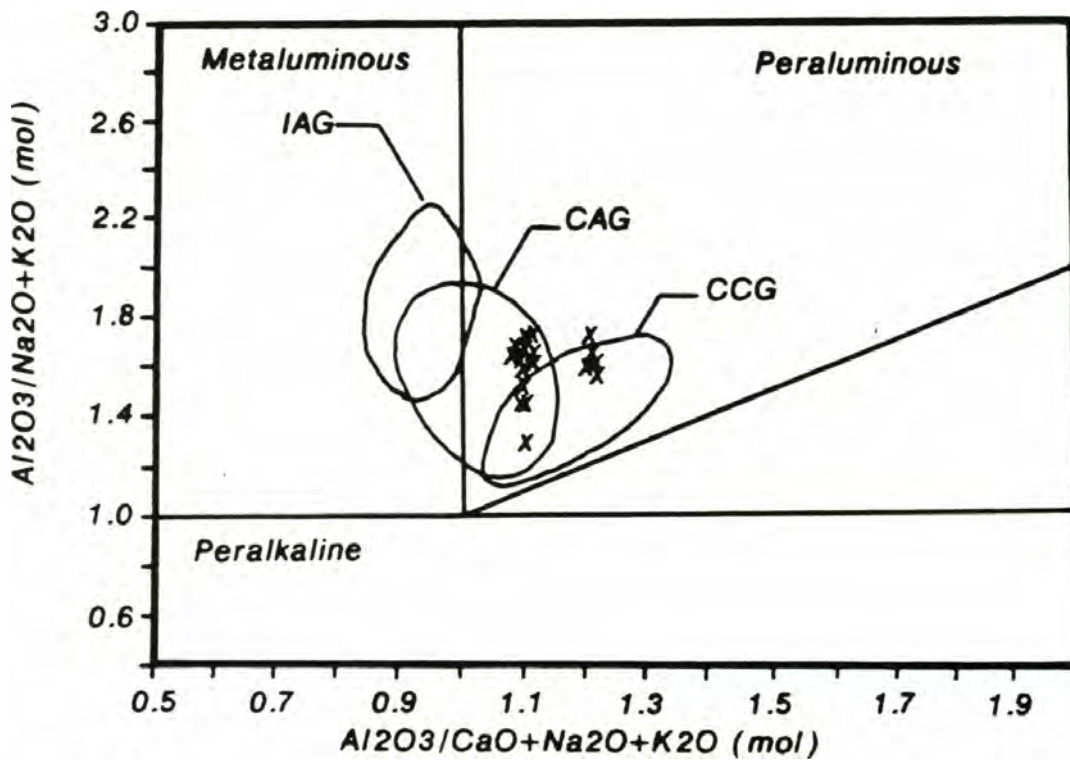


Fig. 3.18: Granitoid discrimination plot (after Maniar and Piccoli, 1989) for the Similkameen granitoids.

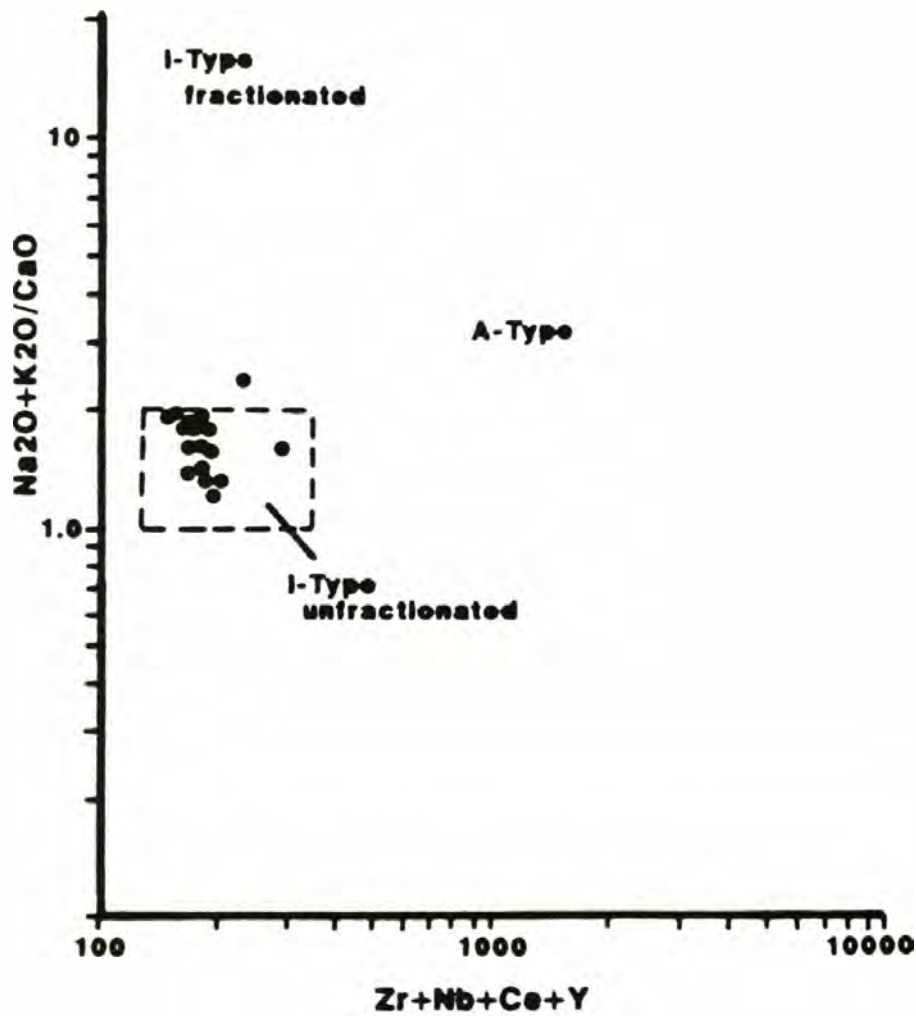


Fig. 3.19: Plot of $\text{Na}_2\text{O}+\text{K}_2\text{O}/\text{CaO}$ versus $\text{Zr}+\text{Nb}+\text{Ce}+\text{Y}$ (after Whalen et al., 1987) showing I-type character for the Similkameen granitoids.

melts from the mafic rocks would produce highly enriched LREE and incompatible element patterns which would be significantly more enriched than the mafic rocks.

As discussed above, a crustal source for the generation of the granitoids is likely. Lower crustal mafic granulites may have been the source for the Similkameen granitoids. Partial melting of a mafic granulite (2 pyroxene + garnet + low feldspar) could produce silicic melts with similar incompatible element profiles (Wilson, 1989) and moderately low initial-Sr ratios with little to no negative Eu anomalies. A granulitic source is attractive because higher degree partial melts (5 -15%) could still produce silicic melts. The volume of melt generated would be greater thus alleviating the problem of how to get high volumes of low degree partial melts from a mantle source.

Mafic Alkaline Suite

The mafic alkaline rocks show light rare earth element (LREE) enriched patterns (Fig. 3.20) consistent with derivation from a garnet-bearing source (Kay and Gast, 1973). Another possibility is that the Similkameen magmas were derived from a LREE-enriched source. The absence of a defined Eu anomaly indicates either magma generation from a feldspar-free source or relatively minor feldspar fractionation within the system. The slopes of the REE patterns are similar for all the alkaline suite samples from the most primitive shonkinite (SMK-207) to the evolved shonkinites and malignites indicating that the LREE/HREE ratios remained constant throughout the evolution of the Similkameen magmas.

The normalized trace element profiles exhibit some variation for selected incompatible elements within the alkaline suite of rocks (Fig. 3.16). For example, the malignites show greater depletions in Nb relative to the shonkinites. Minor elemental variations could represent varying degrees of partial melting and/or crystal fractionation of a homogeneous source region. More significant variations can not be explained by these processes so other possibilities such as magma contamination or partial melting of a chemically heterogeneous source must be addressed. Plots of incompatible trace element ratios with similar KD values are particularly useful because ratios of these elements should remain relatively constant during partial melting and crystal fractionation processes, and thus may provide clues to source region characteristics and magma forming processes.

Incompatible trace element variation is apparent indicating that two distinctive chemical suites are present. The "malignite" series is enriched in Ba but depleted in Nb and Zr relative to the "shonkinite" series. In the plot of Ce/Y versus Zr/Nb (Fig. 3.21), both series have consistent Ce/Y ratios and the variation observed appears to be

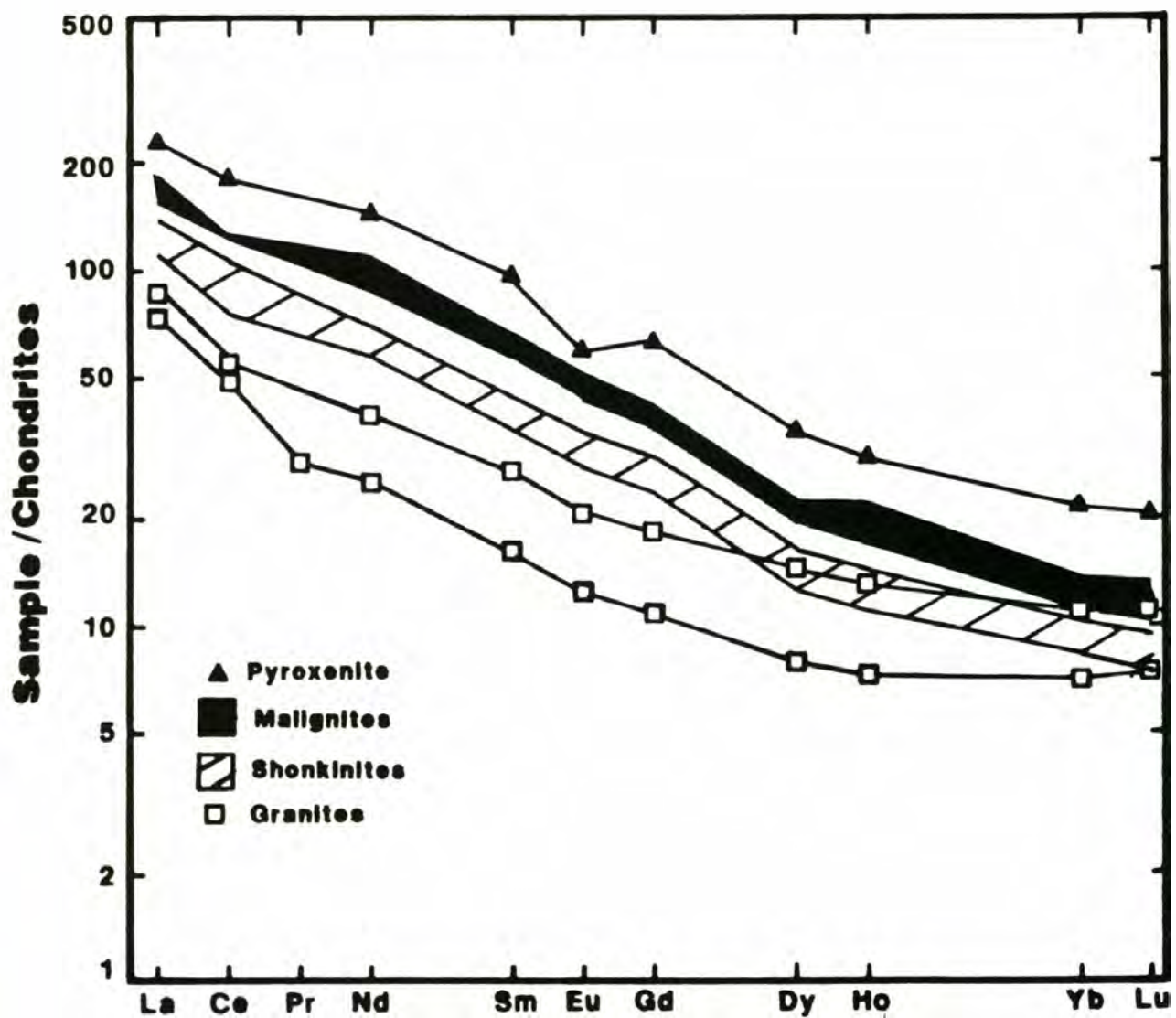


Fig. 3.20: Chondrite normalized REE plot for selected Similkameen samples. Normalization values are after Sun and McDonough (1989).

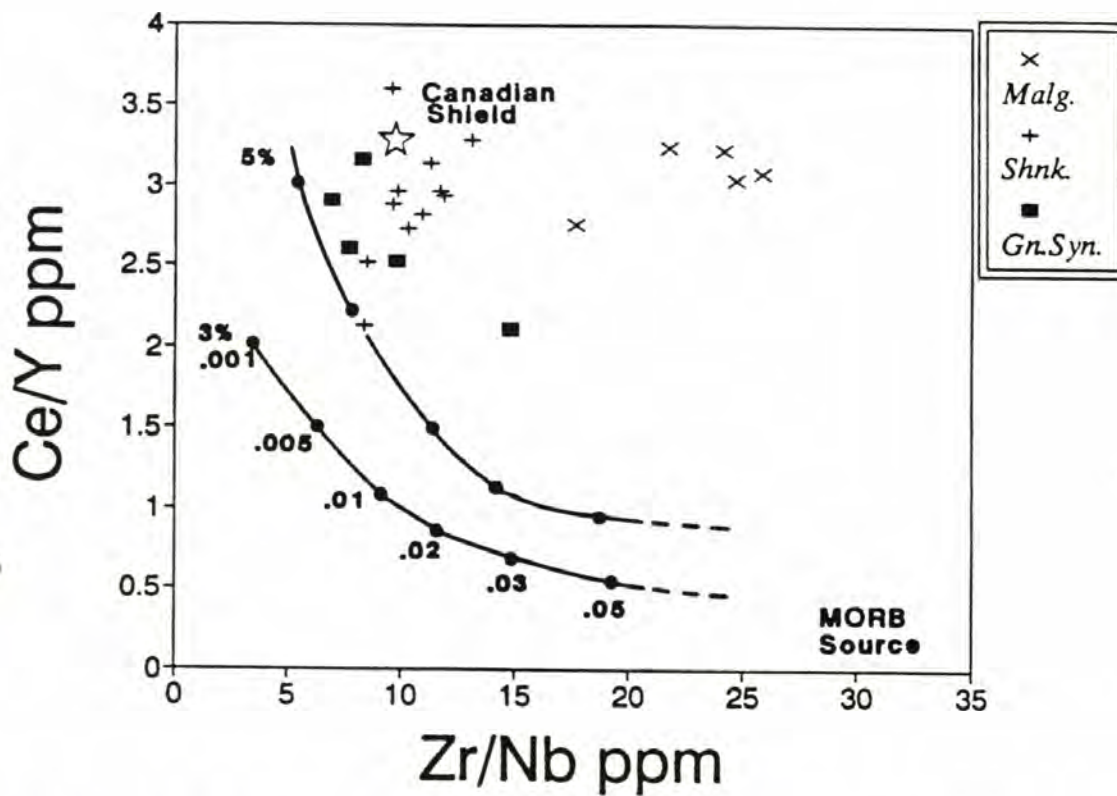


Fig. 3.21: Plot of Ce/Y versus Zr/Nb for the mafic alkaline suite rocks. MORB-source melting curves and crustal values are from Smedley (1988).

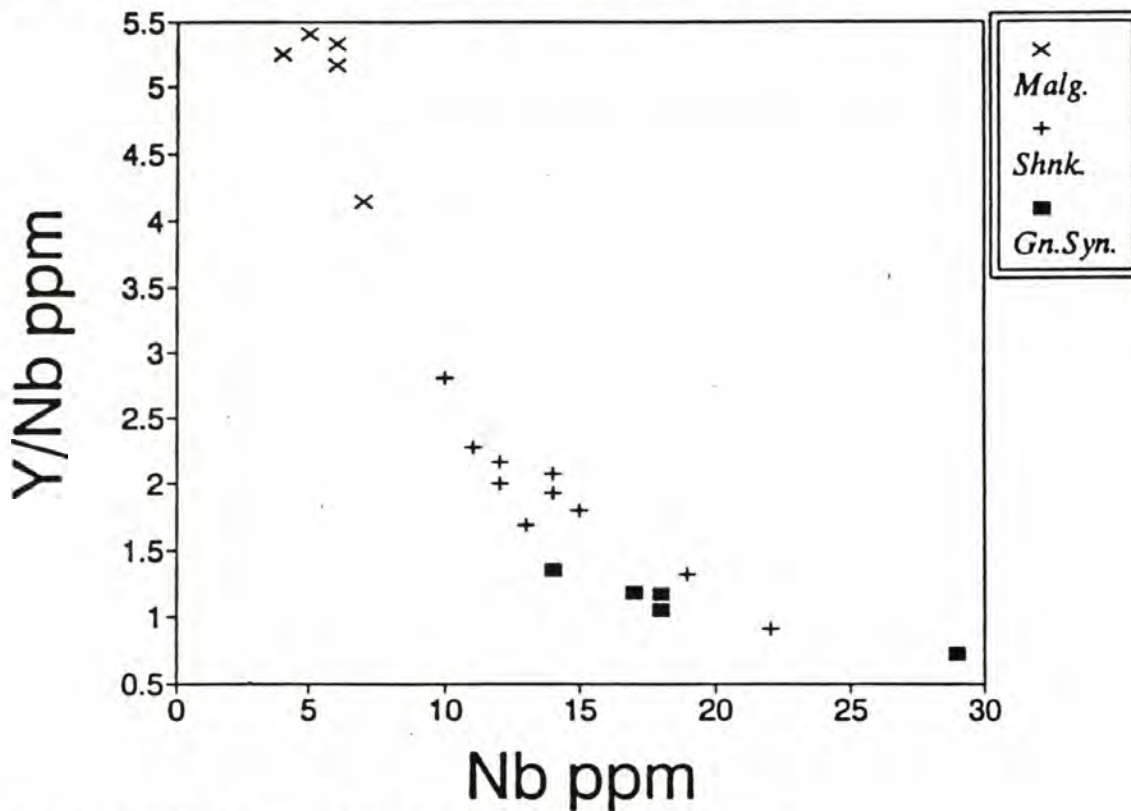


Fig. 3.22: Plot of Y/Nb versus Nb for the mafic alkaline suite.

controlled by Nb concentrations (Fig. 3.22). In Figure 3.23 the samples plot along a disrupted linear OIB-MORB (ocean island basalt, mid ocean ridge basalt) source mantle array with the shonkinite series exhibiting an "enriched" character with respect to the "depleted" character of the malignite series.

Figure 3.24 illustrates the significant Ba-enrichments for the malignite series. The plot of Ba/Zr versus Mg# (Fig. 3.25) establishes that the Ba-enrichments observed are not a function of differentiation; the shonkinite series is well removed from the Ba-enriched malignite series. The variations in Ba concentrations reflect either heterogeneous source component characteristics or magma modifications (e.g., assimilation, chamber recharge, etc..) after initial development of the individual series.

Discussion

From the trace element ratio plots, it appears that two distinctive series exist within the mafic alkaline rocks. The malignites have a depleted signature consistent with a MORB-type source, whereas the shonkinites exhibit incompatible element enrichments suggestive of an OIB-type source component.

Simplified models for the origin of the trace element variations can be tested using published distribution coefficients for various mineral phases when applied to fractional crystallization and partial melting equations. If the observed chemical variations within the alkaline suite originated from primary melting processes (e.g., variable depth melting or progressive partial melting from a mantle source), then the initial melts should have higher incompatible element concentrations relative to the source. The plot of Ce/Y versus Zr/Nb (Fig. 3.21) is particularly useful because small degree partial melts should plot with high Ce/Y and low Zr/Nb ratios. This is because Ce and Nb are incompatible within mantle derived melts when compared to Y and Zr. With continued melting, extracted magmas should contain lower concentrations of Ce and Nb relative to Y and Zr, thus progressive batch melts will plot along a negative sloping curve toward the mantle source composition.

Smedley (1988) argued that variations in Ce/Y versus Zr/Nb ratios for basalts from the Dinantian province are very difficult to explain with variable depth melting or progressive partial melting models because, although the basalts exhibit considerable variability in Ce/Y ratios, the normalized Y concentrations of all the Dinantian basalts show consistent depletion relative to more incompatible elements. If melting were to occur over a range of depths, for example melting of a spinel-bearing to a garnet-bearing source, Y (and other selected HREE's) would become more compatible with increased

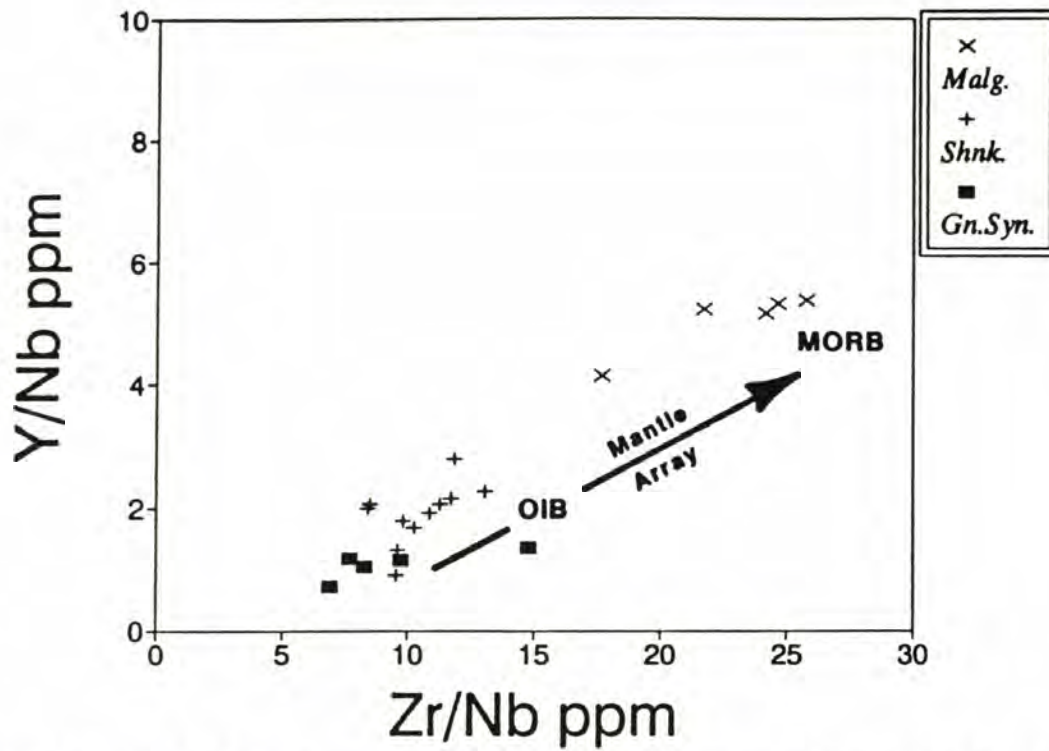


Fig. 3.23: Plot of Y/Nb versus Zr/Nb compositions in mafic alkaline rocks. Samples plot along a disrupted linear mantle array.

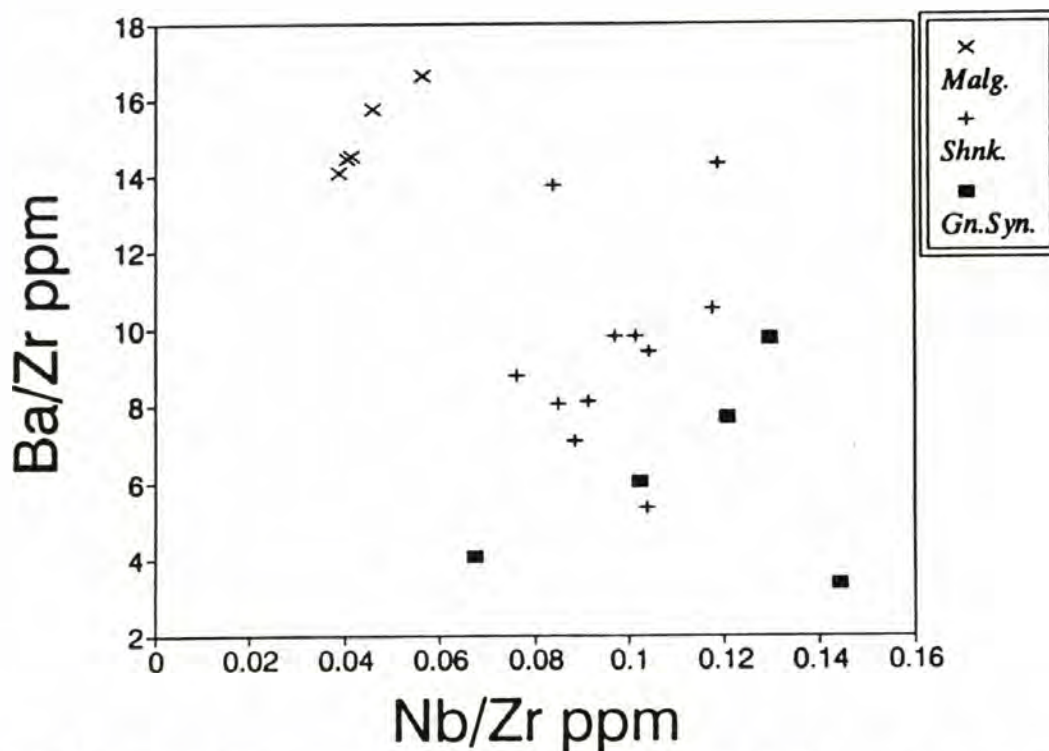


Fig. 3.24: Plot of Ba/Zr versus Nb/Zr compositions within the mafic alkaline rocks. Note the significant enrichments in Ba for the malignite series relative to the shonkinte series.

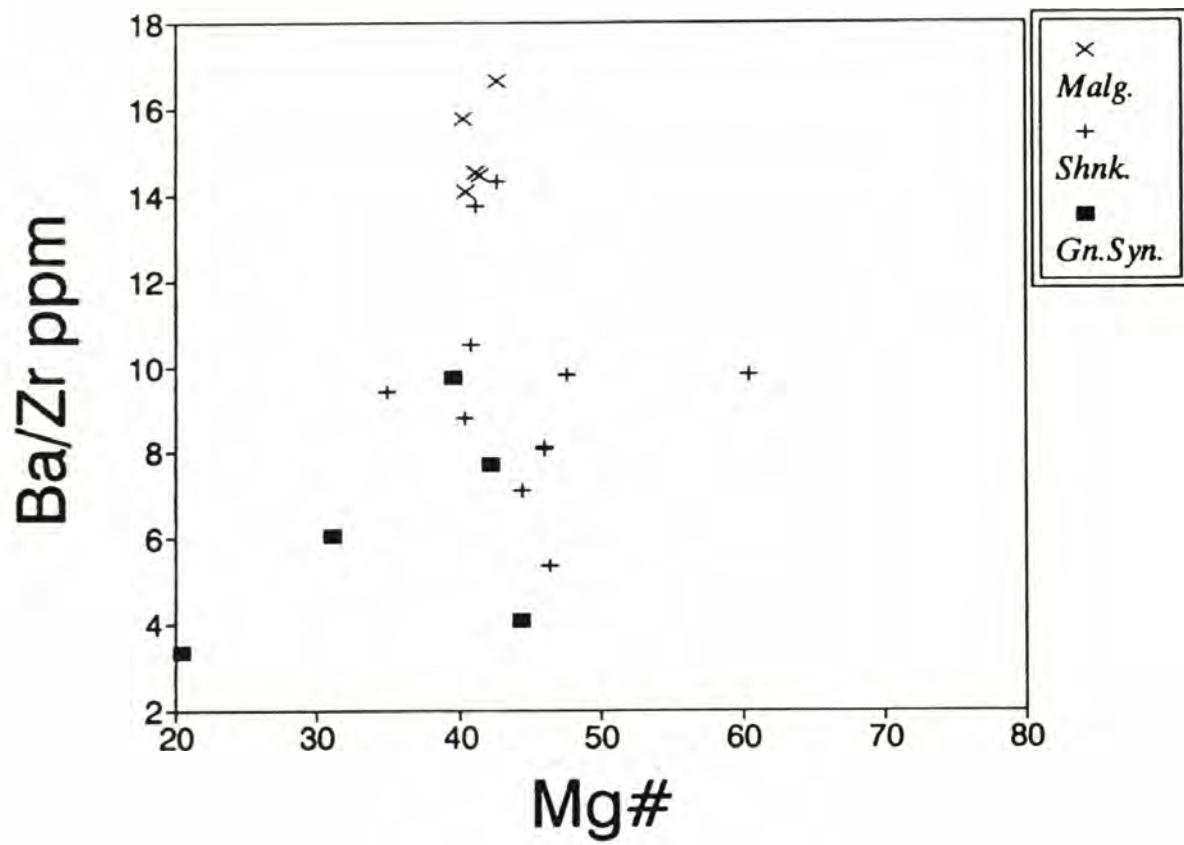


Fig. 3.25: Plot of Ba/Zr versus Mg# for the mafic alkaline suite.

modal abundances of garnet in the source. Therefore, a discernible variation in Y concentrations should be observed. This same argument holds for a progressive partial melting model of a garnet-bearing source. With continued melting and garnet exhaustion, depletion in garnet components (i.e., Y) should be observed in the successive melts as a sharp decline in Y. But, as was pointed out above, the variations in Fig. 3.21 are controlled primarily by Nb concentrations. Partial melting of a phlogopite-bearing source ($D_{Nbphl} = 0.002 - 1.0$) does increase the Zr/Nb ratio some but also decreases the Ce/Y ratios. The relatively constant Ce/Y ratios and the low variability of Y concentrations (Fig. 3.16) within the alkaline rocks of the Similkameen, are probably not due to simple variations in the degree of partial melting.

An alternative model involves the process of fractional crystallization (Rayleigh fractionation) of one or more mineral phases in which Nb is compatible. Samples from the malignite and shonkinite suites do not have substantially different Mg#s which precludes the possibility of dramatically different fractionation histories. As discussed by Smedley (1988), amphibole or clinopyroxene removal may fractionate the Ce/Y ratio but doesn't account for the variations in the Zr/Nb ratios. Phlogopite and/or magnetite fractionation may have been responsible for the variations in Zr/Nb ratios because Nb is moderately to highly compatible ($D_{Nbphl} = 0.002 - 1.0$, $D_{Nbmt} = 0.4 - 2.0$) with these phases in basaltic melts. Fractionation of Nb for values equivalent to the shonkinites to the highest values of the malignites would require $\gg 60\%$ phlogopite or $>30\%$ magnetite removal from a common parent! Either phlogopite or magnetite removal increases the Ce/Y ratio at a greater rate than increases to the Zr/Nb ratio and such variations aren't observed in the mafic rocks. Thus, neither phlogopite nor magnetite fractionation appears to be responsible for the variations in the Zr/Nb ratios.

Mixing of depleted mantle-derived magmas (MORB) with continental crust could explain the Zr/Nb variability. The ratios for Canadian Shield rocks have been plotted with the Similkameen samples (Fig. 3.21) showing a possible mixing trend between the malignite suite and continental crustal rocks, with the shonkinites as intermediate compositions. However, Sr-isotopic evidence precludes this possibility (see above).

A final alternative to explain the Zr/Nb variability between the shonkinite and malignite series is derivation by partial melting and/or mixing within a chemically heterogeneous mantle source. Additionally, there are systematic differences in many other incompatible trace element ratios that cannot be explained by partial melting or fractionation of magmas generated from a homogeneous source region. So, it appears that the trace element variations observed within the two series are a reflection of their source.

Table 3.3 displays the ranges of trace element ratios for the mafic rocks from the Similkameen. It is apparent that the ratios for the shonkinites are intermediate to ratios of the malignites and those of OIBs and OIB sources. For further comparison of possible source components, the trace element ratios for the average MORB source has been included. In most comparisons, the malignites have ratios nearer the MORB source values.

Source component mixing within the regions of arc magma generation has been suggested for such chemical heterogeneities as enrichments of the alkali and alkaline earth elements and depletions in the high-field-strength elements, isotopic discontinuities, and incompatible element ratio variations (Green, 1973; Arculus and Powell, 1986; Hickey et al., 1986; Smedley, 1988; Luhr et al., 1989; Verma and Nelson, 1989). The consistently enriched nature of the shonkinite series relative to the malignite series indicates that mixing of OIB-like melts with depleted magmas or mixing of OIB-like components with slab derived materials could produce the different incompatible element ratios observed in the two suites. The fact that the malignite and shonkinite series have generally similar major element compositions is consistent with mixing in a mantle source region.

The ratios in Table 3.3 that include Ba do not show clear correlations with an enriched component because of the order of magnitude or greater Ba-enrichments (Fig. 3.24) within the malignites. The Ba-enrichments may have been the result of mixing of source magmas with variable amounts of subducted materials such as pelagic sediments (Weaver et al., 1986; Othman et al., 1989). However, Pb/Ce ratios don't correlate with Ba enrichments which indicates little or no involvement of pelagic sediments (Othman et al., 1989). Partial melting of zones rich in phlogopite could produce K and/or Ba-enrichments in the derivative magmas. Wyllie and Sekine (1982) proposed the process of "mantle hybridization", by which hydrous silicic melts derived from fluids released from slab materials react with mantle peridotite to form a hybrid rock composed primarily of phlogopite and pyroxenes. The hybrid rock forms at the expense of the siliceous melts and olivine with additional liberation of water-rich volatiles. Ultimately the hybridized mantle above the slab will become an olivine-free phlogopite and garnet-bearing pyroxenite. This hybridized mantle is thus a convenient K-rich source to produce the potassic magmas by partial melting.

	Malignites	Shonkinites	OIB Source*	MORB Source*	Crust and/or Pelagic Sediments*
Ba/Nb	295 - 363	51 - 115	6 - 19	3.9	21 - 110
La/Nb	6 - 17	2 - 3.5	0.6 - 1.6	1	1.5 - 3.1
Zr/Nb	18 - 26	9.9 - 13	3 - 16	37	8
K/Rb	372 - 560	286 - 416	260 - 490	1060	126 - 455
K/Ba	18 - 40	22 - 47	13 - 40	88	21 - 51
Ba/Rb	11 - 31	7 - 18	11 - 34	12	4 - 13
Ba/La	41 - 51	26 - 51	7 - 17	3.9	14 - 49
La/Y	1.3 - 1.7	1.2 - 1.6	0.7	0.09	0.9
La/Sm	3.95	4.25	2 - 9	1	-

* Values from Verma & Nelson (1989) and references therein.

Table 3.3: Incompatible Element Ratios

Magma Petrogenesis and Tectonic Setting

The geochemical characteristics of the mafic alkaline and calc-alkaline suites indicate that both were derived from sources affected by subduction. Both suites contain alkali and alkaline earth element enrichments with marked depletions of high-field-strength elements characteristic of arc magmas. The Sr-isotopic data and high LREE/HREE ratios for the mafic alkaline rocks are consistent with a mantle origin.

Figure 3.26 depicts a possible model for generation of the Similkameen magmas. Hydrous melts enriched in LREE, alkali, and alkaline earth elements are released from a subducting oceanic crustal slab into the overlying sublithospheric mantle wedge beneath the North American craton. These hydrous silicic fluids or melts react with the overlying peridotite to create heterogeneous K-enriched zones or veins of crystallized phlogopite + pyroxene (Sekine and Wyllie, 1982; Wyllie and Sekine, 1982; Johnston and Wyllie, 1989). The thermal regime of the subduction zone probably requires the crystallization of the K-rich melts before they are able to rise significantly (Wyllie, 1979). The veined peridotite is then entrained by slab-induced downward transport within the mantle wedge but undergoes further partial melting at depth by increased temperatures and the continued infiltration of slab-derived hydrous fluids. The consequent partial melts then coalesce to form mafic potassic melts which then begin their ascent through the overlying sublithospheric mantle wedge.

The origin of enriched versus depleted mantle sources for arc generated magmas is still controversial. Some workers have proposed that the subarc mantle wedge is composed of enriched (OIB-source) asthenosphere (Hickey et al., 1986, 1989; Verma and Nelson, 1989). Other models suggest that the mantle wedge is composed of a depleted (MORB-source) asthenosphere overlain by enriched subcontinental lithosphere (Green, 1973; Kay, 1980; Hickey et al., 1986; O'Brien et al., in press). Still other models call on a stratified wedge in which the deeper portions are composed of OIB-like asthenosphere which is overlain by metasomatically streaked or veined subcontinental lithosphere. In all these, the enriched nature of the subarc asthenosphere or subcontinental lithosphere was developed during earlier enrichment (subduction) episodes.

In Fig. 3.26, the K-rich partial melts originate within the subcontinental lithospheric mantle that contains heterogeneous contamination of "hybridized veined peridotite". The potassic nature and enrichments in alkaline earth elements of the partial melts is inherited by variable amounts of melting and incorporation of the metasomatized veined peridotite. These melts then ascend through and interact with the overlying depleted (MORB-source) subcontinental lithospheric mantle. Depending on the relative

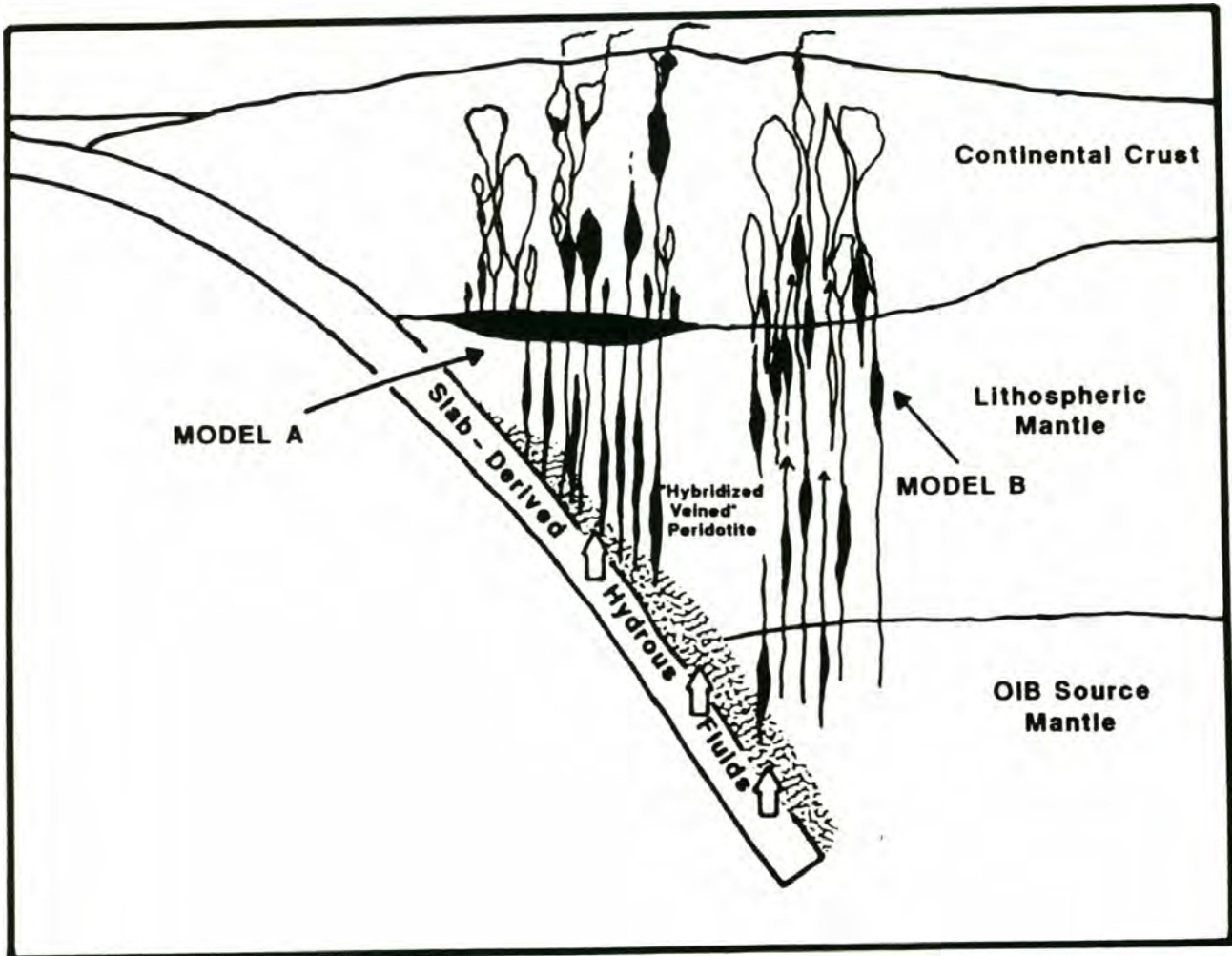


Fig. 3.26: Schematic diagram showing the origin of the Similkameen magmas. Metasomatism or hybridization of mantle peridotite is the result of reaction of slab derived fluids with peridotite to form an enriched, pyroxene and phlogopite-bearing peridotite. The proposed model (Model A) involves the partial melting of "hybridized veined" peridotite to create variably enriched, K-rich mafic melts (dark), which pond at the mantle-crust boundary. Partial melting of a lower crustal mafic granulite forms the parental melts for the calc-alkaline granitoids (white).

degree of interaction with depleted lithosphere, the magmas will progressively incorporate more of a MORB source component.

An alternative model (Fig. 3.26, Model B) poses that the shonkinite magmas originated by partial melting within an enriched OIB-like asthenosphere below the depleted subcontinental lithosphere. Variable amounts of mixing of these OIB-source magmas accompanied by partial melting of the overlying depleted subcontinental lithosphere during ascent produce MORB-like melts.

The source components for the granitoids are problematic but partial melting of a lower crustal mafic granulite is favored (Fig. 3.26). Variable partial melting of a granulitic source could produce the observed trace element and isotopic compositions observed in the Similkameen granitoids.

Melting of the granulite source was triggered by the influx and underplating of hot, hydrous mafic magma at the lower crust-mantle boundary. Magma underplating, i.e., ponding, has been proposed as a heat source to generate melting at lower crustal depths (Hildreth and Moorbath, 1988; Bergantz, 1989). Small amounts of mafic magma were able to ascend farther into the crust along pre-existing zones of weakness to levels that are exposed today. The compositions of the Similkameen mafic melts were indeed water-rich as witnessed by the abundance of hydrous mineral phases and fluid inclusions (see above). Thus with an elevated geotherm at the crust-mantle boundary, which would be expected following collision (of Quesnellia), crustal thickening, and subsequent subduction, the mafic magmas provide a heat source as well as a water source to lower the solidus of the lower crustal materials.

CHAPTER IV CONCLUSIONS

The Similkameen batholith contains two distinctive rock suites; a marginal mafic alkaline suite that has been intruded by several calc-alkaline, I-type granitoid plutons. The mafic rocks are potassic in composition and consist of the rock types malignite, shonkinite, and mafic nepheline syenite. Intimately associated with the mafic rocks are biotite and amphibole-bearing pyroxenite cumulates. The calc-alkaline granitoids vary in composition from monzonite to granodiorite.

Submagmatic deformation fabrics within the marginal mafic phases overprint early magmatic flow fabrics presumably due to the diapiric emplacement of the interior granitoid plutons. Based on petrofabric and structural studies of the batholith, the Similkameen magmas appear to have intruded after the cessation of all regional deformation associated with the collision and subsequent accretion of Quesnellia.

Modeling of major and trace element variations has shown that the mafic alkaline and calc-alkaline suites are not related by crystal fractionation. Within the mafic alkaline suite, major and trace element variations are primarily the result of crystal fractionation of the hydrous assemblage: clinopyroxene + biotite +/- amphibole + apatite + magnetite. Low variations of initial-Sr ratios suggest that assimilation of continental crustal material was relatively minor during the evolution of the Similkameen system.

The observed chemical variations support a subduction-related origin for the Similkameen magmas. Both the mafic alkaline and calc-alkaline suites exhibit enrichments in alkali and alkaline earth elements including Ba, Sr, Rb, and K, with marked depletions in Th, Nb, and Ti. Trace element compositions (high Ba) including REE (high La/Yb ratios) and Sr-isotopic data (low initial-Sr ratios, <0.7040), support a garnet and phlogopite-bearing mantle source for the mafic alkaline rocks. However, variations in trace element ratios indicate that the mantle source was heterogeneous in composition. The malignite series contains incompatible element ratios consistent with variable involvement of a depleted MORB-type source, whereas the shonkinite series appears to have originated from a more enriched OIB-type source. Mixing of subduction-generated melts with variably enriched subcontinental lithospheric mantle, e.g. phlogopite-veined peridotite, could account for the observed variations in trace element abundances. The age of lithospheric mantle enrichment is not well constrained. An alternative model involves subduction related melts mixing with an OIB-like mantle component.

The calc-alkaline granitoids contain moderately high LREE/HREE patterns and low initial-Sr ratios similar to those of the mafic rocks. Concave REE patterns from the

granitoids indicate amphibole fractionation, but the lack of negative Eu anomalies suggests derivation from a source containing little or no feldspar.

The calc-alkaline granitoids were probably derived by low to moderate degree partial melting of a mafic granulite source. High-pressure fractionation of partial melts from a granulite source could produce high-K, silicic magmas. These silicic magmas would lack negative Eu anomalies as well as contain the low initial-Sr ratios and variably enriched trace element compositions similar to those of the Similkameen granitoids. Melting of the lower crustal source could have been triggered by the influx and ponding of the hot, hydrous-mafic magmas at the lower crust-mantle boundary.

REFERENCES

- Abbott, R.N.Jr. 1989. Internal structures in part of the South Mountain batholith, Nova Scotia, Canada. *GSA Bulletin*, 101, 1493-1506.
- Alibert, C., Michard, A., & Albarede, F., 1986. Isotope and trace element geochemistry of Colorado Plateau volcanics. *Geochemica et Cosmochimica Acta*, 50, 2735-2750.
- Allegre, C.J. and Minster, J.F., 1978. Quantitative models of trace element behavior in magmatic processes. *Earth and Planetary Science Letters*, 38, 1-25.
- Archibald, D.A., Glover, J.K., Price, R.A., Farrar, E., Carmichael, D.M. 1983. Geochronology and tectonic implications of magmatism and metamorphism, southern Kootenay Arc and neighboring regions, southeastern British Columbia. Part I: Jurassic to mid-Cretaceous. *Canadian Journal of Earth Sciences*, 20, 1891-1913.
- Arculus, R.J., & Powell, R., 1986. Source component mixing in the regions of arc magma generation. *Journal of Geophysical Research*, 91, 5913-5926.
- Armstrong, R.L. 1982. Cordilleran metamorphic core complexes; From Arizona to southern Canada. *Annual Reviews of Earth and Planetary Sciences*, 10, 129-154.
- Armstrong, R.L. 1988. Mesozoic and early Cenozoic magmatic evolution of the Canadian Cordillera. *Geological Society of America Special Paper* 218, 55-91.
- Armstrong, R.L. & Van Der Heyden, P., 1989. The 2.1 to 2.3 Ga basement under Quesnallia between 47° and 53° N (abs). *Geological Society of America, Abs. w Prog.*, 21, p.51.
- Arth, J.G., Zmuda, C.C., Foley, N.K., Criss, R.E., Patton Jr., W.W., and Miller, T.P., 1989. Isotopic and trace element variations in the Ruby Batholith, Alaska, and the nature of the deep crust beneath the Ruby and Angayucham Terranes. *Journal of Geophysical Research*, 94, 941-955.
- Batchelor, R.A., 1987. Geochemical and petrological characteristics of the Etive granitoid complex, Argyll. *Scottish Journal of Geology*, 23, 227-249.
- Batchelor, R.A., & Bowden, P., 1985. Petrogenetic interpretation of granitoid rock series using multicatonic parameters. *Chemical Geology*, 48, 43-55.
- Bateman, R. 1984. On the role of diapirism in the segregation, ascent and final emplacement of granitoid magmas. *Tectonophysics*, 110, 211-231.
- Bateman, R. 1985. Aureole deformation by flattening around a diapir during in situ ballooning: the Cannibal Creek granite. *Journal of Geology*, 93, 293-310.
- Bateman, P.C., Chappell, B.W., 1979. Crystallization, fractionation, and solidification of the Tuolumne Intrusive Series, Yosemite National Park, California. *GSA Bulletin* 90, 465-482.
- Bateman, P.C., Busacca, A.J., & Sawka, W.N., 1983. Cretaceous deformation in the western foothills of the Sierra Nevada, California. *GSA Bulletin*, 94, 30-42.

- Beard, J.S. and Day, H.W., 1988. Petrology and emplacement of reversely zoned gabbro-diorite plutons in the Smartville Complex, northern California. *Journal of Petrology*, 29, 965-995.
- Bergantz, G.W., 1989. Underplating and partial melting: implications for melt generation and extraction. *Science*, 245, 1093-1095.
- Bence, A.E. and Albee, A.L., 1968. Empirical correction factors for electron microanalysis of silicates and oxides. *Journal of Geology*, 76, 382-403.
- Bonin, B., & Giret, A., 1984. The plutonic alkaline series: the problem of their origin and differentiation, the role of their mineralogical assemblages. *Physics of the Earth and Planetary Interiors*, 35, 212-221.
- Bostock, H.S., 1940. Map of the Keremeos area. GSC Map 341A.
- Bostock, H.S., 1941. Map of the Olalla area. GSC Map 628A.
- Brown, C.G., Thorpe, R.S., and Webb, P.C., 1984. The geochemical characteristics of granitoids in contrasting arcs and comments on magma genesis. *Journal of the Geological Society of London*, 141, 413-426.
- Brown, R.L., Journeay, J.M. 1987. Tectonic denudation of the Shuswap metamorphic terrane of southeastern British Columbia. *Geology*, 15, 142-146.
- Brun, J.P., and Pons, J., 1981. Strain patterns of plutonic emplacement in crust undergoing non-coaxial deformation, Sierra Morena, southern Spain. *Journal of Structural Geology*, 3, 219-230.
- Bryan, W.B., 1986. Linked evolutionary data arrays: a logical structure for petrologic modeling of multisource, multiprocess magmatic systems. *Journal of Geophysical Research*, 91, 5891-5900.
- Bryan, W.B., Finger, L.W., and Chayes, F., 1969. Estimating proportions in petrographic mixing equations by least-squares approximation. *Science*, 163, 926-927.
- Buddington, A., and Burmester, R., 1990. The Similkameen batholith: a mid-Jurassic, post-tectonic complex in the Quesnel terrane, north-central Washington and south-central British Columbia. *GSA Abstracts with Programs*, 22, p.10.
- Campbell, C.D., 1939. The Kruger alkaline syenites of southern British Columbia. *American Journal of Science*, 237, 527-549.
- Cannon, R.W., 1966. Geochronology and petrographic studies of the intrusive rocks of the Oliver area, Oliver, B.C.. Unpub. B.S. thesis, University of British Columbia, Vancouver, pp.23.
- Carroll, M.R. and Wyllie, P.J., 1990. The system tonalite-H₂O at 15 kbar and the genesis of calc-alkaline magmas. *American Mineralogist*, 75, 345-357.
- Castro, A. 1986. Structural pattern and ascent model in the Central Extramadura batholith, Hercynian belt, Spain. *Journal of Structural Geology*, 8, 633-645.

- Chappell, B.W. and White, A.J.R., 1974. Two contrasting granite types. *Pacific Geology*, 8, 173-174.
- Chappell, B.W. and Stephens, W.E., 1988. Origin of infracrustal (I-type) granite magmas. *Transactions of the Royal Society of Edinburgh, Earth Sciences*, 79, 71-86.
- Cogne, J.P., Perroud, H., 1988. Anisotropy of magnetic susceptibility as a strain gauge in the Flamanville granite, NW France. *Physics of the Earth and Planetary Interiors*, 51, 264-270.
- Compton, R.R., 1955. Trondhjemite batholith near Bidwell Bar, California. *GSA Bulletin*, 66, 9-44.
- Coney, P.J., Jones, D.L., and Monger, J.W.H., 1980. Cordilleran suspect terranes. *Nature*, 288, 329-333.
- Coney, P.J., Harms, Tekla, A. 1984. Cordilleran metamorphic core complexes: Cenozoic extensional relics of Mesozoic compression. *Geology*, 12, 550-554.
- Courrioux, G. 1987. Oblique diapirism: the Criffel granodiorite/granite zoned pluton (Southwest Scotland). *Journal of Structural Geology*, 9, 313-330.
- Crock, J.G., Lichte, F.E., and Wildeman, T.R., 1984. The group separation of the rare-earth elements and yttrium from geologic materials by cation-exchange chromatography. *Chemical Geology*, 45, 149-163.
- Daly, R.A. 1906. The Okanogan composite batholith of the Cascade Mtn. system. *GSA Bulletin*, 17, 329-376.
- Daly, R.A. 1912. Geology of the North American Cordillera at the forty-ninth parallel. *Canadian Geological Survey Memoirs*, 38, p.857.
- Davidson, A., 1970. Nepheline-K-feldspar intergrowths from Kaminak Lake, Northwest Territories. *Canadian Mineralogist*, 10, 191-206.
- Deer, W.A., Howie, R.A., & Zussman, J., 1983. *Introduction to the rock-forming minerals*. Longman House, U.K., 528 p.
- de la Roche, H., Leterrier, J., Grand Claude, P., and Marchal, M., 1980. A classification of volcanic and plutonic rocks using R1-R2 diagrams and major element analyses: its relationships with current nomenclature. *Chemical Geology*, 29, 183-210.
- Dell'Angelo, L.N., Tullis, J. 1988. Experimental deformation of partially melted granitic aggregates. *Journal of Metamorphic Geology*, 6, 495-515.
- DePaolo, D.J., 1981. Trace element and isotopic effects of combined wallrock assimilation and fractional crystallization. *Earth and Planetary Science Letters*, 53, 189-202.
- Eggler, D.H., 1987. Solubility of major and trace elements in mantle metasomatic fluids: experimental constraints: in *Mantle Metasomatism*, eds., M.A.Menzies & C.J.Hawkesworth, 21-41. Academic Press Geology Series, London.

- Ellam, R.M., Hawkesworth, C.J., Menzies, M.A., and Rogers, N.W., 1989. The volcanism of southern Italy: role of subduction and the relationship between potassic and sodic alkaline magmatism. *Journal of Geophysical Research*, 94, 4589-4601.
- Ellam, R.M., Hawkesworth, C.J., 1988. Elemental and isotopic variations in subducted related basalts: evidence for a three component model. *Contributions to Mineralogy and Petrology*, 98, 72-80.
- Engels, J.C., 1971. Effects of sample purity on discordant mineral ages found in K-Ar dating. *Journal of Geology*, 79, 609-616.
- Foley, S.F., Venturelli, G., Green, D.H., & Toscani, L., 1987. The ultrapotassic rocks: characteristics, classification, and constraints for petrogenetic models. *Earth and Planetary Science Reviews*, 24, 81-134.
- Fox, K.F., Rinehart, C.D., & Engels, J.C., 1975. K-Ar age of the Similkameen batholith and Kruger Alkalic Complex, Washington and British Columbia. *Journal of Research U.S.G.S.*, 3, 39-43.
- Fox, K.F.Jr., Rinehart, C.D., Engels, J.C., 1977. Plutonism and orogeny in north-central Washington: Timing and regional context. *USGS Professional Paper* 989, 27 p.
- Francalanci, L., 1989. Trace element partition coefficients for minerals in shoshonitic and calc-alkaline rocks from Stromboli Island (Aeolian Arc). *Neus Jahrbuch Miner.Abh.*, 160, 229-247.
- Fudali, R.F., 1963. Experimental studies bearing on the origin of pseudoleucite and associated problems of alkalic rock systems. *GSA Bulletin*, 74, 1101-1126.
- Fuji, T. and Scarfe, C.M., 1982. Petrology of ultramafic nodules from West Kettle River, near Kelowna, southern British Columbia. *Contributions to Mineralogy and Petrology*, 80, 297-306.
- Fujimaki, H., Tatsumoto, M., and Aoki, K., 1984. Partition coefficients of Hf, Zr, and REE between phenocrysts and groundmasses. *Proceedings of the 14th Lunar and Planetary Science Conference, Part 2, Journal of Geophysical Research*, 89(Suppl.), B662-B672.
- Fujinawa, A., 1988. Tholeiitic and calc-alkaline magma series at Adatara volcano, northeast Japan: 1, geochemical constraints on their origin. *Lithos*, 22, 135-158.
- Gabrielse, H. & Reesor, J.E., 1974. The nature and setting of granitic plutons in the central and eastern parts of the Canadian Cordillera. *Pacific Geology*, 8, 109-138.
- Gapais, D., Barbarin, B. 1986. Quartz fabric transition in a cooling syntectonic granite (Hermitage Massif, France). *Tectonophysics*, 125, 357-370.
- Giret, A., Bonin, B., and Leger, J-M., 1980. Amphibole compositional trends in oversaturated and undersaturated alkaline plutonic ring-complexes. *Canadian Mineralogist*, 18, 481-495.

- Gittins, J., Fawcett, J.J., Brooks, C.K., and Rucklidge, J.C., 1980. Intergrowths of nepheline-potassium feldspar and kalsilite-potassium feldspar: a re-examination of the "pseudo-leucite problem". *Contributions to Mineralogy and Petrology*, 73, 119-126.
- Green, D.H., 1973. Experimental melting studies on a model upper mantle composition at high pressure under water-saturated and water-undersaturated conditions. *Earth and Planetary Science Letters*, 19, 37-53.
- Green, T.H., Sie, S.H., Ryan, C.G., and Cousens, D.R., 1989. Proton microprobe-determined partitioning of Nb, Ta, Zr, Sr, and Y between garnet, clinopyroxene, and basaltic magma at high pressure and temperature. *Chemical Geology*, 74, 201-216.
- Green, T.H., and Pearson, N.J., 1987. An experimental study of Nb and Ta partitioning between Ti-rich minerals and silicate liquids at high pressure and temperature. *Geochimica et Cosmochimica Acta*, 51, 55-62.
- Green, T.H., & Pearson, N.J., 1986. Ti-rich accessory phase saturation in hydrous mafic-felsic compositions at high P,T. *Chemical Geology*, 54, 185-201.
- Hammarstrom, J.M., & Zen, E-an, 1986. Aluminum in hornblende: An empirical igneous geobarometer. *American Mineralogist*, 71, 1297-1313.
- Hansen, G.N., 1989. An approach to trace element modeling using a simple igneous system as an example: in *Geochemistry and Mineralogy of Rare Earth Elements*, eds., Lipin, B.R. & McKay, G.A., chap.4, 79-97. The Mineralogical Society of America, Washington, D.C..
- Hanson, G.N., 1978. The application of trace elements to the petrogenesis of igneous rocks of granitic composition. *Earth and Planetary Science Letters*, 38, 26-43.
- Henderson, C.M.B., Pendelbury, K., and Foland, K.A., 1989. Mineralogy and Petrology of the Red Hill Alkaline igneous complex, New Hampshire, U.S.A.. *Journal of Petrology*, 30, 627-666.
- Henry, B. 1988. The magnetic fabrics of the Egletons granite (France): separation and structural implications. *Physics of the Earth and Planetary Interiors*, 51, 253-263.
- Hibbard, M.J. 1970. Myrmekite as a marker between preaqueous and postaqueous phase saturation in granites. *GSA Bulletin*, 90, 1047-1062.
- Hibbard, M.J. 1971. Evolution of a plutonic complex, Okanogan Range, Washington. *GSA Bulletin*, 82, 3013-3048.
- Hibbard, M.J. 1981. The magma mixing origin of mantled feldspars. *Contributions to Mineralogy and Petrology*, 96, 158-170.
- Hibbard, M.J. 1987. Deformation of incompletely crystallized magma systems: granitic gneisses and their tectonic implications. *Journal of Geology*, 95, 543-561.
- Hickey-Vargas, R., Roa, H.M., Escobar, L.L., and Frey, F.A., 1989. Geochemical variations from the Villarrica-Lanin volcanic chain (39.5oS): an evaluation of source heterogeneity, fractional crystallization and crustal assimilation. *Contributions to Mineralogy and Petrology*, 103, 361-386.

- Hickey, R.L., Frey, F.A., Gerlach, D.C., & Lopez-Escobar, L., 1986. Multiple sources for basaltic arc rocks from the southern volcanic zone of the Andes (34o-41oS): Trace element and isotopic evidence for contributions from subducted oceanic crust, mantle, and continental crust. *Journal of Geophysical Research*, 91, 5963-5983.
- Hildreth, W. and Moorbath, S., 1988. Crustal contributions to arc magmatism in the Andes of central Chile. *Contributions to Mineralogy and Petrology*, 13, 1-29.
- Irving, A.J., 1978. A review of experimental studies of crystal/liquid trace element partitioning. *Geochimica et Cosmochimica Acta*, 42, 743-770.
- Jackson, M.P.A., & Talbot, C.J., 1989. Anatomy of mushroom-shaped diapirs. *Journal of Structural Geology*, 11, 211-230.
- Johnston, A.D. and Wyllie, P.J., 1989. The system tonalite-peridotite-H₂O at 30 kbar, with applications to hybridization in subduction zone magmatism. *Contributions to Mineralogy and Petrology*, 102, 257-264.
- Johnson, M.C., & Rutherford, M.J., 1989. Experimental calibration of the aluminum-in-hornblende geobarometer with application to Long Valley caldera (California) volcanic rocks. *Geology*, 17, 837-841.
- Kay, R.W., 1980. Volcanic arc magmas: Implications of a melting-mixing model for element recycling in the crust-upper mantle. *Journal of the Geological Society of London*, 141, 413-426.
- Kay, R.W. and Gast, P.W., 1973. The rare earth content and origin of alkali-rich basalts. *Journal of Geology*, 81, 653-682.
- Kerr, A., 1989. Geochemistry of the trans-Labrador granitoid belt, Canada. A quantitative comparative study of a Proterozoic batholith and possible Phanerozoic counterparts. *Precambrian Research*, 45, 1-17.
- Langmuir, C.H., Vocke, R.D.Jr., Hanson, G.N., and Hart, S.R., 1978. A general mixing equation with applications to islandic basalts. *Earth and Planetary Science Letters*, 37, 380-392.
- Leake, B.E., 1978. Nomenclature of Amphiboles. *Canadian Mineralogist*, 16, 501-520.
- Le Roex, A.P., Dick, H.J.B., Erlank, A.J., Reid, A.M., Frey, F.A., & Hart, S.R., 1983. Geochemistry, mineralogy, and petrogenesis of lavas erupted along the Southwest Indian Ridge between the Bouvet Triple Junction and 11o east. *Journal of Petrology*, 24, 267-318.
- Luhr, J.F. and Kyser, T.K., 1989. Primary igneous analcime: the Colima minettes. *American Mineralogist*, 74, 216-223.
- Luhr, J.F., Allan, J.F., Carmichael, I.S.E., Nelson, S.A., Hasenaka, 1989. Primitive calc-alkaline and alkaline rock types from the western Mexican Volcanic Belt. *Journal of Geophysical Research*, 94(B4), 4515-4530.
- Maniar, P.D., Piccoli, P.M., 1989. Tectonic discrimination of granitoids. *GSA Bulletin*, 101, 635-643.

- Mariano, A.N., 1989. Cathodeluminescence emission spectra of rare earth element activators in minerals: in *Geochemistry and Mineralogy of Rare Earth Elements*, eds., Lipin, B.R. and McKay, G.A., ch.11, 309-348. Mineralogical Society of America, Washington, D.C..
- Marsh, B.D., 1979. Island arc volcanism. *American Journal of Science*, 67, 161-172.
- Marsh, B.D., 1982. On the mechanics of igneous diapirism, stoping, and zone melting. *American Journal of Science*, 282, 808-855.
- McBirney, A.R., 1984. *Igneous Petrology*. San Francisco: Freeman, Cooper, 504 pp.
- Menzies, M. and Halliday, A., 1988. Lithospheric mantle domains beneath the Archean and Proterozoic crust of Scotland. *Journal of Petrology, Special Lithosphere Issue*, 275-302.
- Miller, C.F., 1978. Monzonitic plutons, California, and a model for generation of alkali-rich, near silica-saturated magmas. *Contributions to Mineralogy and Petrology*, 67, 349-355.
- Monger, J.W.H., and Price, R.A., 1979. Geodynamic evolution of the Canadian Cordillera; progress and problems. *Canadian Journal of Earth Sciences*, 19, 770-791.
- Monger, J.W.H., Price, R.A., and Templeman-Kluit, D.J., 1982. Tectonic accretion and the origin of the two major metamorphic and plutonic belts in the Canadian Cordillera. *Geology*, 10, 70-75.
- Morimoto, N., 1988. Nomenclature of pyroxenes. *Mineralogy and Petrology*, 39, 55-76.
- Nelson, D.R., McCulloch, M.T., & Sun, S.S., 1986. The origins of ultrapotassic rocks as inferred from Sr, Nd, and Pb isotopes. *Geochimica et Cosmochimica Acta*, 50, 231-245.
- O'Brien, H.E., 1988. Petrogenesis of the mafic potassic rocks of the Highwood Mountains, Montana. Unpub. Ph.D. Dissertation, Seattle, University of Washington, 293 pp.
- O'Brien, H.E., Irving, A.J., and McCallum, I.S., in press. Eocene potassic magmatism in the Highwood Mountains, Montana: Petrology, geochemistry, and tectonic implications. *GSA Special Paper*.
- Okulitch, A.V., 1984. The role of the Shuswap Metamorphic Complex in Cordilleran tectonism: A review. *Canadian Journal of Earth Sciences*, 21, 1171-1193.
- Othman, D.B., White, W.M., and Patchett, J., 1989. The geochemistry of marine sediments, island arc magma genesis, and crust-mantle recycling. *Earth and Planetary Science Letters*, 94, 1-21.
- Parkinson, D., 1987. U-Pb geochronology and regional geology of the southern Okanogan Valley, British Columbia: The western boundary of a metamorphic core complex. Unpub. M.Sc. thesis, Vancouver, Univ. British Columbia, 149 pp.
- Parrish, R.R. 1981. Geology and regional tectonics of the Nemo Lakes Belt, northern Valhalla Range, British Columbia. *Canadian Journal of Earth Sciences*, 18, 944-958.

- Parrish, R.R., 1979. Geochronology and tectonics of the northern Wolverine Complex, British Columbia. *Canadian Journal of Earth Sciences*, 16, 1428-1438.
- Parrish, R., and Carr, S.D., 1986. Extensional tectonics of southeastern British Columbia: new data and interpretations. *Geological Association of Canada, Programs with Abstracts*, 11, p.112.
- Parrish, R., Carr, S., & Parkinson, D., 1985. Metamorphic complexes and extensional tectonics, southern Shuswap Complex, southeastern British Columbia; in Tempelman-Kluit, D., ed., *Field guides to geology and mineral deposits in the southern Canadian Cordillera: GSA Sec. Mtg., Vancouver, British Columbia, 1985*, 12-15.
- Parrish, R., and Wheeler, J.O., 1983. A U-Pb age of the Kuskanax batholith, southeastern British Columbia. *Canadian Journal of Earth Sciences*, 20, 1751-1756.
- Paterson, S.R., 1989. Cannibal Creek granite: post-tectonic "ballooning" pluton or pre-tectonic piercement diapir: a reply. *Journal of Geology*, 97, 769-771.
- Paterson, S.R. & Tobisch, O.T. 1989. Using pluton ages to date regional deformations: problems with commonly used criteria. *Geology*, 16, 1108-1111.
- Paterson, S.R., Vernon, R.H., & Tobisch, O.T. 1989. A review of criteria for the identification of magmatic and tectonic foliations in granitoids. *Journal of Structural Geology*, 3, 349-363.
- Pearce, J.A., Harris, N.B.W., and Tindle, A.G., 1984. Trace element discrimination diagrams for the tectonic interpretation of granitic rocks. *Journal of Petrology*, 25, 956-983.
- Pearce, J.A., Norry, M.J., 1979. Petrogenetic implications of Ti, Zr, Y, and Nb variations in volcanic rocks. *Contributions to Mineralogy and Petrology*, 69, 33-47.
- Perfit, M.R., Gust, D.A., Bence, A.E., Arculus, R.J., & Taylor, S.R., 1980. Chemical characteristics of island-arc basalts; Implications for mantle sources. *Chemical Geology*, 30, 227-256.
- Pitcher, W.S., 1982. Granite type and tectonic environment. In Hsu, K.J. (ed.) *Mountain Building Processes*, 19-40. London: Academic Press.
- Ramberg, H. 1970. Model studies in relation to intrusion of plutonic bodies. in Newell, G., & Rast, N., eds., *Mechanisms of igneous intrusion. Geological Journal Special Issue 2*, 261-286.
- Ramsay, J.G. 1989. Emplacement kinematics of a granite diapir: the Chindamora batholith, Zimbabwe. *Journal of Structural Geology*, 11, 191-209.
- Read, P.B., Okulitch, A.V. 1977. The Triassic unconformity of south-central British Columbia. *Canadian Journal of Earth Sciences*, 14, 606-638.
- Rinehart, C.D. & Fox, K.F. 1972. *Geology and mineral deposits of the Loomis quadrangle, Okanogan County, Washington. Washington Division of Mines and Geology Bulletin*, 64, 124 pp.

- Roback, R., 1990. U/Pb zircon constraints on the timing of Middle Jurassic plutonism and deformation in the Mount Wilkie area, Kootenay arc, southeast British Columbia. *GSA Abstracts with Programs*, 22, p.78.
- Roddick, J.C., Farrar, E., & Procyshyn, E.L., 1972. Potassium-argon ages of igneous rocks from the area near Hedley, southern British Columbia. *Canadian Journal of Earth Sciences*, 9, 1632-1639.
- Rodgers, N.W., Hawkesworth, C.J., Parker, R.J., Marsh, J.S., 1985. The geochemistry of potassic lavas from Vulsini, central Italy and implications for mantle enrichment processes beneath the Roman region. *Contributions to Mineralogy and Petrology*, 90, 244-257.
- Sekine, T. & Wyllie, P.J., 1982. The system granite-peridotite-H₂O at 30 kbar, with applications to hybridization in subduction zone magmatism. *Contributions to Mineralogy and Petrology*, 81, 190-202.
- Smedley, P.L., 1988. Trace element and isotopic variations in the Scottish and Irish Dinantian volcanism: evidence for an OIB-like mantle source. *Journal of Petrology*, 29, 413-443.
- Steiger, R.H. and Jager, E., 1977. Subcommittee on geochronology: convention on the use of decay constants in geo- and cosmochronology. *Earth and Planetary Science Letters*, 36, 359-362.
- Stoltz, A.J., Varne, R., Wheller, G.E., Foden, J.D., Abbot, M.J., 1988. The geochemistry and petrogenesis of K-rich alkaline volcanics from Batu Tara volcano, eastern Sunda arc. *Contributions to Mineralogy and Petrology*, 98, 374-389.
- Sun, S.S., & McDonough, W.F., 1989. Chemical and isotopic systematics of oceanic basalts: implications for mantle composition and processes. In Saunders, A.D. & Norry, M.J. (eds), *Magmatism in the ocean basins*, Geological Society Special Publication #42, 313-345.
- Sylvester, A.G., Oertel, G., Nelson, C.A., & Christie, J.M., 1978. Papoose Flat pluton: a granite blister in the Inyo Mountains, eastern California. *GSA Bulletin*, 89, 1205-1219.
- Sylvester, P.J., 1989. Post-collisional alkaline granites. *Journal of Geology*, 97, 261-280.
- Tatsumi, Y., Sakuyama, M., Fukuyama, H., and Kushiro, I., 1983. Generation of arc basalt magmas and thermal structure of the mantle wedge in subduction zones. *Journal of Geophysical Research*, 88(B7), 5815-5825.
- Taylor, D. and MacKenzie, W.S., 1975. A contribution to the pseudoleucite problem. *Contributions to Mineralogy and Petrology*, 49, 321-333.
- Tempelman-Kluit, D., & Parkinson, D., 1986. Extension across the Eocene Okanogan crustal shear in southern British Columbia. *Geology*, 14, 318-321.
- Thompson, R.N., Morrison, M.A., Hendry, G.L., and Parry, S.J., 1984. An assessment of the relative roles of crust and mantle in magma genesis: an elemental approach. *Philosophical Transactions of the Royal Society of London*, A310, 549-590.

- Tullis, J., Yund, R.A., 1987. Transition from cataclastic flow to dislocation creep of feldspar: Mechanisms and microstructures. *Geology*, 15, 606-609.
- van Den Eeckhout, B., Grocott, J., & Vissers, R., 1986. On the role of diapirism in the segregation, ascent, and final emplacement of granitoid magmas-discussion. *Tectonophysics*, 127, 161-169.
- van der Molen, I. & Paterson, M.S., 1979. Experimental deformation of partially melted granite. *Contributions to Mineralogy and Petrology*, 70, 299-318.
- Verma, S.P. & Nelson, S.A., 1989. Isotopic and trace element constraints on the origin and evolution of alkaline and calc-alkaline magmas in the northwestern Mexican Volcanic Belt. *Journal of Geophysical Research*, 94(B4), 4531-4544.
- Vernon, R.H., Paterson, S.R., and Geary, E.E., 1989. Evidence for syntectonic intrusion of plutons in the Bear Mountains fault zone, California. *Geology*, 17, 723-726.
- Weaver, B.L., Wood, D.A., Tarney, J., Joron, J.L., 1986. Role of subducted sediment in the genesis of ocean-island basalts: geochemical evidence from South Atlantic Ocean islands. *Geology*, 14, 275-278.
- Whalen, J.B., Currie, K.L., Chappell, B.W., 1987. A-type granites: geochemical characteristics, discrimination and petrogenesis. *Contributions to Mineralogy Petrology*, 95, 407-419.
- Wheeler, J.O., and Gabrielse, H., 1972. The Cordilleran structural province, in Price, R.A., and Douglas, R.J.W., eds., *Variations in tectonic styles in Canada*. Geological Association of Canada Special Paper 11, 1-81.
- Wilson, M., 1989. *Igneous Petrogenesis*. London: Unwin Hyman, 466 pp.
- Wood, D.A., 1979. A variably veined suboceanic upper mantle: Genetic significance for mid-ocean ridge basalts from geochemical evidence. *Geology*, 7, 499-503.
- Worner, G., Zindler, A., Staudigel, H., and Schmincke, H.U., 1986. Sr, Nd, and Pb isotope geochemistry of Tertiary and Quaternary alkaline volcanics from West Germany. *Earth Planetary Science Letters*, 79, 107-119.
- Wyllie, P.J., 1979. Magmas and volatile components. *American Mineralogist*, 64, 469-500.
- Wyllie, P.J., & Sekine, T., 1982. The formation of mantle phlogopite in subduction zone hybridization. *Contributions to Mineralogy and Petrology*, 79, 375-380.
- Xue, X., Badsgaard, H., Irving, A.J., and Scarfe, C.M., in press. Geochemical and isotopic characteristics of lithospheric mantle beneath West Kettle river, British Columbia: evidence from ultramafic xenoliths. *Journal of Geophysical Research*.
- York, D., 1967. Least-squares fitting of a straight line with correlated errors. *Earth and Planetary Science Letters*, 5, 320-324.
- Zhang, X., Nesbitt, B.E., & Muehlenbachs, K., 1989. Gold mineralization in the Okanogan Valley, southern British Columbia: Fluid inclusion and stable isotope studies. *Economic Geology*, 84, 410-424.

APPENDIX A
Petrographic descriptions of Selected
Similkameen Batholith Samples

The following abbreviated descriptions are representative of all the major rock types found within the Similkameen complex (Plates I, II). Not all the samples used for chemical analysis are included here. Abbreviations used include: cpx=clinopyroxene, am=amphibole, biot=biotite, kfsp= microcline, neph=nepheline, pl=plagioclase, mt=magnetite, gt=melanite garnet, sph=sphene, ap=apatite, cc=carbonate, sc= sericite, ep=epidote, mcryst=megacryst, LV= liquid+vapor, VL= vapor+liquid, LVS, liquid+vapor+solid, C.I.= color index.

Pyroxenites

SMK88-137 Pyroxene Hornblendite

Coarse grained, found as a small pod or lens-like body within shonkinite. Contains am (ferroan pargasite) as the dominant mafic. Am is sub- to euhedral but often mantling subhedral cpx. Am contains rare biot inclusions. Accessories: ap, mt, sph, + rare melanite gt. Fairly fresh but with minor micro veinlets of cc, kfsp, sc, ep, and hematite. Pt. count of 709 pts. from section; am= 56.7%, cpx= 27.8%, ap= 8%, mt= 6.8%, sph= .7%.

SMK88-159 Amphibole Pyroxenite

Coarse grained with sub- to euhedral cpx (salitic augite) with moderate reaction to uralite. Ferroan pargasite (.5-7mm) is subhedral with biot inclusions (<5mm). Mt has been replaced by pyrite to varying degrees and with reaction rims of cc+sph. Ep and pyrite are present in hand sample.

This sample is particularly interesting due to the presence of fluid inclusions within the primary mineral phases. Euhedral apatites are characteristically full of fluid inclusions (LV, VL, LVS). Fluid inclusions are also in primary cpx, am, and biot but are not in secondary am or any of the other secondary minerals. The fluid inclusions are presumed to be primary in origin.

SMK88-198 Biotite Pyroxenite

This coarse grained rock has a distinctive cumulate texture with am and large books of biot (.5-10mm). Collected as a boulder from the pyroxenite body along the Prize Mine road. The rock shows moderate alteration; in hand sample ep and cc are present. Prismatic to equant cpx (.5-8mm) are often mantled by am. The sample contains minor

amounts of kfsp which is reflected in the higher SiO₂ content. Apatites are euhedral as intergranular grains and as inclusions in primary mafic grains. The ap contains abundant fluid inclusions (LV +VL). Mt is virtually absent from the rock contributing to the relatively higher Mg#.

This sample like most of the pyroxenitic rocks exhibits a moderate degree of secondary alteration as witnessed by the presence of late am as well as cc, ep, and actinolite. This secondary alteration is considered to be a late magmatic or deuteric alteration primarily because of the overgrowth or interstitial textural nature of the secondary minerals.

SMK88-205 Biotite Pyroxenite

Coarse grained, equigranular with a cumulate texture. In thin section this sample exhibits alignment of cpx laths. Biot is often intergrown with cpx as intergranular grains and as inclusions in cpx as well. Cpx contains poikilitic inclusions of ap, mt, and biot and shows faint oscillatory zoning. Intergranular mt and apt occur as clots together. Euhedral apatite contains abundant micro-fluid inclusions (LV;<1um).

This is essentially a 4-phase rock: cpx + biot + mt + ap in decreasing order of abundance. Note that this rock has the lowest wt.% SiO₂ and highest FeO(t) and P₂O₅ content of all samples throughout the complex (see Appendix B).

SMK88-206 Porphyritic Amphibole Pyroxenite

This rock type occurs as 10-25 cm wide dikes within equigranular med.-grained pyroxenite along the Submarine Mine road. Amphibole phenocrysts (.5-1 cm) are of ferroan pargasite composition and contain inclusions of cpx, ap, mt, & sph. Cpx (diopside) is euhedral equant with an equigranular (<3.5mm) cumulate texture. Kfsp is interstitial and there is a minor amount of pl. Other access. phases include: mt, sph, ap, and biot.

The dikes do not contain chilled margins but in some cases the host pyroxenite margins appear to be sheared indicating that the dikes intruded along fault planes within the earlier crystallized pyroxenite. The phenocrysts appear to be randomly oriented. This may well represent late-stage diking as a result of melt segregation from within the interior of the pyroxenite towards more brittle zones in the cooler, already crystallized outer margins. The faults may be the result of contraction upon crystallization or a deformational response to stress imposed by intruding interior phases (see Chapter 2).

SMK88-210 Amphibole Pyroxenite

Coarse grained pyroxenite with large (<10mm) subhedral am and biot. Cpx shows faint zoning with uraltite replacement along cleavage traces. There are two populations of am; 1) mantling of cpx, and 2) primary subhedral poikilitic grains with abundant ap, mt, & biot inclusions. Amphibole has a deep green pleochroism and the primary grains of am as well as ap contain LV fluid inclusions. Kfsp and pl are moderately altered to sc and ep.

SMK87-2 Biotite Pyroxenite

Typical equigranular biotite pyroxenite found throughout the marginal pyroxenitic phases. Dominated by cpx (90-95%) with a distinctive cumulate texture. Biot (<10%) occurs as interstitial subhedral grains. Kfsp is minor as a late interstitial phase. Ap and mt occur as accessory phases.

SMK87-3 Biotite Pyroxenite

Same as the previous pyroxenite (SMK87-2) except with a greater biot content (32%) within the equigranular matrix. Biot is also prevalent as inclusions within the cpx.

SMK87-26 Biotite Pyroxenite

This rock type exhibits a distinctive pegmatitic texture with abundant books of biot (3-6 cm). The sample contains sub- to euhedral prismatic cpx with abundant euhedral ap (1-3mm) visible in hand sample. Cpx has been replaced to varying degrees by uraltite. Biot cleavages exhibit moderate to extreme deformation. Fluid inclusions are present throughout the primary phases (ap, cpx, biot) but are absent from the secondary uraltite. Carbonate with straight grain boundaries is found in the interstices between cpx and biot and is interpreted as a late magmatic or hydrothermal phase. This sample type was never observed as outcrop but is moderately abundant as float boulders within the talus slopes along the lower portions of the Prize Mine road.

SMK87-42.a,b Hornblendite

For lack of a better name, hornblendite was chosen because of the dominance of euhedral amphibole. Taken from an open pit on the south side of the Similkameen River. The outcrop exhibits a bewildering array of textures that appear to be cumulate or adcumulate in nature but all with a strong foliation. Mafic-rich clots are streaked and felsic dikes crosscutting the foliation are deformed as well. Am and kfsp are the dominant phases with lesser amounts of cpx. The sub- to euhedral am are estimated by petrographic inspection to be pargasitic to hastingsitic in composition. Accessories

include: melanite gt, pl, biot, ap, mt, and zircon. Alteration is moderate with secondary ep, cc, and hematite.

Authors Note About Rock Classification

The classification of malignite, shonkinite, and undersaturated syenites is relatively blurred in the literature especially for mafic alkaline plutonic rocks. In this study the classification of mafic alkaline rocks is defined on the basis of modal abundances of mafic components (cpx, am, etc..) vs nepheline vs alkali feldspar. If the sample contains abundant nepheline with a color index (CI)>45 then the terms shonkinite or malignite are used. If the sample is dominated by alkali feldspar (CI<45) and mafic constituents with virtually no nepheline then the term syenite is used with the appropriate modifiers. If nepheline is present in trace amounts then nepheline is used as a modifier to the syenite classification.

Malignite

SMK88-111.a Pseudoleucite Malignite

Samples 111.a,b, and c are part of the only true malignite body found within the complex. This malignite body makes up a rather small heterogeneous phase characterized by the presence of megacrystic pseudoleucite and vary in ratios of modal felsic vs. mafic components. In all cases the unit exhibits pervasive foliations and lineations defined by aligned and elongated megacrysts.

Pseudoleucites in hand sample range in size from .5 to 4 cm. in length and are often moderately flattened within the plane of foliation. Pseudoleucite has been replaced by a mosaic of intergrown kfsp and neph. Neph is seen in thin section as vermicular or radial intergrowths which have been altered to hydronepheline. The matrix is composed primarily of equant cpx and interstitial kfsp. The sample contains up to 30% nepheline with minor amounts of am, biot, melanite gt. Euhedral prismatic ap and equant mt are common accessory phases. Amph can be primary (subhedral) and as secondary overgrowths of cpx.

SMK88-111.b Pseudoleucite Malignite

Same as sample 111.a except for a higher content of cpx and biot (CI=46). Biot have bent cleavage traces. Note from observation of the whole rock data (Appendix B) that samples 111.b,c are considered ultrapotassic by the definition proposed by Foley et al., (1987).

SMK88-111.c Biotite Shonkinite

This sample is part of the above mentioned malignite body but occurs as a nepheline-poor phase. It contains (CI=60) considerably more cpx, biot, and gt than the above mentioned samples.

Shonkinite

SMK88-125 Shonkinite

Medium grained and for the most part equigranular but the unit does contain sporadic megacrysts of kfsp. CI=40.5. Contains unequal amounts of am to cpx (approximately 75/25%). Amphibole occurs mantling cpx and as primary subhedral grains. Biot is rare as inclusions in am. Kfsp (microcline) is perthitic with tartan twins and neph is altered to hydronepheline or other unidentified zeolites. Apatite and zircon (rare) occur as inclusions in am and cpx.

SMK88-126 Shonkinite

This sample from the same unit (as 88-125 which exhibits a marked lithological heterogeneity), is more mafic than the previous with considerably more cpx to am and less neph. Amphiboles show a sieve-like texture in which they are intergrown with kfsp. Melanite gt is obvious in hand sample.

SMK88-134 Shonkinite

Contains both cpx and am (CI=42), but dominated by cpx. Kfsp and pl (An13 - An20) laths show definite alignment. Also contains accessory melanite gt, ap, sph, and biot.

SMK88-142 Shonkinite

Very typical shonkinite with equigranular, medium-grained texture. Kfsp mcrcrysts (1-2 cm) occur sporadically throughout the unit. Unaltered subhedral nepheline grains (.5-2 mm) are obvious in thin section with kfsp and minor amounts of pl (An31 - An33) in the matrix. Biotite is very minor and cancrinite occurs as a late interstitial phase.

SMK88-200 Shonkinite

Abundant nepheline with cpx and am. Melanite gt intergrown with green biotite. Apatite as euhedral grains with fluid inclusions and cancrinite as an interstitial phase.

SMK88-207 Shonkinite

Very mafic sample (CI=75) with zoned cpx. Kfsp is interstitial with very minor amounts of pl. Biotite is as inclusions in cpx and as replacement of cpx along cleavage traces. Amphibole is mantling cpx and mt is virtually absent.

Syenites

SMK88-168 Augite Syenite

This strongly foliated syenite has cpx as the dominant mafic phase. Amphibole does occur but essentially as overgrowths to cpx. Kfsp laths are surrounded by a finer grained mosaic of kfsp, pl, myrmekite, and trace amounts of quartz. Accessory phases include: sph, ap, mt, and zircon.

The foliated fabric that characterizes this rock in the field is accentuated in thin section by the strong alignment of kfsp laths. The mosaic of kfsp and pg represents a late or more likely subsolidus deformational overprint and annealing to a primary magmatic flow fabric (see Chapter 2).

SMK88-187 Syenite

Subporphyritic with phenos of kfsp (7-15 mm) within an equigranular matrix of kfsp, pl, and biot. Melanite gt is anhedral, intergrown with sph. Other accessories include; mt, ap, and zircon.

SMK88-188, 189 Mafic Nepheline Syenite

Subporphyritic with aligned zoned mcrysts of kfsp in medium grained foliated matrix of kfsp, am, and cpx (CI=31). Amphibole occurs as primary grains and mantling cpx. Contains approximately 3% nepheline which is well altered. Ap and mt as euhedral intergranular grains and as inclusions. Melanite gt with am mantling cpx as sieve-like texture or as skeletal stringers into kfsp.

SMK88-204 Mafic Nepheline Syenite

This well foliated sample contains flattened phenocrysts of kfsp in a medium grained matrix of cpx. Amphibole mantles cpx and biot occurs as inclusions in cpx. The sample does contain approximately 3% neph but is considered a syenite based on the CI=34.

Gneissic Syenitic Rocks

SMK88-167 Gneissic Syenite/Shonkinite

This sample is characteristic of the outermost gneissic unit. Contains a penetrative foliation as well as mineral lineation. Kfsp twins are aligned in the plane of foliation and aligned biot clots define the lineation which is length parallel to the foliation. Melanite gt is intergrown with green biot. Epidote and varying amounts of muscovite constitute the remainder of the major mineral phases. Apatite is euhedral and zircon is subhedral, both which occur as inclusions within sph and kfsp (rare). Magnetite has been replaced to varying degrees by pyrite. No cpx or am are present.

There has been a substantial amount of recrystallization of kfsp; primary zoned subhedral grains are rare. See Chapter 2 for discussion of fabric. Due to the higher % of mafics (gt, biot, and mt) and the relatively low SiO₂ content, this sample may have been considered a shonkinite prior to deformation and recrystallization.

SMK88-211 Gneissic Syenite

Same as above but with distinctively lesser amounts of mafics but yet has a lower SiO₂ content. This sample is from a felsic-rich layer approximately 15cm thick within the gneissic unit.

SMK88-212 Gneissic Syenite

From same outcrop as above but the sample represents a zone of uniform felsic-rich, mafic-rich layering. Grain size is fine to medium. Note there is very little difference in bulk composition between 88-211 & 88-212 (see Appendix B).

SMK87-8.A Gneissic Syenite

One cpx grain in total disequilibrium and is almost completely replaced by biot, ep, and mt. One am grain was observed and it too had been reacted and was surrounded by biot, ep, and mt.

Trachytoid Rocks

SMK88-158 Trachytoid Mafic Monzonite

This rock type is characterized by its distinctive trachytoid fabric defined by the alignment of zoned kfsp megacrysts. The mcrysts are always zoned and never deformed. The kfsp zoning is mimicked by inclusions of pl and biot aligned along internal crystal faces of the kfsp presumably by synneusis during continual crystallization. Mafics (am + cpx) are aligned within the plane of foliation. Amphibole content is generally higher than cpx content. Amphibole occurs mantling cpx and as primary subhedral grains. Plagioclase is within the groundmass as sub- to anhedral grains (<1mm). Spene is euhedral and up to 10mm in length. Other access. phases include: mt, biot, ap, and gt. CI=26.

SMK88-169 Trachytoid Monzonite

Same as above with large (3-5cm in length) zoned kfsp mcrysts. Amphibole is anhedral and occurs mantling cpx and as inclusions within subhedral cpx. Some cpx as inclusions in am. Contains 1-2% quartz. Biot is a minor access with sph, mt, and ap. CI=24.

SMK88-190 Mafic Nepheline Syenite

Megacrysts of kfsp with trachytoid fabric in medium grained foliated matrix of kfsp, fresh nepheline, cpx, am, biot, and melanite gt. Access. phases include: sph, ap, zircon, and cancrinite.

There appears to be a reaction relation of early cpx to am, gt, biot, +/-sph. There also appears to be some degree of recrystallization of kfsp. This may represent late fluid reaction (subsolidus) and recrystallization during deformation or a metasomatic infiltration and reaction.

Granitoid Rocks

Similkameen Valley Pluton

SMK88-113 Monzonite

A sub-porphyrific, coarse grained variety with mcrysts of kfsp (1-2cm). Foliation is faint but aligned am and feldspar laths are obvious in thin section. Pl composition ranges from An₃₇ to An₃₂. Quartz is anhedral interstitial and moderately undulose. Amphibole (hornblende) contains inclusions of biot, sph, ap, and mt. Minor alteration products of feldspars and am include: ep, chlorite, and sc.

SMK88-114 Quartz Monzonite

Going inward to the interior this sample typifies the increase in quartz content from the outer monzonitic phases. Same as 113 but with higher qtz content.

SMK88-120 Quartz Monzonite

From locality used for U-Pb and Rb-Sr dating. Moderately fresh, coarse grained sub-porphyrific with mcrysts of kfsp (1-3 cm) and euhedral pl (An₃₂ - An₂₆) with inclusions of am, sph, and ap. Biotite is subhedral with jagged edges indicating reaction and occurs as euhedral inclusions in am. Amphibole (hornblende) exhibits oscillatory zoning. Accessory minerals include: sph, mt, zircon, and ap and a CI=12.

SMK88-136 Quartz Monzodiorite

Same as 88-120 but with significant cpx (CI=20) which is either rimmed by amph or has reacted to am or ep, mt, and hematite. Some euhedral mt contains biot inclusions.

SMK88-163 Quartz Monzodiorite

From Hurley Peak area; grades into qtz monzonite (88-164) away from the contact with the Kobau Formation. Essentially the same as above but with no cpx (CI=23). Biot is rare and gone to chlorite. Euhedral ap and mt intergrown as small intergranular clusters (<1mm). The accessory content is slightly higher in this sample than 88-164.

SMK88-192 Quartz Monzodiorite

Same as 88-136 but this sample is the only granitoid with fluid inclusions which are present within apatite.

SMK88-196 Granodiorite

From Barber Mtn., this granodiorite (CI=14) is a gradational equivalent to the qtz monzonite of 88-120. Very similar mineralogically and texturally to 88-120. Plagioclase

composition ranges from An₃₆ (cores) to An₂₃ (rims). Contains accessory euhedral allanite as inclusions in kfsp.

SMK88-195 Granite

This coarse-grained, sub-porphyritic sample exemplifies the gradational zonation to higher SiO₂ contents from the border zone inward for granitoids of the eastern field area. Same as 88-195 except for higher qtz content. Hornblende is the dominant mafic with lesser amounts of sub- to anhedral biot. Biot has jagged edges indicating reaction relation and has been replaced by chlorite.

Granitic Rocks of the Snowy Mountain Area

SMK88-214 Monzodiorite

Coarse grained unit with aligned feldspars and mafics. This unit intrudes the Harry Lake granodiorite (SMK88-183). On Snowy Mtn. this unit is subporphyritic with mcrcrysts of kfsp (1-3cm).

SMK88-176 Quartz Monzonite

Coarse grained, sub-porphyritic phase of the Snowy Mtn. Unit. Kfsp euhedral mcrcrysts (1-3cm) are aligned in the foliation. Plagioclase compositions are from An₃₅ (cores) to An₂₈ (rims). Zoned euhedral am (hornblende) contain inclusions of biot and some biot mantles am. Intergranular biot is sub- to anhedral but has very irregular grain boundaries which indicate unstable reaction. Accessories include: ap, mt, sph, and zircon.

Harry Lake Unit

The location of this unit is centralized around the Harry Lake area, due west of Snowy Mtn. hence the name the Harry Lake Unit. The body appears to continue to the south of Snowy Mtn. in the upper portions of the Snehumption Creek drainage (sample 88-175, see Plate II) but absolute correlation is difficult due to the significant difference in whole rock chemistry (see Appendix B).

SMK88-183 Quartz Monzonite

A medium grained equigranular unit with variable amounts of am vs cpx. This sample is dominated by am as the mafic mineral and cpx occurs as cores to some of the amph and as relict corroded grains. Plagioclase composition ranges from An₃₄ (cores) to An₂₈ (rims). Kfsp (microcline) is commonly perthitic with some myrmekite and tartan

twinning. Quartz occurs as a late interstitial mineral. Feldspars exhibit moderately deformed twin planes. Accessory phases include: ap, mt, and sph.

SMK88-213 Quartz Monzonite

This sample is the same as 88-183 but with cpx as the dominant mafic mineral. Cpx is equant to prismatic subhedral with somewhat jagged edges. Hornblende does occur as subhedral grains and also mantling cpx. Biot is also present as sub- to anhedral grains. Epidote is an alteration product of the feldspars and mafics.

Granodiorite of Upper Snehumpton Creek

This eqigranular, medium-grained unit is very similar in field appearance to the Harry Lk. Unit (88-183) but note the significant difference in whole rock chemistry. This unit can have variable amounts of biot and am (hornblende); some occurrences dominated by am, others relatively devoid of am. On textural grounds, this unit is significantly distinctive from the granitoid rocks of the eastern field area (SMK88-120, 195, 196, etc..) and is considered a separate intrusive phase.

SMK88-175 Granodiorite

Biotite-rich sample; biot is sub- to anhedral occupying interstices between feldspars. Contains large (4-7mm) subhedral, equant quartz that are characteristic in hand sample. In thin section zones of equant qtz inclusions are around the outer margins of zoned (oscillatory) pl. Myrmekite is common. Accessory phases include: mt, sph, ap, and zircon.

Schlieren Zone

SMK87-24.a

This sample is from a contact zone between the marginal mafic phase and the main phase granitoids. The gradational contact zone represents a transition from shonkinitic rocks to interior granitic rocks along the northwesterly face of Ellemeham Mtn (see Plate I). The outcrop from which this sample was taken contains mafic-rich cumulate zones interlayered with felsic-rich monzonitic material exhibiting schlieren fabrics.

Dominated by subhedral cpx mantled and partially replaced by pargasitic am. Cpx-rich clots have cumulate texture. Kfsp dominates the felsic zones with lesser amounts of pl. The larger kfsp grains have corroded edges. A fine grained mosaic of kfsp and pl

surround the larger feldspar grains. Apatite & sph are accessory minerals with a virtual absence of mt.

Alaskites

Alaskite occurs predominately as veins or dikes which crosscut both the granitoids and the mafic alkaline assemblages. One large mappable alaskite body is located along the southeast portion of the batholith (Plates I, II) within the outer mafic assemblages. Agmatites of mafic rocks (pyroxenites and shonkinites) with alaskitic matrix occur sporadically along the southeast margin. Crosscutting relations make it clear that many of the alaskites are associated to post-granitoid emplacement; most likely late-stage differentiation products from the granitoids. But other alaskites within the marginal mafic rocks can't be linked unequivocally to the granitoids based on field relations.

SMK88-170 Alaskite

This leucogranite contains 36% (modal) microcline, 34% plagioclase, 28% quartz, and 2% mafics. Plagioclase compositions range from An₁₀ to An₂₃. Mafics include biotite and amphibole altered to chlorite and epidote. The feldspars are prismatic and in parallel alignment interpreted as a magmatic flow alignment. Accessory constituents include: sph, mt, zircon, & allanite. Quartz veins (1-2 cm width) cut primary alaskite.

SMK87-25 Alaskite

Identical to SMK88-170. Myrmekite present and pl contain normal and oscillatory zoning with albite twinning. Microcline contains tartan twinning. Feldspars exhibit moderate alteration to sericite and epidote.

Xenoliths

SMK87-13.a

Ovoid shaped, biot-rich xenolith within qtz monzonite. Fine grained with subhedral biot and am. Zoned andesine pl with albite twinning. Accessory phases include: mt, ap, sph, and zircon. Epidote has partially replaced biot and am.

SMK87-14

Biotite-rich with am; biot and am to chlorite and epidote. Plagioclase and kfsp altered to ep and sc. Minor subhedral sphene.

SMK87-20

Amphibole-rich xenolith from the intrusive breccia zone due west of the Kabba Texas mine. There are two different am compositions; euhedral hornblendes with slightly jagged edges are the most abundant, the second am (pargasite) present is anhedral with deep blue-green pleochroism and also occurs as overgrowths on some of the hornblende. Euhedral biot inclusions occur within the hornblende. Sub- to anhedral kfs with curved grain boundaries with myrmekite. Plagioclase (An₁₅) and minor qtz. High amount of zircon but still accessory with mt and ap. The ap grains contain fluid inclusions. This mafic xenolith is presumed to be of igneous origin.

Kobau Formation Country Rocks

SMK87-7 Biotite Schist

This sample was collected approximately 30 m from the contact with pyroxenite on the eastern border. Strongly foliated with aligned amphibole porphyroblasts (0.5 mm, in the foliation plane) that have been pseudomorphed by non-oriented biotite. Finer grained groundmass composed of biot, am, pl, qtz, and ep. The aligned amphibole is presumed to be synkinematic with regional metamorphism and the non-oriented biot pseudomorphs are contact metamorphic in origin. See Chapter 2 for discussion.

SMK87-15 Hornfelsed Metabasalt

Fine grained and well foliated with micro-folds. Alternating layers of actinolite with pl and qtz. Some actinolite is idioblastic and up to 1.0 mm with 180 degree grain boundaries. Plagioclase and qtz layers are composed of idiomorphic grains with 180 degree grain junctions. Biot-rich foliated masses are within the am-rich layers. Epidote is found as idiomorphic masses.

SMK88-16 Metachert

Garnet-rich with non-foliated masses of ep, qtz, cc, pl, and minor pyrite. This sample collected approximately 200 m from the contact with monzonite along the southern border.

SMK89-305,306 Garnet Biotite Schist

Garnet porphyroblasts are pre- to synkinematic. Garnets are idioblastic but exhibit deformation (pull apart texture) with broken edges and contain pl and qtz inclusions. The fine grained foliated matrix is composed of biot, pl, qtz, gt, mt, & hematite. This sample was collected within a small pod of gt-bearing metapelite along the southeastern border

approximately 100 m from the contact with syenitic gneiss. The garnets predate any contact metamorphism related to emplacement of the batholith.

APPENDIX B

XRF Whole Rock, Major and Trace Element Data

Whole rock analyses on 50 powdered samples were carried out at the Grant Institute of Geology, University of Edinburgh (England), by Professor R.S. Babcock and Dodie James. Samples were powdered (<200 μm) by the author using a Spex tungsten-carbide shatterbox. XRF analyses were made on pressed powder pellets with a Phillips model XRF. Ferric-ferrous iron determinations were made by the author following the meta-vanadate method.

REE Data

REE analyses were performed on powdered samples carried out at the University of Washington by the author under the guidance of Dr. A.J. Irving. REE solutions were made by dissolving approximately 0.7 grams of rock powder in a $\text{HClO}_4\text{-HF-HNO}_3$ mixture. Centrifuged residues from this mixture were fused with NaOH in Ag crucibles and readded to the initial mixture. Separation of REE's were done using cation exchange chromatography following the procedure of Crock et al. (1984). REE analyses were obtained with a Baird PS-1 inductively-coupled plasma emission spectrometer (ICP).

Table B.1 Similkameen Batholith XRF Whole Rock Data

	111.a	111.b	111.c	113	114	120	125	134	136	137
SiO ₂	50.40	49.13	47.95	64.27	65.01	65.84	51.40	50.51	60.57	38.30
TiO ₂	0.90	1.03	1.01	0.44	0.43	0.40	0.80	0.95	0.61	1.68
Al ₂ O ₃	16.49	15.03	14.66	16.31	16.43	15.98	16.77	15.36	16.54	5.18
Fe ₂ O ₃	4.19	5.01	5.18	1.78	1.95	1.80	3.26	4.94	2.80	11.03
FeO	4.64	5.23	4.97	2.40	2.12	2.07	4.84	5.30	3.07	9.40
MnO	0.22	0.26	0.26	0.13	0.12	0.12	0.19	0.23	0.16	0.44
MgO	2.80	3.36	3.26	1.49	1.33	1.32	3.36	3.33	2.01	9.11
CaO	7.78	9.23	9.09	4.45	4.41	4.07	7.48	8.70	5.50	19.71
Na ₂ O	2.45	1.82	1.96	4.06	3.98	3.94	3.37	2.99	3.93	0.39
K ₂ O	7.12	6.94	6.92	3.20	3.13	3.58	5.57	5.02	3.78	0.68
P ₂ O ₅	0.65	0.78	0.76	0.21	0.19	0.19	0.54	0.74	0.35	1.88
LOI	1.80	1.81	1.87	0.72	0.65	0.35	0.93	0.70	0.41	0.74
Total	99.43	99.62	97.89	99.46	99.75	99.64	98.52	98.77	99.74	98.53
						PPM				
Ni	9	9	10	5	3	4	12	9	7	22
Cr	4	5	4	1	2	2	22	5	6	32
V	312	354	348	79	75	71	224	305	129	721
Sc	16	15	20	8	6	8	17	17	13	50
Cu	150	126	141	3	4	3	102	146	27	361
Zn	96	118	117	68	52	61	95	115	80	180
Sr	2685	2571	2445	710	715	642	1349	2187	930	1061
Rb	159	155	153	95	87	120	139	84	104	15
Zr	129	148	145	115	108	107	183	119	115	143
Nb	5	6	6	11	10	10	19	10	10	4
Ba	1814	2141	2106	997	935	919	978	1635	1052	856
Pb	2	1	nd	10	9	14	10	3	10	nd
Th	nd	nd	nd	6	6	10	nd	nd	5	nd
La	37	53	52	24	21	22	38	41	27	88
Ce	83	97	100	39	35	33	72	82	40	170
Nd	41	53	52	15	16	16	36	44	22	96
Y	27	32	31	19	18	18	25	28	21	46
Mg#	40.50	41.45	41.21	42.88	41.22	42.12	46.38	41.22	42.41	49.61

SMK111.a - Malignite
 SMK111.b - Malignite
 SMK111.c - Shonkinite
 SMK113 - Monzonite
 SMK114 - Quartz Monzodiorite

SMK120 - Quartz Monzonite
 SMK125 & 126 - Shonkinite
 SMK134 - Mafic Syenite
 SMK136 - Quartz Monzonite
 SMK137 - Biotite Pyroxenite

Table B.1 (cont)

	142	158	159	161	162	163	164	167	168	169
SiO ₂	50.69	53.45	39.68	62.04	63.55	59.58	64.49	56.41	63.12	56.27
TiO ₂	0.89	0.79	1.74	0.52	0.40	0.57	0.44	0.42	0.39	0.64
Al ₂ O ₃	16.17	16.50	3.69	16.74	15.51	17.25	15.94	20.45	16.61	17.28
Fe ₂ O ₃	4.57	4.20	12.21	2.41	1.67	2.80	2.01	1.78	1.94	3.52
FeO	4.96	3.90	10.99	2.83	2.18	2.91	2.21	2.17	1.65	3.06
MnO	0.21	0.21	0.25	0.14	0.11	0.16	0.14	0.14	0.11	0.18
MgO	3.54	2.56	10.58	1.90	1.35	2.04	1.52	0.84	1.30	2.22
CaO	8.70	6.89	17.37	5.19	3.88	5.47	4.22	3.43	3.50	6.20
Na ₂ O	4.01	4.11	0.26	3.87	3.71	4.22	3.93	4.71	5.72	4.52
K ₂ O	4.61	4.61	0.36	3.22	3.42	3.08	3.69	7.41	5.21	4.29
P ₂ O ₅	0.71	0.42	0.40	0.28	0.19	0.33	0.21	0.19	0.17	0.39
LOI	0.43	0.32	0.45	0.68	0.65	0.85	0.60	1.63	0.42	0.56
Total	99.49	97.97	97.99	99.82	96.62	99.26	99.40	99.56	100.14	99.14
					PPM					
Ni	8	9	85	6	5	6	5	4	7	8
Cr	5	11	303	5	1	4	3	1	10	8
V	288	205	810	106	72	122	82	80	70	171
Sc	19	12	79	12	5	10	10	4	5	13
Cu	166	88	280	14	2	27	5	36	6	29
Zn	96	108	122	78	47	83	71	73	36	95
Sr	1553	1761	234	757	623	894	623	1553	885	1773
Rb	95	81	17	95	109	84	125	181	130	91
Zr	158	119	33	113	108	116	104	176	207	101
Nb	14	14	nd	9	10	10	11	18	14	12
Ba	1119	1252	79	994	921	1167	924	1066	849	1445
Pb	13	6	2	10	11	9	13	15	8	8
Th	2	nd	nd	7	11	5	9	5	7	nd
La	43	36	20	28	29	28	31	31	34	23
Ce	91	73	10	43	39	46	43	53	40	51
Nd	43	32	7	23	16	24	21	24	15	28
Y	29	29	12	21	18	22	21	21	19	24
Mg#	44.44	40.84	50.03	43.63	42.57	43.51	43.59	31.20	44.42	42.66

SMK142 - Shonkinite
 SMK158 - Mafic Monzonite
 SMK159 - Hornblende Pyroxenite
 SMK161 - Quartz Monzodiorite
 SMK162 - Quartz Monzonite

SMK163 - Quartz Monzodiorite
 SMK164 - Quartz Monzonite
 SMK167 - Gneissic Syenite
 SMK168 - Syenite
 SMK169 - Monzonite

Table B.1 (cont)

	170	175	176	179	183	187	188	189	190	192
SiO ₂	76.50	68.00	64.85	63.70	55.82	55.66	48.58	53.51	54.45	59.05
TiO ₂	0.05	0.29	0.43	0.47	0.76	0.40	1.00	0.77	0.51	0.64
Al ₂ O ₃	13.15	16.19	16.42	16.37	17.30	21.07	15.12	17.62	19.64	16.82
Fe ₂ O ₃	0.34	1.24	1.74	2.10	3.31	1.56	5.43	3.91	2.47	2.90
FeO	0.30	1.47	2.31	2.47	3.99	1.65	5.41	3.68	2.26	3.36
MnO	0.02	0.12	0.11	0.13	0.16	0.14	0.25	0.19	0.14	0.17
MgO	0.01	0.90	1.33	1.52	2.81	0.38	3.72	2.35	1.16	2.21
CaO	0.89	3.52	4.14	4.66	6.96	2.65	9.21	6.76	3.89	5.97
Na ₂ O	4.10	4.37	3.86	3.95	3.90	4.55	2.82	3.84	4.99	4.13
K ₂ O	4.33	2.80	3.73	3.36	3.47	8.46	4.52	5.88	8.00	3.21
P ₂ O ₅	0.01	0.13	0.20	0.23	0.40	0.11	0.81	0.51	0.25	0.37
LOI	0.23	0.53	0.57	0.65	nd	2.67	2.69	0.72	0.88	0.35
Total	99.93	99.56	99.67	99.60	98.43	99.29	99.57	99.74	98.64	99.17

	PPM									
Ni	4	3	5	5	7	3	11	7	5	16
Cr	nd	1	2	2	7	nd	6	1	1	7
V	6	42	77	91	186	65	325	212	104	139
Sc	nd	2	9	10	15	2	21	11	2	13
Cu	nd	nd	3	4	49	18	147	109	26	26
Zn	13	67	50	61	78	75	118	90	82	83
Sr	159	640	697	703	846	1856	2469	1712	2442	979
Rb	222	81	100	99	90	201	67	118	164	90
Zr	62	102	119	114	99	201	124	144	211	113
Nb	2	9	11	10	10	29	7	11	22	11
Ba	85	1309	1085	897	979	676	2065	1266	1982	1032
Pb	18	13	8	8	6	10	2	12	8	9
Th	33	4	10	8	4	7	nd	nd	3	7
La	19	22	29	30	27	42	42	39	30	34
Ce	9	25	38	46	35	61	80	82	72	51
Nd	nd	18	20	18	21	22	46	39	30	26
Y	3	16	22	21	24	21	29	25	20	24
Mg#	2.68	41.45	40.82	41.43	44.98	20.51	42.70	40.38	35.01	43.03

SMK170 - Alaskite

SMK175 - Granodiorite

SMK176 - Quartz Monzonite

SMK179 - Quartz Monzodiorite

SMK183 - Granodiorite

SMK187 - Gneissic Syenite

SMK188 - Malignite

SMK189 - Shonkinite

SMK190 - Mafic Syenite

SMK192 - Quartz Monzodiorite

Table B.1 (cont)

	193	194	195	196	198	199	200	202	204	205
SiO ₂	63.80	65.41	66.92	66.51	48.93	61.14	50.03	41.36	53.38	36.30
TiO ₂	0.41	0.42	0.35	0.36	0.72	0.56	0.86	1.54	0.69	1.99
Al ₂ O ₃	17.30	15.89	15.98	16.07	4.74	16.74	16.10	9.45	18.07	9.77
Fe ₂ O ₃	1.83	1.92	1.57	1.54	2.89	2.59	4.63	9.50	3.84	10.01
FeO	1.73	2.11	1.73	1.79	6.46	2.79	4.69	9.74	3.11	11.02
MnO	0.10	0.12	0.10	0.11	0.21	0.14	0.19	0.36	0.16	0.45
MgO	1.12	1.26	1.05	1.05	12.51	1.95	3.68	5.84	2.12	8.27
CaO	3.78	4.07	3.61	3.77	20.40	4.83	8.47	15.31	5.99	16.32
Na ₂ O	5.18	3.92	4.08	4.04	0.48	3.98	3.73	1.65	3.01	1.42
K ₂ O	4.03	3.46	3.22	3.36	0.78	3.78	5.59	1.72	6.68	1.56
P ₂ O ₅	0.18	0.20	0.16	0.16	0.21	0.31	0.64	1.57	0.46	2.04
LOI	0.30	0.49	0.63	0.35	1.28	0.53	0.71	0.87	0.98	1.06
Total	99.75	99.26	99.40	99.12	99.59	99.33	99.33	98.91	98.49	100.22
					PPM					
Ni	6	4	5	4	47	9	10	25	7	20
Cr	3	1	nd	3	118	7	13	24	4	17
V	70	76	52	57	265	111	258	448	200	650
Sc	6	7	6	6	77	11	18	36	11	50
Cu	4	4	2	5	15	30	144	162	76	62
Zn	44	64	57	57	71	74	89	149	87	222
Sr	1119	631	700	687	266	889	1411	1266	1938	784
Rb	109	122	105	109	34	116	162	43	129	14
Zr	165	102	106	109	45	191	141	108	87	210
Nb	13	10	8	8	2	17	12	9	4	21
Ba	921	824	1007	1039	259	1163	1137	478	1371	397
Pb	9	12	12	12	2	11	8	2	6	nd
Th	3	10	7	10	nd	11	nd	nd	nd	4
La	27	30	22	30	2	41	36	32	27	117
Ce	37	36	29	52	10	64	77	54	68	235
Nd	20	16	13	20	10	29	33	34	34	109
Y	19	18	15	15	13	22	26	40	21	65
Mg#	40.68	40.24	40.58	40.22	72.85	43.82	46.10	39.66	40.35	45.79

SMK193 - Quartz Monzonite
 SMK194 - Quartz Monzodiorite
 SMK195 - Granite
 SMK196 - Granodiorite
 SMK198 - Biotite Pyroxenite

SMK199 - Quartz Monzonite
 SMK200 - Shonkinite
 SMK202 - Pyroxenite
 SMK204 - Mafic Nepheline Syenite
 SMK205 - Biotite Pyroxenite

Table B.1 (cont)

	206	207	208	209	210	211	212	214	219
SiO ₂	39.36	49.32	73.53	49.80	43.28	55.79	56.03	58.35	40.60
TiO ₂	1.51	0.78	0.09	0.96	1.35	0.59	0.54	0.54	1.60
Al ₂ O ₃	9.06	13.59	14.50	15.57	7.47	19.12	19.56	18.16	3.67
Fe ₂ O ₃	9.60	3.34	0.37	4.20	7.00	3.67	3.46	2.94	11.02
FeO	9.32	5.83	0.51	5.58	8.03	2.32	2.14	2.58	10.45
MnO	0.37	0.18	0.02	0.21	0.40	0.16	0.16	0.16	0.25
MgO	5.74	6.86	0.17	4.23	9.05	1.72	1.79	1.80	10.95
CaO	15.18	9.13	1.51	9.37	17.58	4.74	4.09	5.94	18.15
Na ₂ O	1.54	2.21	4.50	3.37	1.39	4.40	4.16	4.61	0.31
K ₂ O	1.71	5.36	4.15	3.83	0.85	5.76	6.66	3.27	0.37
P ₂ O ₅	1.51	0.74	0.03	0.75	1.48	0.29	0.30	0.28	0.57
LOI	0.23	0.98	0.20	0.93	0.71	0.85	0.88	0.40	0.68
Total	95.14	98.31	99.57	98.79	98.60	99.41	99.76	99.03	98.61
				PPM					
Ni	14	72	4	12	23	7	7	8	83
Cr	15	205	nd	16	67	12	9	2	333
V	610	266	16	306	454	134	128	110	746
Sc	37	24	1	24	54	5	8	10	82
Cu	261	96	2	19	17	34	27	7	149
Zn	180	84	6	98	172	88	86	60	114
Sr	1794	1361	552	1781	423	1870	1482	1274	223
Rb	20	107	135	79	27	120	152	55	16
Zr	165	134	53	148	193	131	149	123	32
Nb	9	13	4	15	14	17	18	7	2
Ba	1758	1313	435	1453	166	1279	1147	1349	72
Pb	nd	7	12	5	4	11	11	5	1
Th	nd	1	22	nd	5	nd	1	nd	nd
La	68	26	8	37	70	24	29	24	12
Ce	145	60	16	80	150	52	60	51	11
Nd	82	33	6	41	79	26	30	24	9
Y	46	22	5	27	54	20	19	22	14
Mg#	39.79	60.53	28.85	47.65	56.30	39.56	42.24	41.83	52.69

SMK206 - Hornblende Pyroxenite
 SMK207 - Shonkinite
 SMK208 - Alaskite
 SMK209 - Mafic Nepheline Syenite
 SMK210 - Biotite Pyroxenite

SMK211 - Gneissic Syenite
 SMK212 - Gneissic Shonkinite
 SMK214 - Monzodiorite
 SMK219 - Biotite Pyroxenite

Table B.2 ICP Whole Rock Trace Element Analyses

Sample	111.b	183	188	189	195	200	207	209	210
					ppm				
La	56.56	27.11	46.860	43.91	22.92	42.96	34.44	43.45	71.69
Ce	101.94	43.76	100.420	86.34	38.97	75.54	61.80	85.41	160.17
Nd	65.15	23.29	52.74	40.93	15.15	41.83	34.75	42.51	88.03
Sm	12.97	5.35	11.04	8.19	3.14	8.41	7.02	8.82	18.94
Eu	3.72	1.53	3.18	2.42	0.91	2.35	2.06	2.54	4.34
Gd	10.71	4.81	9.27	7.06	2.82	7.43	6.19	7.79	16.49
Dy	7.15	4.66	6.30	5.03	2.56	5.23	4.08	5.18	11.44
Ho	1.58	0.93	1.22	0.89	0.52	1.04	0.80	1.04	2.13
Yb	2.88	2.29	2.28	2.1	1.49	2.13	1.77	2.12	4.56
Lu	0.44	0.36	0.34	0.31	0.23	0.31	0.25	0.30	0.67
Y	33.64	25.67	28.41	24.31	15.72	25.01	20.35	25.68	55.20

APPENDIX C

Microprobe Data

The following appendix includes mineral composition data obtained by Professor R.S. Babcock on the Grant Institute of Geology, University of Edinburghs' Camebax microprobe. Data were corrected using the Bence-Albee correction procedure (Bence and Albee, 1968).

Table C.1 Clinopyroxene Compositions

	111.B-1	125.A-1	125.A-2	125.C	206.A-1	142.A-1	142.A-2	142.B	159.B
SiO2	51.16	47.19	46.89	47.25	46.18	49.15	46.63	50.55	52.82
Al2O3	6.13	6.02	6.21	6.05	6.36	4.43	6.07	3.34	1.08
TiO2	0.58	1.00	1.07	1.11	1.42	0.77	1.21	0.66	0.13
FeO*	13.32	13.62	12.47	12.50	12.25	8.55	12.49	8.25	5.34
MnO	0.41	0.45	0.46	0.38	0.49	0.35	0.49	0.37	0.18
MgO	6.36	8.33	8.93	9.03	8.85	11.71	8.72	12.37	14.6
Cr2O3	0.00	0.01	0.00	0.01	0.00	0.00	0.00	0.00	0.00
CaO	18.45	21.71	22.04	22.51	22.53	22.73	22.04	22.75	24.96
Na2O	3.61	1.65	1.46	1.36	1.05	1.16	1.45	1.03	0.15
Total	100.02	99.98	99.53	100.20	99.13	98.85	99.10	99.32	99.26

FeO* = total Fe

Cations Based on 6 Oxygens

Si	1.94	1.82	1.81	1.81	1.79	1.87	1.81	1.91	1.97
Al	0.27	0.27	0.28	0.27	0.29	0.20	0.28	0.15	0.05
Ti	0.02	0.03	0.03	0.03	0.04	0.02	0.04	0.02	0.00
Fe	0.42	0.44	0.40	0.40	0.40	0.27	0.41	0.26	0.17
Mn	0.01	0.01	0.02	0.01	0.02	0.01	0.02	0.01	0.01
Mg	0.36	0.48	0.51	0.52	0.51	0.66	0.50	0.70	0.81
Cr	0.00	0.00	0.00	0.00	0.00	0.00	0.00	0.00	0.00
Ca	0.75	0.90	0.91	0.92	0.94	0.93	0.92	0.92	1.00
Na	0.27	0.12	0.11	0.10	0.08	0.09	0.11	0.08	0.01
Total	4.04	4.08	4.07	4.07	4.06	4.05	4.07	4.04	4.01

	206.A-2	206.B	206.C	111.B-2	111.B-3	111.B-1 = Rim	206.C = Rim
SiO2	46.92	45.60	45.91	46.49	47.16	125.A-1 = Core	111.B-2 = Core
Al2O3	5.63	6.98	6.08	5.89	4.98	125.A-2 = Rim	111.B-3 = Core
TiO2	1.18	1.56	1.36	1.28	1.27	125.C = Core	142.A-1 = Core
FeO*	11.93	12.73	12.37	11.89	13.03	206.A-1 = Core	142.A-2 = Rim
MnO	0.49	0.43	0.46	0.46	0.49	206.A-2 = Rim	142.B = Core
MgO	9.28	8.80	8.95	9.05	8.65	206.B = Rim	159.B = Core
Cr2O3	0.00	0.00	0.00	0.00	0.00		
CaO	22.49	22.72	22.61	22.16	21.90		
Na2O	1.05	0.95	1.07	1.49	1.60		
Total	98.97	99.77	98.81	98.71	99.08		

FeO* = total Fe

Cations Based on 6 Oxygens

Si	1.82	1.76	1.79	1.82	1.82
Al	0.26	0.32	0.28	0.26	0.27
Ti	0.03	0.05	0.04	0.03	0.03
Fe	0.39	0.41	0.40	0.39	0.44
Mn	0.02	0.01	0.02	0.02	0.01
Mg	0.54	0.51	0.52	0.54	0.48
Cr	0.00	0.00	0.00	0.00	0.00
Ca	0.93	0.94	0.94	0.93	0.90
Na	0.08	0.07	0.08	0.08	0.12
Total	4.06	4.07	4.07	4.06	4.08

Table C.2 Amphibole Compositions

	AM111.b-1	AM111.b-2	AM111.d-1	AM111.d-2	AM120.a-1	AM125.b	AM125.ov	AM125.c
Na ₂ O	3.07	2.92	2.68	2.84	1.53	2.65	2.37	2.52
MgO	6.96	6.81	6.51	6.08	11.28	7.34	7.37	7.44
Al ₂ O ₃	12.13	12.36	11.55	12.22	8.58	13.20	13.40	13.47
SiO ₂	37.64	37.51	37.60	39.26	43.64	38.23	38.01	38.48
K ₂ O	2.29	2.39	2.43	2.61	1.15	2.23	2.22	2.19
CaO	10.28	10.43	10.38	9.72	11.46	10.81	11.18	11.21
TiO ₂	1.20	1.10	0.85	0.77	1.69	2.10	2.30	2.20
MnO	0.59	0.56	0.60	0.54	0.77	0.52	0.48	0.49
FeO*	22.62	22.72	23.95	22.51	16.55	20.72	20.31	20.37
Total	96.78	96.80	96.55	96.55	96.65	97.80	97.64	98.37

FeO* = total Fe

Cations Based on 23 Oxygens

Na	0.95	0.91	0.84	0.88	0.45	0.80	0.72	0.76
Mg	1.66	1.62	1.57	1.44	2.56	1.71	1.72	1.72
Al	2.29	2.33	2.20	2.29	1.54	2.43	2.47	2.46
Si	6.02	6.00	6.07	6.25	6.66	5.97	5.94	5.96
K	0.47	0.49	0.50	0.53	0.22	0.44	0.44	0.43
Ca	1.76	1.79	1.80	1.66	1.87	1.81	1.87	1.86
Ti	0.14	0.13	0.10	0.09	0.19	0.25	0.27	0.26
Mn	0.08	0.08	0.08	0.07	0.10	0.07	0.06	0.06
Fe	3.03	3.04	3.23	3.00	2.11	2.71	2.65	2.64
Total	16.40	16.39	16.39	16.21	15.72	16.19	16.14	16.15

	AM120.a-2	AM120.c-1	AM120.c-2	AM120.d	AM125.a	AM159.a	AM159.b	AM206.a-1
Na ₂ O	1.23	1.27	1.37	1.28	2.64	1.67	1.93	1.71
MgO	10.63	11.87	10.54	11.45	7.84	10.09	11.13	8.08
Al ₂ O ₃	8.51	7.67	8.82	7.47	12.77	10.95	11.90	13.37
SiO ₂	44.54	44.98	43.26	45.47	38.78	41.20	41.01	37.61
K ₂ O	0.89	0.91	1.13	0.89	2.04	1.40	1.20	2.62
CaO	11.48	11.40	11.36	11.36	10.94	11.97	12.18	11.63
TiO ₂	0.77	1.36	1.22	1.30	2.47	1.80	1.43	2.99
MnO	1.08	0.82	0.90	0.97	0.49	0.24	0.19	0.51
FeO*	17.86	15.86	17.45	16.39	19.67	17.57	15.50	19.24
Total	96.99	96.14	96.05	96.58	97.64	96.89	96.47	97.76

FeO* = total Fe

Cations Based on 23 Oxygens

Na	0.36	0.37	0.41	0.38	0.80	0.50	0.57	0.52
Mg	2.41	2.69	2.42	2.59	1.82	2.31	2.53	1.87
Al	1.53	1.38	1.60	1.34	2.34	1.98	2.14	2.45
Si	6.78	6.84	6.67	6.89	6.03	6.33	6.26	5.86
K	0.17	0.18	0.22	0.17	0.40	0.27	0.23	0.52
Ca	1.87	1.86	1.88	1.85	1.82	1.97	1.99	1.94
Ti	0.09	0.16	0.14	0.15	0.29	0.21	0.16	0.35
Mn	0.14	0.11	0.12	0.12	0.06	0.03	0.02	0.07
Fe	2.27	2.02	2.25	2.08	2.56	2.26	1.98	2.51
Total	15.63	15.59	15.71	15.56	16.11	15.86	15.90	16.08

Table C.2 (cont)

	AM206.a-2	AM206.b	AM142.a	AM142.a	
Na ₂ O	1.68	1.71	2.42	2.37	Am111.b-1 = Core
MgO	8.19	7.97	7.24	8.68	Am111.b-2 = Rim
Al ₂ O ₃	13.26	13.13	13.26	12.48	Am111.d-1 = Core
SiO ₂	37.35	37.81	38.09	38.86	Am111.d-2 = Rim
K ₂ O	2.56	2.50	2.21	2.22	Am120.a-1 = Core
CaO	11.68	11.65	11.23	11.52	Am120.a-2 = Rim
TiO ₂	2.90	2.87	2.47	2.69	Am120.c-1 = Core
MnO	0.46	0.49	0.58	0.50	Am120.c-2 = Core
FeO*	18.76	19.11	20.24	18.30	Am120.d = Core
Total	96.84	97.24	97.74	97.62	Am125.a = Core
FeO* = to					Am125.b = Core
					Am125.ov = overgrowth of cpx
Na	0.51	0.52	0.73	0.71	Am125.c = overgrowth of cpx
Mg	1.92	1.86	1.68	2.00	Am206.a-1 = Core
Al	2.45	2.42	2.44	2.28	Am206.a-2 = Rim
Si	5.86	5.91	5.95	6.02	Am206.b = Rim
K	0.51	0.50	0.44	0.44	
Ca	1.96	1.95	1.88	1.91	
Ti	0.34	0.34	0.29	0.31	
Mn	0.06	0.06	0.08	0.07	
Fe	2.46	2.50	2.64	2.37	
Total	16.08	16.05	16.13	16.11	

Table C.3 Biotite Compositions

	Bi111.a-1	Bi111.a-2	Bi111.b	Bi120.a	Bi120.b	Bi159.a	Bi159.b	
Na2O	0.06	0.07	0.14	0.07	0.04	0.04	0.04	
MgO	9.71	9.54	10.73	11.47	12.33	13.72	12.95	Bi111.a-1 = Rim
Al2O3	17.86	17.74	15.27	15.16	15.25	15.09	15.25	Bi111.a-2 = Core
SiO2	34.30	34.06	34.02	37.10	37.12	35.79	35.53	Bi111.b = Core
K2O	10.17	10.06	9.79	9.71	9.69	9.94	9.61	Bi120.a = Rim
CaO	0.06	0.00	0.00	0.00	0.02	0.00	0.00	Bi120.b = Rim
TiO2	1.80	1.74	2.41	2.08	1.53	1.69	1.22	Bi159.a = Core
MnO	0.59	0.58	0.53	0.85	0.76	0.22	0.21	Bi159.b = Core
FeO*	20.48	20.57	21.84	19.02	18.62	16.97	18.52	
Total	95.03	94.36	94.73	95.46	95.36	93.46	93.33	

FeO* = total Fe

Cations Based on 23 Oxygens

Na	0.02	0.02	0.04	0.02	0.01	0.01	0.01
Mg	2.35	2.33	2.63	2.73	2.93	3.31	3.15
Al	3.42	3.42	2.96	2.85	2.86	2.88	2.93
Si	5.57	5.58	5.60	5.92	5.91	5.80	5.80
K	2.11	2.10	2.06	1.98	1.97	2.05	2.00
Ca	0.01	0.00	0.00	0.00	0.00	0.00	0.00
Ti	0.22	0.21	0.30	0.25	0.18	0.21	0.15
Mn	0.08	0.08	0.07	0.11	0.10	0.03	0.03
Fe	2.78	2.82	3.01	2.54	2.48	2.30	2.53
Total	16.56	16.56	16.67	16.40	16.46	16.59	16.59

Table C.4 Oxide Compositions

	Mt142.a	Mt159.a	Mt206.a		Am120.b
Na2O	0.01	0.01	0.03	Na2O	0.02
MgO	0.02	0.02	0.03	MgO	0.01
Al2O3	0.16	0.06	0.06	Al2O3	1.44
SiO2	0.08	0.04	0.02	SiO2	29.05
TiO2	0.54	0.03	0.05	CaO	26.37
Cr2O3	0.04	0.18	0.04	TiO2	36.24
MnO	0.30	0.11	0.28	MnO	0.24
FeO*	91.28	91.37	91.39	FeO*	1.72
Total	92.43	91.82	91.90	Total	95.09

FeO* = total Fe

Cations Based on 4 Oxygens

Na	0.00	0.00	0.02	Mt142.a = Magnetite
Mg	0.01	0.01	0.02	Mt159.a = Magnetite
Al	0.08	0.03	0.03	Mt206.a = Magnetite
Si	0.03	0.02	0.00	Am120.b = Sphene
Ti	0.17	0.00	0.02	
Cr	0.01	0.06	0.01	
Mn	0.10	0.04	0.10	
Fe	31.34	31.76	31.76	
Total	31.76	31.93	31.96	

Table C.5 Feldspar Compositions

	Kf111	Kf120	Kf125	Kf142.b	Kf206	Pl120	Pl142.a	
Na ₂ O	0.98	0.52	0.89	0.96	0.69	7.56	7.72	Kf111 = Core
MgO	0.00	0.01	0.00	0.01	0.01	0.01	0.01	Kf120 = Megacryst Core
Al ₂ O ₃	18.78	18.60	18.93	18.68	19.32	24.54	24.24	Kf125 = Core
SiO ₂	63.78	64.44	64.31	63.70	62.07	60.21	59.54	Kf142.b = Core
K ₂ O	15.28	16.16	15.72	15.03	14.69	0.08	0.21	Kf206 = Interstitial
CaO	0.02	0.00	0.01	0.16	0.02	6.34	6.09	Pl120 = Core
FeO*	0.08	0.06	0.00	0.08	0.11	0.14	0.16	Pl142.b = Core
BaO	0.43	0.86	0.50	0.30	1.78	0.00	0.01	
Total	99.35	100.65	100.36	98.92	98.69	98.88	97.98	

FeO* = total Fe

Cations Based on 8 Oxygens

	Kf111	Kf120	Kf125	Kf142.b	Kf206	Pl120	Pl142.a
Na	0.35	0.19	0.32	0.35	0.25	2.63	2.72
Mg	0.00	0.00	0.00	0.00	0.00	0.00	0.00
Al	4.13	4.06	4.12	4.11	4.31	5.20	5.19
Si	11.89	11.92	11.88	11.90	11.74	10.82	10.81
K	3.63	3.81	3.71	3.58	3.55	0.02	0.05
Ca	0.00	0.00	0.00	0.03	0.00	1.22	1.18
Fe	0.01	0.00	0.00	0.01	0.02	0.02	0.02
Ba	0.03	0.06	0.04	0.02	0.13	0.00	0.00
Total	20.05	20.05	20.07	20.01	20.00	19.91	19.98

Table C.6 Garnet Compositions

	Gt111.d-1	Gt111.c-1	Gt11	Gt111.	Gt111.c-2	Gt111.d-2	
SiO ₂	35.62	34.60	34.55	35.17	34.72	34.83	Gt111.d-1 = Rim
TiO ₂	2.77	2.75	3.21	2.42	2.46	2.53	Gt111.c-1 = Core
Al ₂ O ₃	10.14	5.07	5.72	4.91	5.21	5.08	Gt111 = Rim
Cr ₂ O ₃	0.00	0.01	0.02	0.02	0.02	0.01	Gt111.b = Rim
FeO*	13.66	21.07	20.62	21.51	21.41	21.58	Gt111.c-2 = Rim
MnO	0.60	0.60	0.64	0.60	0.62	0.60	Gt111.d-2 = Core
MgO	0.05	0.29	0.32	0.26	0.26	0.27	
CaO	35.03	32.98	32.26	32.76	32.57	32.88	
Total	97.87	97.38	97.34	97.67	97.27	97.77	

FeO* = total Fe

Cations Based on 24 Oxygens

	Gt111.d-1	Gt111.c-1	Gt11	Gt111.	Gt111.c-2	Gt111.d-2
Si	5.98	6.10	6.06	6.18	6.12	6.12
Ti	0.35	0.37	0.42	0.32	0.33	0.33
Al	2.01	1.05	1.18	1.02	1.08	1.05
Cr	0.00	0.00	0.00	0.00	0.00	0.00
Fe	1.92	3.12	3.02	3.16	3.16	3.17
Mn	0.09	0.09	0.10	0.09	0.09	0.09
Mg	0.01	0.08	0.08	0.07	0.07	0.07
Ca	6.30	6.23	6.06	6.16	6.15	6.19
Total	16.66	17.01	16.93	17.00	17.01	17.02

APPENDIX D

Rb-Sr Isotopic Compositions

Twentyfour whole rock samples from representative lithologic units throughout the Similkameen batholith were analyzed for Sr isotopic compositions in the geochronology laboratory at the University of British Columbia. The work was conducted by the author under the guidance Dita Runkle and Professor Richard Lee Armstrong.

Excess rock powders obtained for whole rock, major and trace element analysis were used. Rb and Sr concentrations were determined by replicate analyses of pressed powder pellets using X-ray fluorescence. United States Geological Survey rock standards were used for calibration; mass absorption coefficients were obtained from Mo K-alpha Compton scattering measurements. Rb/Sr ratios have a precision of 2% (one sigma) where both concentrations exceed 50 ppm. Sr isotopic compositions were measured on unspiked samples dissolved in teflon beakers with HF and prepared using standard ion exchange techniques. Sr isotopic measurements were made on a Vacuum-Generators Isomass 54R mass spectrometer automated with a Hewlett-Packard HP-85 computer. Measured ratios have been normalized to a $^{87}\text{Sr}/^{86}\text{Sr}$ ratio of 0.1194 and adjusted so that the National Bureau of Standards standard SrCO_3 (SRM 987) gives a $^{87}\text{Sr}/^{86}\text{Sr}$ ratio of 0.71019 ± 0.00002 and the Eimer and Amend Sr standard a ratio of 0.70800 ± 0.00002 . The precision of a single $^{87}\text{Sr}/^{86}\text{Sr}$ ratio is less than 0.0001 (one sigma). Any exceptions are noted. Rb-Sr dates are based on a Rb decay constant of $1.42 \times 10^{-11} \text{y}^{-1}$ (Steiger and Jager, 1977). The regressions are calculated according to the technique of York (1967). Errors reported are one standard deviation or the standard error of the mean, unless otherwise noted.

Table D.1 Sr Isotopic Compositions of the Similkameen Batholith Samples

SAMPLE	ROCK TYPE	Rb* ppm	Sr*	87Rb/86Sr	87Sr/86Sr**	87Sr/86Sr(T)
SMK-111.A	Malignite	167.0	2773	0.174	0.70419 ±5	0.703769
SMK-120	Granodiorite	120.0	654	0.529	0.70548 ±5	0.704201
SMK-126	Shonkinite	124.0	1490	0.240	0.70445 ±5	0.703870
SMK-134	Shonkinite	89.0	2237	0.115	0.70411 ±5	0.703832
SMK-142	Shonkinite	100.0	1600	0.181	0.70435 ±5	0.703913
SMK-158	Mafic Syenite	86.0	1811	0.137	0.70445 ±5	0.704119
SMK-159	Bt-Pyroxenite	19.8	283	0.202	0.70453 ±5	0.704042
SMK-167	Gneissic Syenite	183.0	1575	0.335	0.70471 ±5	0.703900
SMK-169	Mafic Syenite	95.9	1797	0.154	0.70437 ±5	0.703998
SMK-175	Granodiorite	81.0	636	0.369	0.70481 ±5	0.703918
SMK-179	Monzonite	99.2	711	0.404	0.70501 ±5	0.704034
SMK-189	Mafic Syenite	120.0	1735	0.200	0.70441 ±5	0.703927
SMK-190	Mafic Syenite	172.0	2470	0.201	0.70442 ±5	0.703934
SMK-195	Monzonite	105.0	699	0.433	0.70508 ±5	0.704033
SMK-200	Shonkinite	166.0	1461	0.329	0.70479 ±5	0.703995
SMK-205	Bt-Pyroxenite	17.1	798	0.062	0.70398 ±5	0.703830
SMK-206	A-Pyroxenite	26.1	1899	0.040	0.70395 ±5	0.703853
SMK-207	Shonkinite	113.0	1431	0.228	0.70429 ±5	0.703739
SMK-208	Alaskite	135.0	552	0.710	0.70573 ±5	0.704014
SMK-209	Shonkinite	83.0	1840	0.131	0.70412 ±5	0.703803
SMK-210	Bt-Pyroxenite	28.3	435	0.189	0.70428 ±5	0.703823
SMK-213	Granodiorite	115.0	976	0.340	0.70488 ±5	0.704058
SMK-25	Alaskite	455.0	125	10.55	0.72737 ±5	0.701872
SMK-170	Alaskite	218.0	153	4.10	0.71321 ±5	0.703301

* Rb and Sr concentrations by XRF

** Errors for samples are 1 sigma, values for SRM987 are:
87Sr/86Sr= 0.71019 ± 0.00002.

87Sr/86Sr(T) calculated for age of T=170 Ma

Table D.2 AFC Modeling Data

Sample	Rock Type	87Sr/86Sr 170Ma	Sr ppm 170Ma
Contaminant			
SH-A	Paragneiss	.7202	447
SH-D	Bi-Plg Granulite	.7071	717
SH-T	Paragneiss	.7126	369
Parent			
	Rock Type	87Sr/86Sr 170Ma	Sr ppm 170Ma
SMK126	Shonkinite	.7039	1336
SMK189	Shonkinite	.7039	1609
SMK207	Shonkinite	.7037	1279
SMK188	Malignite	.7038	2321
SMK111.a	Malignite	.7038	2524

APPENDIX E
Results of Mass-Balance Calculations

The following data are the results of mass-balance comparisons the crystal fractionation and mixing modeling presented in Chapter 3. Fractionation runs utilized the program GPP by Dr. A. McBirney of the University of Oregon. The mixing calculations were done with the program MULTIFIT by W.M. Bryan (1986).

Fractionation Runs

	PARENT	125.A	142.A	D43	111.BI	DAUGHTER
SI02	48.58	47.19	0.08	0.47	34.02	50.40
TIO2	1.00	1.00	0.54	0.00	2.41	0.90
AL2O3	15.12	6.02	0.16	0.00	15.27	16.49
FE2O3	0.00	0.00	0.00	0.00	0.00	0.00
FEO	10.30	13.62	91.28	0.51	21.84	8.41
MNO	0.25	0.45	0.30	0.06	0.53	0.22
MGO	3.72	8.33	0.02	0.08	10.73	2.80
CAO	9.21	21.71	0.00	53.87	0.00	7.78
NA2O	2.82	1.65	0.01	0.11	0.14	2.45
K2O	4.52	0.00	0.00	0.00	9.79	7.12
H2O+	2.69	0.00	0.00	0.23	0.00	1.80
H2O-	0.00	0.00	0.00	0.00	0.00	0.00
P2O5	0.81	0.00	0.00	39.97	0.00	0.65

(PARENT-MINERALS=DAUGHTER)

PARENT: 188
 DAUGHTER: 111.A

	SOL'N	% CUMULATE
188	1.000	
125.A	-0.120	72.500
142.A	-0.011	6.907
D43	-0.004	2.548
111.BI	-0.030	18.044
111.A	0.834	

R SQUARED = 0.827

	PARENT ANALYSIS	DAUGHTER ANALYSIS	DAUGHTER CALC	WEIGHTED RESID
SI02	53.64	55.91	55.96	-0.05
TIO2	1.11	1.00	1.07	-0.04
AL2O3	16.70	18.29	18.50	-0.21
FEO	11.37	9.33	9.34	-0.02
MNO	0.27	0.24	0.23	0.00
MGO	4.11	3.10	3.25	-0.15
CAO	10.17	8.63	8.63	0.00
NA2O	3.11	2.72	3.48	-0.31
K2O	4.99	7.90	5.57	0.81
P2O5	0.89	0.72	0.80	-0.04

	PARENT	125.A	142.A	D43	111.BI	DAUGHTER
SiO2	50.40	47.19	0.08	0.47	34.02	53.38
TiO2	0.90	1.00	0.54	0.00	2.41	0.69
Al2O3	16.49	6.02	0.16	0.00	15.27	18.07
Fe2O3	0.00	0.00	0.00	0.00	0.00	0.00
FeO	8.41	13.62	91.28	0.51	21.84	6.57
MnO	0.22	0.45	0.30	0.06	0.53	0.16
MgO	2.80	8.33	0.02	0.08	10.73	2.12
CaO	7.78	21.71	0.00	53.87	0.00	5.99
Na2O	2.45	1.65	0.01	0.11	0.14	3.01
K2O	7.12	0.00	0.00	0.00	9.79	6.68
H2O+	1.80	0.00	0.00	0.23	0.00	0.98
H2O-	0.00	0.00	0.00	0.00	0.00	0.00
P2O5	0.65	0.00	0.00	39.97	0.00	0.46

(PARENT-MINERALS=DAUGHTER)

PARENT: 111.A
 DAUGHTER: 204

	SOL'N	% CUMULATE
111.A	1.000	
125.A	-0.082	56.941
142.A	-0.010	7.219
D43	-0.015	10.199
111.BI	-0.037	25.641
204	0.856	

R SQUARED = 0.366

	PARENT ANALYSIS	DAUGHTER ANALYSIS	DAUGHTER CALC	WEIGHTED RESID
SiO2	55.91	59.15	59.00	0.14
TiO2	1.00	0.76	0.94	-0.09
Al2O3	18.29	20.02	20.02	0.01
FeO	9.33	7.27	7.26	0.01
MnO	0.24	0.18	0.21	-0.00
MgO	3.10	2.35	2.28	0.07
CaO	8.63	6.63	6.73	-0.10
Na2O	2.72	3.33	3.00	0.13
K2O	7.90	7.40	8.74	-0.47
P2O5	0.72	0.51	-0.08	0.30

	PARENT	125.A	142.A	D43	111.BI	DAUGHTER
SIO2	48.58	47.19	0.08	0.47	34.02	53.38
TIO2	1.00	1.00	0.54	0.00	2.41	0.69
AL2O3	15.12	6.02	0.16	0.00	15.27	18.07
FE2O3	0.00	0.00	0.00	0.00	0.00	0.00
FEO	10.30	13.62	91.28	0.51	21.84	6.57
MNO	0.25	0.45	0.30	0.06	0.53	0.16
MGO	3.72	8.33	0.02	0.08	10.73	2.12
CAO	9.21	21.71	0.00	53.87	0.00	5.99
NA2O	2.82	1.65	0.01	0.11	0.14	3.01
K2O	4.52	0.00	0.00	0.00	9.79	6.68
H2O+	2.69	0.00	0.00	0.23	0.00	0.98
H2O-	0.00	0.00	0.00	0.00	0.00	0.00
P2O5	0.81	0.00	0.00	39.97	0.00	0.46

(PARENT-MINERALS=DAUGHTER)

PARENT: 188
DAUGHTER: 204

	SOL'N	% CUMULATE
188	1.000	
125.A	-0.193	67.654
142.A	-0.021	7.230
D43	-0.015	5.286
111.BI	-0.057	19.830
204	0.715	

R SQUARED = 0.659

	PARENT ANALYSIS	DAUGHTER ANALYSIS	DAUGHTER CALC	WEIGHTED RESID
SIO2	53.24	58.50	58.42	0.08
TIO2	1.10	0.75	1.03	-0.14
AL2O3	16.57	19.80	20.15	-0.34
FEO	11.28	7.19	7.20	-0.00
MNO	0.27	0.18	0.20	-0.00
MGO	4.08	2.32	2.45	-0.13
CAO	10.10	6.56	6.64	-0.08
NA2O	3.09	3.29	3.85	-0.22
K2O	4.95	7.32	6.04	0.64
P2O5	0.89	0.51	0.12	0.20

UNWEIGHTED INPUT DATA:

	PARENT	125.A	142.A	D43	111.BI	DAUGHTER
SIO2	49.80	47.19	0.08	0.47	34.02	51.40
TIO2	0.96	1.00	0.54	0.00	2.41	0.80
AL2O3	15.57	6.02	0.16	0.00	15.27	16.77
FE2O3	0.00	0.00	0.00	0.00	0.00	0.00
FEO	9.36	13.62	91.28	0.51	21.84	7.77
MNO	0.21	0.45	0.30	0.06	0.53	0.19
MGO	4.23	8.33	0.02	0.08	10.73	3.36
CAO	9.37	21.71	0.00	53.87	0.00	7.48
NA2O	3.37	1.65	0.01	0.11	0.14	3.37
K2O	3.83	0.00	0.00	0.00	9.79	5.57
H2O+	0.93	0.00	0.00	0.23	0.00	0.93
H2O-	0.00	0.00	0.00	0.00	0.00	0.00
P2O5	0.75	0.00	0.00	39.97	0.00	0.54

(PARENT-MINERALS=DAUGHTER)

PARENT: 209
DAUGHTER: 125

	SOL'N	% CUMULATE
209	1.000	
125.A	-0.117	74.735
142.A	-0.007	4.624
D43	-0.008	5.363
111.BI	-0.024	15.278
125	0.843	

R SQUARED = 0.742

	PARENT ANALYSIS	DAUGHTER ANALYSIS	DAUGHTER CALC	WEIGHTED RESID
SIO2	53.67	55.90	55.88	0.02
TIO2	1.03	0.86	1.00	-0.07
AL2O3	16.77	18.24	18.55	-0.31
FEO	10.09	8.45	8.46	-0.01
MNO	0.23	0.21	0.18	0.00
MGO	4.55	3.66	3.87	-0.22
CAO	10.09	8.13	8.17	-0.04
NA2O	3.63	3.66	4.07	-0.20
K2O	4.13	6.06	4.58	0.74
P2O5	0.81	0.59	0.43	0.08

UNWEIGHTED INPUT DATA:

	PARENT	125.A	D43	111.BI	DAUGHTER
SIO2	49.80	47.19	0.47	34.02	50.69
TIO2	0.96	1.00	0.00	2.41	0.89
AL2O3	15.57	6.02	0.00	15.27	16.17
FE2O3	0.00	0.00	0.00	0.00	0.00
FEO	9.36	13.62	0.51	21.84	9.07
MNO	0.21	0.45	0.06	0.53	0.21
MGO	4.23	8.33	0.08	10.73	3.54
CAO	9.37	21.71	53.87	0.00	8.70
NA2O	3.37	1.65	0.11	0.14	4.01
K2O	3.83	0.00	0.00	9.79	4.61
H2O+	0.93	0.00	0.23	0.00	0.43
H2O-	0.00	0.00	0.00	0.00	0.00
P2O5	0.75	0.00	39.97	0.00	0.71

(PARENT-MINERALS=DAUGHTER)

PARENT: 209
 DAUGHTER: 142

	SOL'N	% CUMULATE
209	1.000	
125.A	-0.064	78.199
D43	-0.001	1.779
111.BI	-0.016	20.022
142	0.918	

R SQUARED = 0.354

	PARENT ANALYSIS	DAUGHTER ANALYSIS	DAUGHTER CALC	WEIGHTED RESID
SIO2	53.67	54.32	54.41	-0.09
TIO2	1.03	0.95	1.01	-0.03
AL2O3	16.77	17.33	17.53	-0.20
FEO	10.09	9.72	9.58	0.15
MNO	0.23	0.22	0.20	0.00
MGO	4.55	3.80	4.15	-0.35
CAO	10.09	9.32	9.34	-0.02
NA2O	3.63	4.30	3.83	0.24
K2O	4.13	4.94	4.30	0.32
P2O5	0.81	0.77	0.80	-0.02

UNWEIGHTED INPUT DATA:

	PARENT	125.A	125.B	D43	DAUGHTER
SIO2	51.40	47.19	38.23	0.47	53.51
TIO2	0.80	1.00	2.10	0.00	0.77
AL2O3	16.77	6.02	13.20	0.00	17.62
FE2O3	0.00	0.00	0.00	0.00	0.00
FEO	7.77	13.62	20.72	0.51	7.20
MNO	0.19	0.45	0.52	0.06	0.19
MGO	3.36	8.33	7.34	0.08	2.35
CAO	7.48	21.71	10.81	53.87	6.76
NA2O	3.37	1.65	2.65	0.11	3.84
K2O	5.57	0.00	2.23	0.00	5.88
H2O+	0.93	0.00	0.00	0.23	0.72
H2O-	0.00	0.00	0.00	0.00	0.00
P2O5	0.54	0.00	0.00	39.97	0.51

(PARENT-MINERALS=DAUGHTER)

PARENT: 125
DAUGHTER: 189

	SOL'N	% CUMULATE
125	1.000	
125.A	-0.042	45.625
125.B	-0.049	53.185
D43	-0.001	1.190
189	0.907	

R SQUARED = 0.752

	PARENT ANALYSIS	DAUGHTER ANALYSIS	DAUGHTER CALC	WEIGHTED RESID
SIO2	56.07	57.74	57.34	0.40
TIO2	0.87	0.83	0.79	0.02
AL2O3	18.30	19.02	19.12	-0.10
FEO	8.48	7.77	7.50	0.27
MNO	0.21	0.21	0.18	0.00
MGO	3.67	2.54	3.22	-0.68
CAO	8.16	7.30	7.25	0.05
NA2O	3.68	4.14	3.82	0.16
K2O	6.08	6.35	6.57	-0.10
P2O5	0.59	0.55	0.59	-0.02

UNWEIGHTED INPUT DATA:

	PARENT	125.A	142.A	D43	111.BI	DAUGHTER
SIO2	50.69	47.19	0.08	0.47	34.02	53.51
TIO2	0.89	1.00	0.54	0.00	2.41	0.77
AL2O3	16.17	6.02	0.16	0.00	15.27	17.62
FE2O3	0.00	0.00	0.00	0.00	0.00	0.00
FEO	9.07	13.62	91.28	0.51	21.84	7.20
MNO	0.21	0.45	0.30	0.06	0.53	0.19
MGO	3.54	8.33	0.02	0.08	10.73	2.35
CAO	8.70	21.71	0.00	53.87	0.00	6.76
NA2O	4.01	1.65	0.01	0.11	0.14	3.84
K2O	4.61	0.00	0.00	0.00	9.79	5.88
H2O+	0.43	0.00	0.00	0.23	0.00	0.72
H2O-	0.00	0.00	0.00	0.00	0.00	0.00
P2O5	0.71	0.00	0.00	39.97	0.00	0.51

(PARENT-MINERALS=DAUGHTER)

PARENT: 142
DAUGHTER: 189

	SOL'N	% CUMULATE
142	1.000	
125.A	-0.109	59.712
142.A	-0.005	2.717
D43	-0.013	6.959
111.BI	-0.056	30.612
189	0.817	

R SQUARED = 0.594

	PARENT ANALYSIS	DAUGHTER ANALYSIS	DAUGHTER CALC	WEIGHTED RESID
SIO2	54.46	57.74	57.55	0.20
TIO2	0.96	0.83	0.84	-0.01
AL2O3	17.38	19.02	19.25	-0.23
FEO	9.75	7.77	7.76	0.01
MNO	0.22	0.21	0.17	0.00
MGO	3.81	2.54	2.69	-0.15
CAO	9.35	7.30	7.37	-0.07
NA2O	4.31	4.14	5.04	-0.45
K2O	4.95	6.35	5.29	0.47
P2O5	0.77	0.55	0.11	0.22

UNWEIGHTED INPUT DATA:

	PARENT	125.A	142.A	D43	111.BI	DAUGHTER
SIO2	50.69	47.19	0.08	0.47	34.02	56.41
TIO2	0.89	1.00	0.54	0.00	2.41	0.42
AL2O3	16.17	6.02	0.16	0.00	15.27	20.45
FE2O3	0.00	0.00	0.00	0.00	0.00	0.00
FEO	9.07	13.62	91.28	0.51	21.84	3.77
MNO	0.21	0.45	0.30	0.06	0.53	0.14
MGO	3.54	8.33	0.02	0.08	10.73	0.84
CAO	8.70	21.71	0.00	53.87	0.00	3.43
NA2O	4.01	1.65	0.01	0.11	0.14	4.71
K2O	4.61	0.00	0.00	0.00	9.79	7.41
H2O+	0.43	0.00	0.00	0.23	0.00	1.63
H2O-	0.00	0.00	0.00	0.00	0.00	0.00
P2O5	0.71	0.00	0.00	39.97	0.00	0.19

(PARENT-MINERALS=DAUGHTER)

PARENT: 142
DAUGHTER: 167

	SOL'N	% CUMULATE
142	1.000	
125.A	-0.254	68.143
142.A	-0.016	4.156
D43	-0.019	5.083
111.BI	-0.084	22.618
167	0.627	

R SQUARED = 0.628

	PARENT ANALYSIS	DAUGHTER ANALYSIS	DAUGHTER CALC	WEIGHTED RESID
SIO2	55.22	63.32	63.23	0.09
TIO2	0.97	0.47	0.74	-0.14
AL2O3	17.62	22.95	23.23	-0.27
FEO	9.88	4.23	4.23	0.00
MNO	0.23	0.15	0.08	0.01
MGO	3.86	0.95	1.03	-0.08
CAO	9.48	3.85	3.95	-0.11
NA2O	4.37	5.29	6.27	-0.34
K2O	5.02	8.32	6.48	0.55
P2O5	0.78	0.21	-0.37	0.29

UNWEIGHTED INPUT DATA:

	PARENT	125.A	125.B	142.A	D43	DAUGHTER
SiO2	50.69	47.19	38.23	0.08	0.47	55.79
TiO2	0.89	1.00	2.10	0.54	0.00	0.59
Al2O3	16.17	6.02	13.20	0.16	0.00	19.12
Fe2O3	0.00	0.00	0.00	0.00	0.00	0.00
FeO	9.07	13.62	20.72	91.28	0.51	5.62
MnO	0.21	0.45	0.52	0.30	0.06	0.16
MgO	3.54	8.33	7.34	0.02	0.08	1.72
CaO	8.70	21.71	10.81	0.00	53.87	4.74
Na2O	4.01	1.65	2.65	0.01	0.11	4.40
K2O	4.61	0.00	2.23	0.00	0.00	5.76
H2O+	0.43	0.00	0.00	0.00	0.23	0.85
H2O-	0.00	0.00	0.00	0.00	0.00	0.00
P2O5	0.71	0.00	0.00	0.00	39.97	0.29

(PARENT-MINERALS=DAUGHTER)

PARENT: 142
DAUGHTER: 211

	SOL'N	% CUMULATE
142	1.000	
125.A	-0.128	39.040
125.B	-0.191	58.121
142.A	0.003	-0.964
D43	-0.013	3.802
211	0.671	

R SQUARED = 0.085

	PARENT ANALYSIS	DAUGHTER ANALYSIS	DAUGHTER CALC	WEIGHTED RESID
SiO2	55.22	61.50	61.35	0.15
TiO2	0.97	0.65	0.61	0.02
Al2O3	17.62	21.08	21.04	0.04
FeO	9.88	6.20	6.18	0.01
MnO	0.23	0.18	0.09	0.01
MgO	3.86	1.90	1.88	0.02
CaO	9.48	5.22	5.24	-0.02
Na2O	4.37	4.85	5.38	-0.19
K2O	5.02	6.35	6.79	-0.13
P2O5	0.78	0.33	0.17	0.08

UNWEIGHTED INPUT DATA:

	PARENT	125.A	111.BI	142.A	D43	DAUGHTER
SIO2	51.40	47.19	34.02	0.08	0.47	65.84
TIO2	0.80	1.00	2.41	0.54	0.00	0.40
AL2O3	16.77	6.02	15.27	0.16	0.00	15.98
FE2O3	0.00	0.00	0.00	0.00	0.00	0.00
FEO	7.77	13.62	21.84	91.28	0.51	3.69
MNO	0.19	0.45	0.53	0.30	0.06	0.12
MGO	3.36	8.33	10.73	0.02	0.08	1.32
CAO	7.48	21.71	0.00	0.00	53.87	4.07
NA2O	3.37	1.65	0.14	0.01	0.11	3.94
K2O	5.57	0.00	9.79	0.00	0.00	3.58
H2O+	0.93	0.00	0.00	0.00	0.23	0.35
H2O-	0.00	0.00	0.00	0.00	0.00	0.00
P2O5	0.54	0.00	0.00	0.00	39.97	0.19

(PARENT-MINERALS=DAUGHTER)

PARENT: 125
 DAUGHTER: 120

	SOL'N	% CUMULATE
125	1.000	
125.A	0.124	%-44.693
111.BI	-0.311	%112.003
142.A	0.004	-1.518
D43	-0.095	34.209
120	0.722	

R SQUARED = 16.446

	PARENT ANALYSIS	DAUGHTER ANALYSIS	DAUGHTER CALC	WEIGHTED RESID
SIO2	55.36	68.79	68.43	0.36
TIO2	0.86	0.41	0.19	0.11
AL2O3	18.07	16.70	18.69	-1.99
FEO	8.37	3.86	3.88	-0.02
MNO	0.21	0.12	0.10	0.00
MGO	3.62	1.38	1.25	0.12
CAO	8.06	4.25	5.48	-1.23
NA2O	3.63	4.11	5.23	-0.67
K2O	6.00	3.74	3.56	0.10
P2O5	0.58	0.20	-6.24	3.22

UNWEIGHTED INPUT DATA:

	PARENT	120.A	PL120	KSP120	D43	142.A	DAUGHTER
SiO2	65.84	43.64	60.21	64.44	0.47	0.08	66.92
TiO2	0.40	1.69	0.00	0.00	0.00	0.54	0.35
Al2O3	15.98	8.58	24.54	18.60	0.00	0.16	15.98
Fe2O3	0.00	0.00	0.00	0.00	0.00	0.00	0.00
FeO	3.69	16.55	0.14	0.06	0.51	91.28	3.14
MnO	0.12	0.77	0.00	0.00	0.06	0.30	0.10
MgO	1.32	11.28	0.01	0.01	0.08	0.02	1.05
CaO	4.07	11.46	6.34	0.00	53.87	0.00	3.61
Na2O	3.94	1.53	7.56	0.52	0.11	0.01	4.08
K2O	3.58	1.15	0.08	16.16	0.00	0.00	3.22
H2O+	0.35	0.00	0.00	0.00	0.23	0.00	0.63
H2O-	0.00	0.00	0.00	0.00	0.00	0.00	0.00
P2O5	0.19	0.00	0.00	0.00	39.97	0.00	0.16

(PARENT-MINERALS=DAUGHTER)

PARENT: 120
 DAUGHTER: 195

	SOL'N	% CUMULATE
120	1.000	
120.A	-0.034	34.890
PL120	-0.021	21.823
KSP120	-0.036	36.793
D43	-0.004	3.636
142.A	-0.003	2.858
195	0.903	

R SQUARED = 0.010

	PARENT ANALYSIS	DAUGHTER ANALYSIS	DAUGHTER CALC	WEIGHTED RESID
SiO2	68.79	70.18	70.22	-0.04
TiO2	0.41	0.36	0.39	-0.01
Al2O3	16.70	16.76	16.76	-0.00
FeO	3.86	3.30	3.30	-0.00
MnO	0.12	0.11	0.10	0.00
MgO	1.38	1.10	1.07	0.03
CaO	4.25	3.79	3.82	-0.03
Na2O	4.11	4.28	4.29	-0.00
K2O	3.74	3.38	3.41	-0.02
P2O5	0.20	0.17	0.01	0.08

UNWEIGHTED INPUT DATA:

	PARENT	120.A	PL120	DAUGHTER
SIO2	59.05	43.64	60.21	60.57
TIO2	0.64	1.69	0.00	0.61
AL2O3	16.82	8.58	24.54	16.54
FE2O3	0.00	0.00	0.00	0.00
FEO	5.97	16.55	0.14	5.59
MNO	0.17	0.77	0.00	0.16
MGO	2.21	11.28	0.01	2.01
CAO	5.97	11.46	6.34	5.50
NA2O	4.13	1.53	7.56	3.93
K2O	3.21	1.15	0.08	3.78
H2O+	0.35	0.00	0.00	0.41
H2O-	0.00	0.00	0.00	0.00
P2O5	0.37	0.00	0.00	0.35

(PARENT-MINERALS=DAUGHTER)

PARENT: 192
 DAUGHTER: 136

	SOL'N	% CUMULATE
192	1.000	
120.A	-0.068	40.025
PL120	-0.101	59.975
136	0.831	

R SQUARED = 0.175

	PARENT ANALYSIS	DAUGHTER ANALYSIS	DAUGHTER CALC	WEIGHTED RESID
SIO2	62.19	63.53	63.40	0.14
TIO2	0.67	0.64	0.66	-0.01
AL2O3	17.71	17.35	17.45	-0.10
FEO	6.29	5.86	6.12	-0.25
MNO	0.18	0.17	0.15	0.00
MGO	2.33	2.11	1.83	0.28
CAO	6.28	5.77	5.76	0.01
NA2O	4.35	4.12	4.14	-0.01
K2O	3.38	3.96	3.96	0.00
P2O5	0.39	0.37	0.47	-0.05

UNWEIGHTED INPUT DATA:

	PARENT	120.A	PL120	KSP120	142.A	DAUGHTER
SIO2	64.85	43.64	60.21	64.44	0.08	66.92
TIO2	0.43	1.69	0.00	0.00	0.54	0.35
AL2O3	16.42	8.58	24.54	18.60	0.16	15.98
FE2O3	0.00	0.00	0.00	0.00	0.00	0.00
FEO	3.88	16.55	0.14	0.06	91.28	3.14
MNO	0.11	0.77	0.00	0.00	0.30	0.10
MGO	1.33	11.28	0.01	0.01	0.02	1.05
CAO	4.14	11.46	6.34	0.00	0.00	3.61
NA2O	3.86	1.53	7.56	0.52	0.01	4.08
K2O	3.73	1.15	0.08	16.16	0.00	3.22
H2O+	0.57	0.00	0.00	0.00	0.00	0.63
H2O-	0.00	0.00	0.00	0.00	0.00	0.00
P2O5	0.20	0.00	0.00	0.00	0.00	0.16

(PARENT-MINERALS=DAUGHTER)

PARENT: 176
DAUGHTER: 195

	SOL'N	% CUMULATE
176	1.000	
120.A	-0.052	25.599
PL120	-0.084	41.166
KSP120	-0.063	30.766
142.A	-0.005	2.469
195	0.796	

R SQUARED = 0.065

	PARENT ANALYSIS	DAUGHTER ANALYSIS	DAUGHTER CALC	WEIGHTED RESID
SIO2	67.91	70.18	70.18	0.00
TIO2	0.45	0.36	0.44	-0.04
AL2O3	17.20	16.76	16.73	0.02
FEO	4.06	3.30	3.30	0.00
MNO	0.11	0.11	0.08	0.00
MGO	1.39	1.10	0.96	0.14
CAO	4.33	3.79	3.95	-0.16
NA2O	4.04	4.28	4.10	0.11
K2O	3.90	3.38	3.45	-0.04
P2O5	0.21	0.17	0.26	-0.05

UNWEIGHTED INPUT DATA:

	PARENT	120.A	142.A	D43	KSP120	DAUGHTER
SIO2	66.92	43.64	0.08	0.47	64.44	68.00
TIO2	0.35	1.69	0.54	0.00	0.00	0.29
AL2O3	15.98	8.58	0.16	0.00	18.60	16.19
FE2O3	0.00	0.00	0.00	0.00	0.00	0.00
FEO	3.14	16.55	91.28	0.51	0.06	2.59
MNO	0.10	0.77	0.30	0.06	0.00	0.12
MGO	1.05	11.28	0.02	0.08	0.01	0.90
CAO	3.61	11.46	0.00	53.87	0.00	3.52
NA2O	4.08	1.53	0.01	0.11	0.52	4.37
K2O	3.22	1.15	0.00	0.00	16.16	2.80
H2O+	0.63	0.00	0.00	0.23	0.00	0.53
H2O-	0.00	0.00	0.00	0.00	0.00	0.00
P2O5	0.16	0.00	0.00	39.97	0.00	0.13

(PARENT-MINERALS=DAUGHTER)

PARENT: 195
 DAUGHTER: 175

	SOL'N	% CUMULATE
195	1.000	
120.A	-0.019	32.619
142.A	-0.004	7.093
D43	-0.001	2.178
KSP120	-0.034	58.110
175	0.942	

R SQUARED = 0.008

	PARENT ANALYSIS	DAUGHTER ANALYSIS	DAUGHTER CALC	WEIGHTED RESID
SIO2	70.18	71.04	71.10	-0.07
TIO2	0.36	0.31	0.35	-0.02
AL2O3	16.76	16.92	16.89	0.03
FEO	3.30	2.70	2.70	-0.00
MNO	0.11	0.13	0.10	0.00
MGO	1.10	0.94	0.92	0.02
CAO	3.79	3.67	3.68	-0.01
NA2O	4.28	4.57	4.49	0.04
K2O	3.38	2.93	2.94	-0.01
P2O5	0.17	0.14	0.11	0.02

UNWEIGHTED INPUT DATA:

	PARENT	120.A	142.A	D43	PL120	KSP120	DAUGHTER
SIO2	55.82	43.64	0.08	0.47	60.21	64.44	59.05
TIO2	0.76	1.69	0.54	0.00	0.00	0.00	0.64
AL2O3	17.30	8.58	0.16	0.00	24.54	18.60	16.82
FE2O3	0.00	0.00	0.00	0.00	0.00	0.00	0.00
FEO	6.97	16.55	91.28	0.51	0.14	0.06	5.97
MNO	0.16	0.77	0.30	0.06	0.00	0.00	0.17
MGO	2.81	11.28	0.02	0.08	0.01	0.01	2.21
CAO	6.96	11.46	0.00	53.87	6.34	0.00	5.97
NA2O	3.90	1.53	0.01	0.11	7.56	0.52	4.13
K2O	3.47	1.15	0.00	0.00	0.08	16.16	3.21
H2O+	0.00	0.00	0.00	0.23	0.00	0.00	0.35
H2O-	0.00	0.00	0.00	0.00	0.00	0.00	0.00
P2O5	0.40	0.00	0.00	39.97	0.00	0.00	0.37

(PARENT-MINERALS=DAUGHTER)

PARENT: 183
 DAUGHTER: 192

	SOL'N	% CUMULATE
183	1.000	
120.A	-0.167	28.850
142.A	-0.017	2.952
D43	-0.011	1.911
PL120	-0.270	46.780
KSP120	-0.113	19.506
192	0.422	

R SQUARED = 0.366

	PARENT ANALYSIS	DAUGHTER ANALYSIS	DAUGHTER CALC	WEIGHTED RESID
SIO2	58.84	62.19	62.32	-0.13
TIO2	0.80	0.67	1.16	-0.24
AL2O3	18.24	17.71	17.86	-0.15
FEO	7.35	6.29	6.30	-0.02
MNO	0.17	0.18	0.07	0.01
MGO	2.96	2.33	2.25	0.08
CAO	7.34	6.28	6.45	-0.16
NA2O	4.11	4.35	3.89	0.27
K2O	3.65	3.38	3.48	-0.06
P2O5	0.42	0.39	-0.40	0.40

UNWEIGHTED INPUT DATA:

	PARENT	120.A	142.A	D43	PL120	KSP120	DAUGHTER
SIO2	55.82	43.64	0.08	0.47	60.21	64.44	68.00
TIO2	0.76	1.69	0.54	0.00	0.00	0.00	0.29
AL2O3	17.30	8.58	0.16	0.00	24.54	18.60	16.19
FE2O3	0.00	0.00	0.00	0.00	0.00	0.00	0.00
FEO	6.97	16.55	91.28	0.51	0.14	0.06	2.59
MNO	0.16	0.77	0.30	0.06	0.00	0.00	0.12
MGO	2.81	11.28	0.02	0.08	0.01	0.01	0.90
CAO	6.96	11.46	0.00	53.87	6.34	0.00	3.52
NA2O	3.90	1.53	0.01	0.11	7.56	0.52	4.37
K2O	3.47	1.15	0.00	0.00	0.08	16.16	2.80
H2O+	0.00	0.00	0.00	0.23	0.00	0.00	0.53
H2O-	0.00	0.00	0.00	0.00	0.00	0.00	0.00
P2O5	0.40	0.00	0.00	39.97	0.00	0.00	0.13

(PARENT-MINERALS=DAUGHTER)

PARENT: 183
 DAUGHTER: 175

	SOL'N	% CUMULATE
183	1.000	
120.A	-0.235	28.810
142.A	-0.026	3.230
D43	-0.016	1.995
PL120	-0.382	46.774
KSP120	-0.157	19.192
175	0.183	

R SQUARED = 3.520

	PARENT ANALYSIS	DAUGHTER ANALYSIS	DAUGHTER CALC	WEIGHTED RESID
SIO2	58.84	71.04	71.34	-0.30
TIO2	0.80	0.31	1.97	-0.83
AL2O3	18.24	16.92	17.31	-0.40
FEO	7.35	2.70	2.71	-0.01
MNO	0.17	0.13	-0.17	0.03
MGO	2.96	0.94	0.67	0.27
CAO	7.34	3.67	4.18	-0.51
NA2O	4.11	4.57	3.40	0.70
K2O	3.65	2.93	3.35	-0.25
P2O5	0.42	0.14	-2.47	1.30

Mixing Runs

SOLUTION ARRAY

	179	120	136
●↔			
SiO2	63.70	65.84	60.57
TiO2	0.47	0.40	0.61
Al2O3	16.37	15.98	16.54
FeO*	4.36	3.69	5.59
MnO	0.13	0.12	0.16
MgO	1.52	1.32	2.01
CaO	4.66	4.07	5.50
Na2O	3.95	3.94	3.93
K2O	3.36	3.58	3.78
P2O5	0.23	0.19	0.35

⊙▽

VARIABLE ARRAY

	209	194
●↔		
SiO2	49.80	65.41
TiO2	0.96	0.42
Al2O3	15.57	15.89
FeO*	9.36	3.84
MnO	0.21	0.12
MgO	4.23	1.26
CaO	9.37	4.07
Na2O	3.37	3.92
K2O	3.83	3.46
P2O5	0.75	0.20

	179			120			136		
	CALC	OBSVD	DIFF	CALC	OBSVD	DIFF	CALC	OBSVD	DIFF
SiO2	63.81	63.70	0.11	65.86	65.84	0.02	60.74	60.57	0.17
TiO2	0.48	0.47	0.01	0.41	0.40	0.01	0.59	0.61	-0.02
Al2O3	15.89	16.37	-0.48	15.95	15.98	-0.03	15.85	16.54	-0.69
FeO*	4.48	4.36	0.12	3.78	3.69	0.09	5.60	5.59	0.01
MnO	0.13	0.13	0.00	0.12	0.12	-0.00	0.15	0.16	-0.01
MgO	1.60	1.52	0.08	1.22	1.32	-0.10	2.20	2.01	0.19
CaO	4.68	4.66	0.02	4.01	4.07	-0.06	5.76	5.50	0.26
Na2O	3.87	3.95	-0.08	3.94	3.94	0.00	3.76	3.93	-0.17
K2O	3.51	3.36	0.15	3.47	3.58	-0.11	3.59	3.78	-0.19
P2O5	0.26	0.23	0.03	0.19	0.19	0.00	0.37	0.35	0.02

⊙▽

CALCULATED WEIGHT FRACTIONS AND SUMS RESIDUALS SQUARED

●↔

	SOL. NO. 1	SOL. NO. 2	SOL. NO. 3
209	0.1135	-0.0137	0.3162
194	0.8891	1.0173	0.6879
SUM R SQ`D	0.2887	0.0344	0.6720

SOLUTION ARRAY

	179	120	136
●↔			
SiO2	63.70	65.84	60.57
TiO2	0.47	0.40	0.61
Al2O3	16.37	15.98	16.54
FeO*	4.36	3.69	5.59
MnO	0.13	0.12	0.16
MgO	1.52	1.32	2.01
CaO	4.66	4.07	5.50
Na2O	3.95	3.94	3.93
K2O	3.36	3.58	3.78
P2O5	0.23	0.19	0.35

⊙▽

VARIABLE ARRAY

	188	195
●↔		
SiO2	48.58	66.92
TiO2	1.00	0.35
Al2O3	15.12	15.98
FeO*	10.30	3.14
MnO	0.72	0.10
MgO	3.25	1.05
CaO	9.21	3.61
Na2O	2.82	4.08
K2O	4.52	3.22
P2O5	0.81	0.16

	179			120			136		
	CALC	OBSVD	DIFF	CALC	OBSVD	DIFF	CALC	OBSVD	DIFF
SiO2	63.80	63.70	0.10	65.83	65.84	-0.01	60.75	60.57	0.18
TiO2	0.48	0.47	0.01	0.41	0.40	0.01	0.59	0.61	-0.02
Al2O3	15.90	16.37	-0.47	16.01	15.98	0.03	15.80	16.54	-0.74
FeO*	4.52	4.36	0.16	3.75	3.69	0.06	5.80	5.59	0.21
MnO	0.22	0.13	0.09	0.15	0.12	0.03	0.33	0.16	0.17
MgO	1.47	1.52	-0.05	1.24	1.32	-0.08	1.87	2.01	-0.14
CaO	4.69	4.66	0.03	4.10	4.07	0.03	5.70	5.50	0.20
Na2O	3.86	3.95	-0.09	4.00	3.94	0.06	3.65	3.93	-0.28
K2O	3.48	3.36	0.12	3.35	3.58	-0.23	3.72	3.78	-0.06
P2O5	0.28	0.23	0.05	0.21	0.19	0.02	0.40	0.35	0.05

⊙▽

CALCULATED WEIGHT FRACTIONS AND SUMS RESIDUALS SQUARED

●↔

	SOL. NO. 1	SOL. NO. 2	SOL. NO. 3
188	0.1899	0.0828	0.3675
195	0.8155	0.9237	0.6410
SUM R SQ`D	0.2894	0.0715	0.7948

Mixing & Fractionation

SOLUTION ARRAY

	134	158
SiO2	50.51	53.45
TiO2	0.95	0.79
Al2O3	15.36	16.50
FeO*	9.75	7.68
MnO	0.23	0.21
MgO	3.33	2.56
CaO	8.70	6.89
Na2O	2.99	4.11
K2O	5.02	4.61
P2O5	0.74	0.32

VARIABLE ARRAY

	188	195
SiO2	48.58	66.92
TiO2	1.00	0.35
Al2O3	15.12	15.98
FeO*	10.30	3.14
MnO	0.72	0.10
MgO	3.25	1.05
CaO	9.21	3.61
Na2O	2.82	4.08
K2O	4.52	3.22
P2O5	0.81	0.16

	134			158		
	CALC	OBSVD	DIFF	CALC	OBSVD	DIFF
SiO2	50.54	50.51	0.03	53.80	53.45	0.35
TiO2	0.96	0.95	0.01	0.79	0.79	-0.00
Al2O3	15.34	15.36	-0.02	15.23	16.50	-1.27
FeO*	9.82	9.75	0.07	7.95	7.68	0.27
MnO	0.68	0.23	0.45	0.52	0.21	0.31
MgO	3.10	3.33	-0.23	2.53	2.56	-0.03
CaO	8.84	8.70	0.14	7.36	6.89	0.47
Na2O	2.95	2.99	-0.04	3.18	4.11	-0.93
K2O	4.46	5.02	-0.56	4.06	4.61	-0.55
P2O5	0.77	0.74	0.03	0.60	0.32	0.28

CALCULATED WEIGHT FRACTIONS AND SUMS RESIDUALS SQUARED

	SOL. NO. 1	SOL. NO. 2
188	0.9285	0.6762
195	0.0812	0.3131
SUM R SQ'D	0.5960	3.3621

Mixing & Fractionation (cont.)

UNWEIGHTED INPUT DATA:

	PARENT	125.A	125.B	142.A	D43	DAUGHTER
SiO2	50.40	47.19	38.23	0.08	0.47	53.51
TiO2	0.97	1.00	2.10	0.54	0.00	0.77
Al2O3	15.67	6.02	13.20	0.16	0.00	17.62
Fe2O3	0.00	0.00	0.00	0.00	0.00	0.00
FeO	9.81	13.62	20.72	91.28	0.51	7.20
MnO	0.24	0.45	0.52	0.30	0.06	0.19
MgO	3.60	8.33	7.34	0.02	0.08	2.35
CaO	8.90	21.71	10.81	0.00	53.87	6.76
Na2O	3.04	1.65	2.65	0.01	0.11	3.84
K2O	4.38	0.00	2.23	0.00	0.00	5.88
H2O+	0.00	0.00	0.00	0.00	0.23	0.72
H2O-	0.00	0.00	0.00	0.00	0.00	0.00
P2O5	0.74	0.00	0.00	0.00	39.97	0.51

(PARENT-MINERALS=DAUGHTER)

PARENT: 134.CA
 DAUGHTER: 189

	SOL'N	% CUMULATE
134.CA	1.000	
125.A	-0.112	46.195
125.B	-0.124	51.354
142.A	-0.004	1.469
D43	-0.002	0.983
189	0.759	

R SQUARED = 0.295

	PARENT ANALYSIS	DAUGHTER ANALYSIS	DAUGHTER CALC	WEIGHTED RESID
SiO2	53.78	56.97	57.24	-0.27
TiO2	1.04	0.82	0.85	-0.02
Al2O3	16.72	18.76	18.87	-0.11
FeO	10.47	7.66	7.70	-0.03
MnO	0.26	0.21	0.18	0.00
MgO	3.84	2.51	2.54	-0.04
CaO	9.50	7.20	7.17	0.03
Na2O	3.24	4.09	3.57	0.31
K2O	4.67	6.26	5.78	0.29
P2O5	0.79	0.54	0.87	-0.17